Západočeská univerzita v Plzni

Fakulta aplikovaných věd

DOCTORAL THESIS

2009 Ing. Jana Hájková

Západočeská univerzita v Plzni
Fakulta aplikovaných věd

Disertační práce

k získání akademického titulu doktor
v oboru

Informatika a výpočetní technika

Zpracování dat pro simulaci dopadu laserového paprsku

Ing. Jana Hájková

Školitel: Doc. Ing. Pavel Herout, Ph.D.

Katedra: Katedra informatiky a výpočetní techniky

Plzeň, 2009

University of West Bohemia
Faculty of Applied Sciences

Doctoral Thesis

in partial fulfillment of the requirements for the degree of
Doctor of Philosophy
in specialization

Computer Science and Engineering

Data Processing for Simulation of Laser Beam Impact

Ing. Jana Hájková

Supervisor: Doc. Ing. Pavel Herout, Ph.D.

Department: Department of Computer Science and Engineering

Plzeň, 2009

Prohlášení

Předkládám tímto k posouzení a obhajobě disertační práci zpracovanou za závěr doktorského studia na Fakultě aplikovaných věd Západočeské univerzity v Plzni.

Prohlašuji, že jsem tuto práci vypracovala samostatně s použitím odborné literatury a dostupných pramenů uvedených v seznamu, který je součástí této práce

V Plzni, 7. 7. 2009 Ing. Jana Hájková

Data Processing for Simulation of Laser Beam Impact

Ing. Jana Hájková

Abstract

This work deals with several important parts of laser engraving simulation process. At the beginning, it gives a broader overview of the project of laser simulation, which is processed at the University of West Bohemia in Pilsen. The physical background of interaction between the laser beam and the processed material are outlined. All important parts of the simulation are described; several other problems are also discussed to get a global overview of the whole process. The input data sets are described and the way of their acquisition is shown.

The main content of the thesis is formed by the methodology for solving several subproblems used especially in the phase of data processing. Methods for data parameterization and methods for automatic heat-affected area detection are described in detail. The main idea of each described method is explained and its problems and possible ways of their elimination are discussed.

As a part of the thesis, two basic ideas of simulation methods and several methods for system verification are outlined. At the end of the thesis, possible plans for future research are introduced.

Data Processing for Simulation of Laser Beam Impact

Ing. Jana Hájková

Abstrakt

Práce se zabývá několika důležitými částmi procesu simulace laserového gravírování. V úvodu práce je popsán celý projekt laserové simulace zpracovávaný na Západočeské univerzitě v Plzni. Pro získání celkového přehledu o řešené problematice jsou zde popsané všechny podstatné části simulace a zároveň je v úvodu práce nastíněna řada problémů, které bude nutné v rámci řešení projektu vzít v úvahu, včetně základních informací o interakci laseru a zpracovávaného materiálu během procesu laserového vypalování. Součástí práce je popis formátu používaných reálných dat a způsob jejich získávání.

Hlavní náplní disertační práce je návrh metodiky řešení části zpracování vstupních dat. Jsou zde detailně popsány metody pro parametrizaci dat a metody pro automatickou detekci oblasti povrchu materiálu modifikované laserem v průběhu vypalování. U jednotlivých metod je vždy vysvětlena hlavní myšlenka a také problémy, u kterých jsou navržené možnosti řešení. Všechny popsané metody jsou testovány na stejné vybrané skupině vzorků zvolených z důvodu jejich specifických vlastností.

Jako součást práce jsou také naznačené dvě metody vlastní simulace laserového gravírování a několik metod verifikace simulace a porovnávání vzorků. V závěru disertační práce jsou navržené možnosti dalšího výzkumu.

Acknowledgements

At this place I would like to thank all the people who have helped me during my Ph. D. studies. First, great thanks go to my supervisor Doc. Ing. Pavel Herout, Ph. D. for his support during my research and Ph. D. thesis finalization.

Great thanks go to all my colleagues in the Department of Computer Science and Engineering who were discussing many scientific problems with me. They gave me various inspiring ideas and theories, which have helped me in my research.

I would like to thank the experts from non-computer-science groups cooperating on the project, Doc. Ing. Milan Honner, Ph. D. from the New Technologies Research Center and Doc. Ing. Petr Girg, Ph. D. from the Department of Mathematics.

Last but not least, my great thanks belong to my family for its support and understanding during my Ph. D. studies. Special thanks go to Michal, my greatest moral support.

Table of Content

1 Introduction

1.1 Project Description

At the beginning, the whole Ph.D. work was prepared as a part of a large multi-departmental project. The cooperation has started at the end of 2006 and it had several participants: three departments of the University of West Bohemia – the Department of Computer Science and Engineering, the Department of Physics and the Department of Cybernetics. Except these three university departments, a hi-tech company Lintech [Lintech] should also participate on this project and support it. The global overview of the planned project is described in [Háj08a]. The aim of the project was to develop a real laser equipment (HW device) for engraving any described experiment into a proper material. This device should have also several SW parts, which should control the laser and simulate its function.

Experts from the Department of Physics have a big experience with lasers and their usage, so they should choose, operate and service the laser equipment. The group from the Department of Cybernetics has a big experience with the control of various devices, so they should be responsible for direct control of the laser device. We were asked to provide IT support and to add a software which will be able to simulate the engraving process and to visualize and evaluate the measured results of real experiments in detail. The last partner of the project, the commercial firm Lintech, has planned to use the system for common technical tasks. After some time of the project existence, we also started to cooperate with another partner from the University of West Bohemia. We involved experts from the Department of Mathematics. The aim of the cooperation between the Department of Mathematics and the Department of Computer Science and Engineering was to search for the optimal algorithm for processed samples parts recognition and their comparison.

Of course, somebody could think that such devices that we planned to design, are already available for commercial use. That is partly true. However, the existing devices do not enable affecting all the engraving parameters and so they do not take advantage of all the possible usages of the device, which would increase the quality of the experiments results. Moreover, they are fundamentally meant for technological operations and not for any ambitious research experiments. They also do not enable to use simulation for various kinds of optimization. Another problem that can be prevented by the simulation is based on not fully deterministic results of the engraving operations, which cause that engraved experiments need sometimes to be repeated several times using different laser settings to obtain the optimal result. The repeated engraving process is costly and time consuming and for this reason, laser simulation is a desirable part of the laser engraving system.

After approximately one year of preparatory works, it has appeared that it would not be possible to buy all the necessary HW components in time and that is why our project had to change. We have started to use an already existing laser that was provided by the Lintech company. This device does not enable all the intended settings, but its facilities are broad enough to perform most of the physical experiments and to provide real data, which could be used as the input for the simulation system and the system for exploring the measured data. In the following description, only the SW parts of the project will be explained.

The whole simulation process is a complicated system of various tasks that had to be provided in the proper sequence and, if possible, in the as-automatic-as-possible way. All the important tasks are shown in Fig. 1. To provide a simulation of the engraving process, data sets from the real samples have to be measured and the results saved into some data files. These files should be loaded step by step into the sample editor, where they are processed (pulses detected, parameterized, etc.). After the parameterization of all the samples from the input data set, each sample can be described by a set of parameters and also the laser settings and material quality descriptions are summarized. In order to simulate an experiment, it is necessary to prepare data describing the experiment that can be used as an input for the simulator. The results of the simulation have to be validated and verified using data obtained by measuring a real experiment engraved with the same parameters. According to the results of the verification, the parametric description and the laser and material specification could be affected to get the reliable simulation model that would produce as realistic results as possible. Both the simulation results and the real measured samples can be further visualized, evaluated and various statistics could be computed for them to get a set of promising experiments which should be finally engraved into the real material.

The simulation can be performed either unassisted in a batch mode or controlled by a human in an interactive mode. During the batch mode, all results should be saved and logged, so that the best results could be chosen after the simulation finishes. In the case of the interactive mode, the engraving process can be optimized on-the-fly. For example, the speed of engraving or quality of the result could be chosen as criterions for the optimization. The simulator should also enable to view all samples (both the real and the simulated ones) in a 2D and a 3D viewer. Finally, at the end of the simulation process, the final engraved sample (the simulation experiment) is created.

It is evident that in order to prepare all parts of the simulation system, a lot of work has to be done. Only some tasks are solved by this Ph. D. thesis.

1.2 Fields of Cooperation

As mentioned in the previous section, the work comes out from a cooperation with experts in other fields of research, such as mathematics or physics.

The cooperation with the Department of Mathematics is important for data analysis and design of methods and algorithms for data preprocessing. The mathematical view has helped us to find another approaches and solutions for problems, which were showing up during our research. From our cooperation, a method using image filtering followed by isolines searching has resulted. It is described in Section 5.2.4 and its results are outlined in Section 6.1.4.

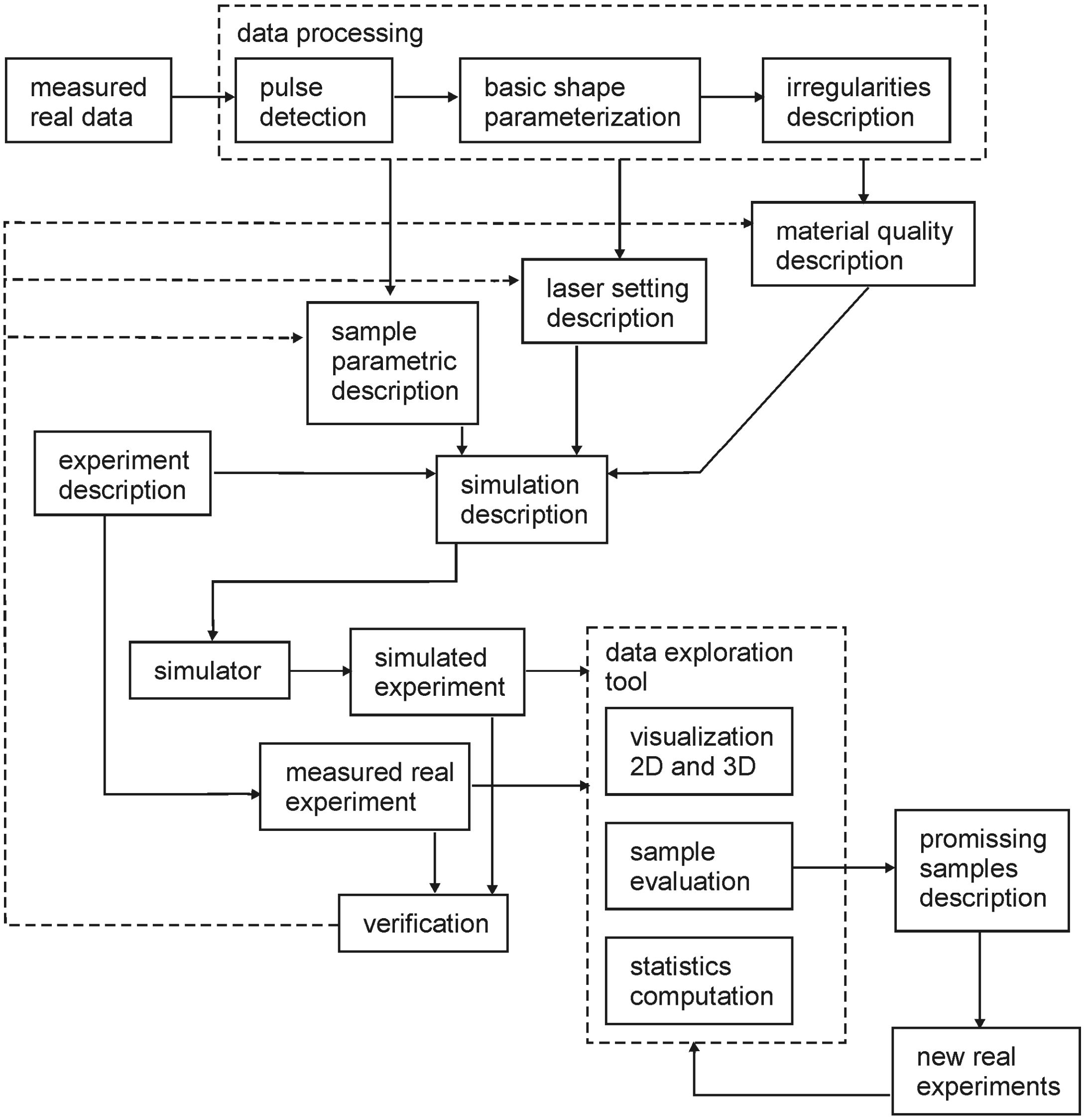

Fig. 1: Sequence of tasks of the SW part of the project.

More intensive cooperation was established with the working group from the Department of Physics, more concretely, with the experts from the New Technologies Research Centre at the University of West Bohemia. To start our work, we needed to obtain real data to get a satisfactory imagination about a form of the data to be processed and to understand the engraving process well. From our colleagues, we have received several real measured samples engraved into steel and cermet and then we have started to analyze them. Later, we have also received one complete measured experiment engraved into steel. More information about data acquisition process and its description can be found in Chapter 3. We have taken an advantage from our cooperation with Lintech and so all experiments were prepared there so far. Despite their willingness to cooperate, the data acquisition was a little bit more complicated, because the laser equipment for engraving the real samples had to be borrowed for each experiment.

When we get all the required data we could start to work on the simulation system itself. Our cooperation has continued during the system development, because we had to pass necessary information and discuss the current results with them. Of course, we also want to keep the cooperation in the future, until our shared plans are finished.

1.3 Ways of Research

For our work, use real data sets as the input for the simulation system, but they cannot be processed directly. First, the data has to be preprocessed and transformed into the suitable form. The transformation should run in several steps and so it is important to design a methodology for data preprocessing at the beginning of our research. Without doing that, we would not be able to continue with any other steps of the simulation.

Data preprocessing consists of several parts. Because only a part of the material surface is affected by the laser beam during the engraving process, it is important to detect this area of the sample. If we want this operation to be performed automatically, an algorithm for the automatic detection needs to be designed.

All processed real samples should also be parameterized. The sample parameterization should be self-regulating and so it would be good to find some dependence of the parameters on the real conditions, which were used for the sample engraving. If any such dependence can be found, we would be able to describe samples which were not really engraved. Computed parameters can be used for samples description, comparison, but also for generating new samples. For generating samples, a set of appropriate methods needs to be designed.

When the input data is preprocessed, the simulation itself can start. The simulation process, all its parts and problems to solve are described in detail in Section 2.1. To prepare the simulation itself, a lot of tasks has to be researched. The validation and verification of the simulation results is an integral part of the whole simulation process as well.

But as mentioned in the review of the concept of doctoral thesis [Háj08b], to solve all the outlined ways of the project, it would take much more time than available for one Ph. D. research. That is why we have decided to select the most important parts and to work only on them. We had to start from the beginning, and so the first methods, which had to be designed, are those for data preprocessing.

1.4 Aims of the Ph.D. Work

Aims of this thesis can be summarized into four points. First, the general methodology for processing the real input data sets needs to be designed. It should result into a parametric description of a general sample engraved into any material.

Artificial sample surface generation relates to the sample parameterization process. That is why our second aim is to concentrate on the methodology of sample surface generation based on the parametric sample description.

Next important part of the data processing is the automatic detection of the pulse in any real or simulated sample surface. The detection should be further used for the automation of sample parameterization described above and also for the validation and verification of the simulation model.

Finally, to be able to test all the designed methods and to evaluate the real measured and simulated samples, a data exploration and simulation tool should be implemented.

1.5 A Thesis Organization

This thesis can be divided into several parts. In Chapter 1, the whole project is described, parts of the project, which we should work on, are outlined and our cooperation with other groups working on the project is shown. The physical processes running during the laser engraving and also several already existing similar projects from other researches are summarized in Chapter 2.

Several problems of the process simulation (concretely from the data preprocessing part) are chosen and their research is described in detail. Each problem is outlined first, methods for solving it are analyzed and, finally, all the designed methods are tested on the real samples and their results are discussed.

The first solved problem is the process of the pulse parameterization and its approximation that is shown in Chapter 3. As a part of this chapter, the way of data acquisition and the format of real measured data are also outlined. Results of methods designed for the sample parameterization and approximation can be found in Chapter 4.

The second problem, which we are interested in, is the process of automatic detection of the material sample area affected by the laser beam during the real laser engraving process. Several algorithms are shown in Chapter 5 and their successfulness and result comparison can be seen in Chapter 6.

The simulation itself is not the main topic of this thesis. As it was described above, many steps have to be done and a lot of methods for the data processing should be designed before the simulation itself. For all that, some primary approaches for the simulation are outlined in Chapter 7 and also some methods how to compare two samples (for example the real sample with the simulated one) are shown in Chapter 8.

As a part of our research, the simulation system including the sample 2D and 3D viewer was created and its usage for the visualization and evaluation of real experiments corresponds with the aims of the whole project. It was prepared to test all the designed methods and approaches. The system and its basic functions are outlined in Chapter 9. Some other possible ways of further research, which have appeared over the time, are described in Chapter 10. Finally, Chapter 11 concludes the thesis.

2 State of the Art

To obtain a general overview about already existing projects solving the analogous problems, we were searching in papers and books for references of any existing solutions. Because we are interested in relatively specialized problems, no descriptions and solutions of analogous problems are usually accessible and that is why only related problems and especially methods applicable to our solutions will be described in the following state of the art.

In the following sections, the laser-engraving process and its physical background are described, along with the process of engraving simulation, its problems, reasons for doing it and its possible techniques.

2.1 Laser-Engraving Process

To simulate the laser-engraving process, we should understand the process of laser engraving and material ablation in detail. During the engraving process, the surface of the material is exposed to an intense pulsed laser beam that creates a rapid rise in local temperature. The surface is warming up and the material starts to ablate. The material, which is ablated, redeposites around the irradiated area and damages the surrounding material. Finally, at the exposure site, a pit with a transition ring around it is left behind. The relief of such sample can be seen in Fig. 2.

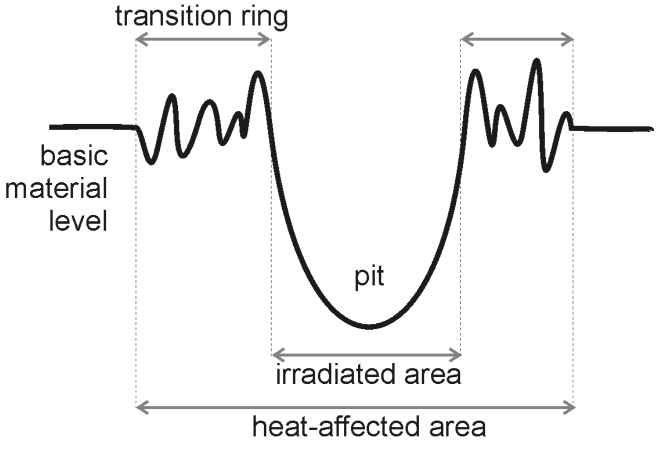

Fig. 2: Relief of a sample and the used terminology.

We can explain the whole process more concretely. Laser beam is an electromagnetic radiation. When this radiation (EL) strikes a surface of the material, some radiation is reflected (R), some absorbed (A) and some transmitted (T) as shown in Fig. 3.

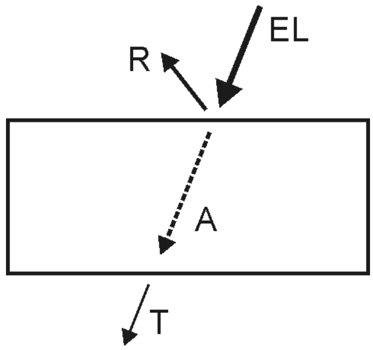

Fig. 3 : Schematic representation of the reflected (R), absorbed (A) and transmitted (T) electromagnetic radiation (EL).

For the laser processing of a material, the most important is the absorption of the radiation. As the electromagnetic radiation passes through the material, the absorbed radiation causes excitation of free electrons (in metals), vibrating in the structure of the material (in insulators), or both (in semiconductors). We detect all these processes as heat. The heat generated at the surface directly affected by the laser beam is conducted into the material. The temperature distribution in the material depends on the thermo-physical properties of the material (e.g., absorptivity, thermal conductivity, density, etc.) and also on the parameters of the laser (e.g., intensity, wavelength, coherence, angle of incidence, etc.). The evolution of surface temperature during a single pulse (outlined as the gray rectangle) is shown in Fig. 4

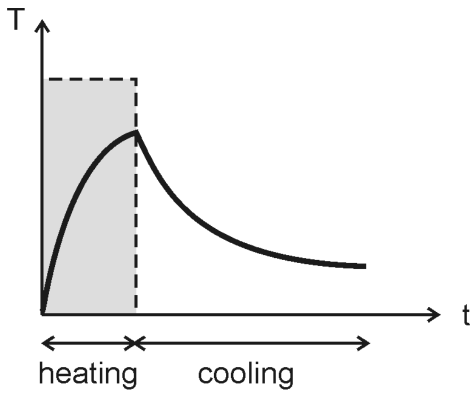

Fig. 4: Schematic evolution of the surface temperature during a single laser beam pulse.

If the laser intensity is high enough, the incident material heats, melts and if it reaches the boiling point, it starts to vaporize. These three described phases can be seen from the cross-section view in Fig. 5. The solid arrows signal the laser beam direction, dashed arrows show the heat conduction in the material and the melted and vaporized material is highlighted with the gray color.

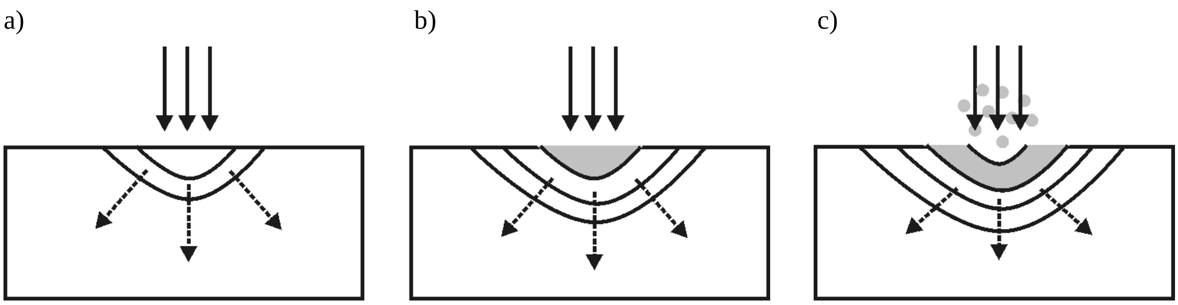

Fig. 5: Phases of interaction of laser and material: a) heating; b) melting; c) vaporization.

Once the vaporization is initiated, the interactions between the resulting vapor and the incident laser beam become important in determining the effect of the laser irradiation on the material. The vapor ionizes and the highly ionized vapor is called plasma. The building of plasma further influences the interaction of the laser beam and the material, because it forms near the evaporating so-called plasma coupling (see Fig. 6) which confines the intensity of the laser beam. The whole process and the details related to the plasma phase are described in [Steen91] or [Dah08].

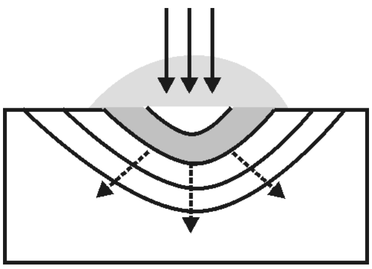

Fig. 6: Material with plasma coupling.

Vaporized particles, which are not affected by the laser beam, move away from the surface of the material, loose their energy and so the vapor becomes significantly cooler and less dense than the vapor in equilibrium with the surface. As mentioned in [Anis68], approximately 18% of the vapor particles condense back to the surface of the material. Moreover, the evolving vapor from the surface exerts a recoil pressure on the surface, which causes a melt expulsion. It is schematically shown in Fig. 7.

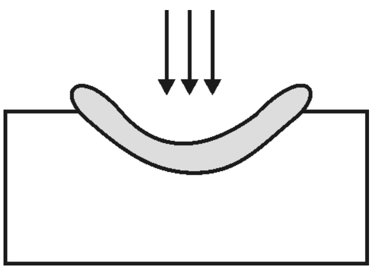

Fig. 7: Schematic representation of melt expulsion process.

The previous description relates to the situation, when laser irradiates engraving continuously and the material is heated during the whole engraving constantly. If we engrave more laser beam pulses, the temperature of the material increases during each laser pulse and this is followed by cooling during the time between the adjacent pulses. Since the cooling is not complete during the short duration between the laser pulses, the initial temperature during heating with the subsequent pulses is always higher than that during heating with preceding pulses. The evolution of temperature of such sample is shown in Fig. 8.

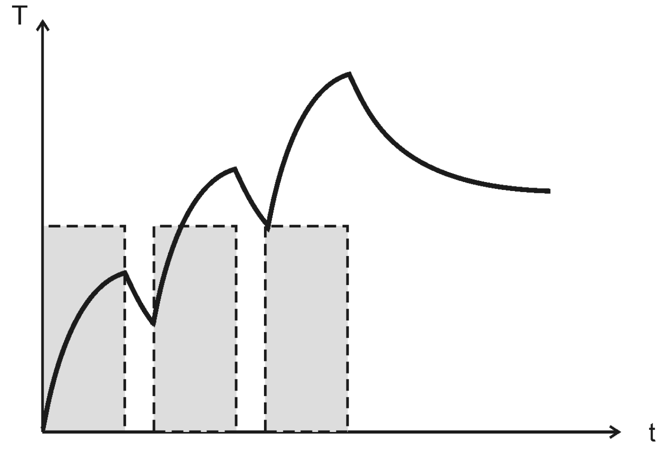

Fig. 8: Schematic evolution of surface temperature during engraving multiple laser beam pulses into the same point.

Another complication of the whole process description would be caused by motion of the laser beam during the engraving process. In this case, each following pulse is engraved partially into a material heated by the preceding laser pulse and partially into a cool material that has not been affected by any laser engraving yet. More details are described in [Dah08].

To sum up, the result of the engraving process depends on the used material, its roughness, parameters of the laser that is used for the engraving process, its angle of incidence according to the material surface and, of course, on number and positioning of pulses engraved into the material and many other facts. For example, [Bulg07] distinguishes a “gentle” and a “strong” ablation and discusses its results on the example of the Al_2O_3.

2.2 Laser-Engraving Simulation

The laser-engraving simulation should be able to create a sample surface according to the description of the experiment that should be engraved and the material and laser qualities. The simulated sample should correspond to the real one engraved into the same material with the same laser settings. This should be proved in the validation and verification process that has to be an inseparable part of the simulation model.

First, the simulation system must be able to form the material surface after engraving one laser pulse or more laser pulses into the same place on the used material surface. An example of a single laser pulse engraved into cermet can be seen from the top view as the gray scale image in Fig. 9a. The lighter is the area in the sample, the higher is the surface in that place.

If we are able to simulate engraving a single laser pulse or pulses engraved into a single point, we can start simulation of laser pulses engraved next to each other with a partial overlap. For this purpose, the description of both pulses interaction will be the most important. An example of pulses engraved into steel during a laser beam motion with the speed 100mm/s and frequency of 50 kHz is shown in Fig. 9b. If we are able to engrave pulses along any trajectory, we can engrave any shape describable by the curve.

a) b)

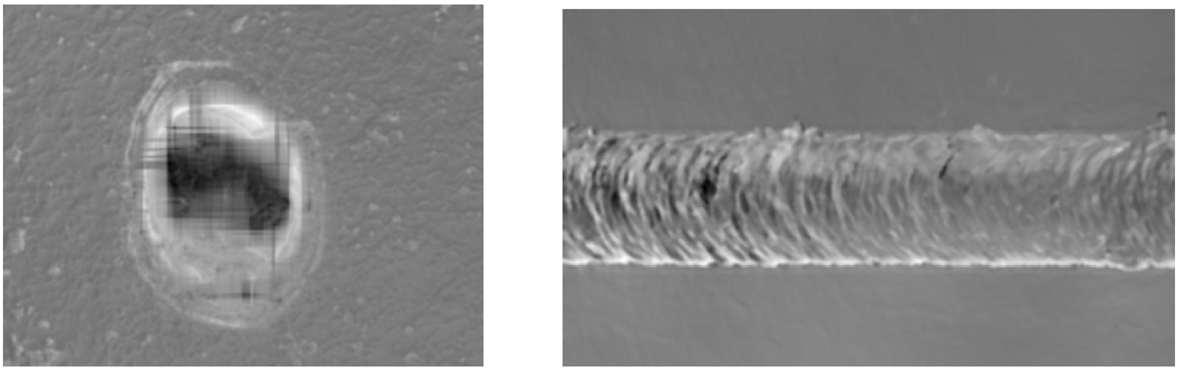

Fig. 9: An example of a) a single laser pulse engraved into cermet; b) pulses engraved into steel during a laser beam motion with the speed 100mm/s and frequency of 50 kHz. Both samples are shown in a top view in the form of a gray scale image.

Moreover, if the laser-engraved pulses are placed next to each other in several rows, we can use this principle for simulation of engraving laser pulses into an area. The height map of several engraved rows is shown in Fig. 10. The areal engraving creates a specific structure on the surface of the material. Because of the light reflecting in the modified parts of the material surface, it makes an impression of changing color. This effect is used in the technological process of laser scribing.

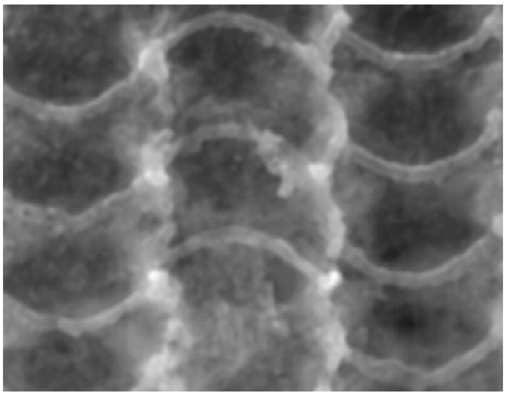

Fig. 10: Pulses placed next to each other in several vertical rows creating the continuous engraved area.

Independently of the pattern we want to engrave, laser simulation should be processed in a very high resolution to catch all the important details. As described in Section 3.2, samples we are working with have the real dimensions of 256×192µm and they are represented by 1024×768 values of the height map. The real sample of these dimensions is hardly visible without microscope. But let’s imagine a sample of the real dimensions of several millimeters or even centimeters, which is quite realistic. The amount of values needed for such sample representing is far higher than it would be possible to process in the real time. So far we are working with comparatively small data, but because the simulation has to be able to process also larger data, either a smaller resolution of the simulation or some algorithm for level of detail height maps processing [Lueb02] should be used.

The simulation of an experiment engraved into a given material surface could be processed individually for each selected setting of the laser and the results could be evaluated manually. This can be time demanding and thus the simulation could test several laser settings and find the optimal result, which could be further engraved into the real material. Such tests can be provided either offline with the possibility of the backward consideration or online on-the-fly.

2.2.1 Simulation Problems

It does not seem to be a very complicated task to simulate the ideal engraving process. But the real situation, that should be simulated, has to take into account various irregularities and inaccuracies of the real materials and measured samples.

All samples are measured in hight resolution and so, inaccuracies are visible on the material. Not only the roughness of the basic unengraved material, but also some local defects, can be found in some samples. These local defects cannot be seen by eye, but they can influence the result of the engraving process. The simulation should run in the same precision. The probability of irregularities can be decreased by polishing the used material, but this cannot be done each time. Unfortunately, it is also not technically possible to measure the material before the engraving and to set the exact point where to engrave. That is why we cannot suppose using an ideal material without any so local defects and the simulation has to manage it.

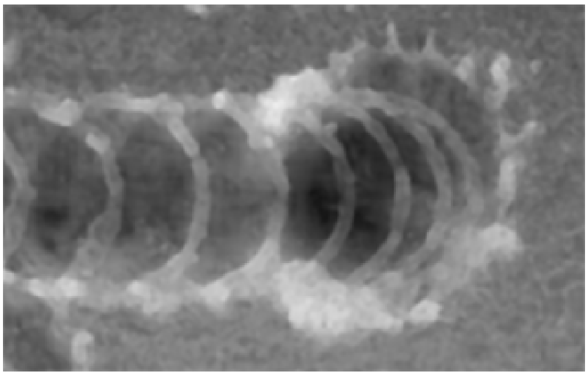

Fig. 11: Inaccuracies caused by starting the laser motion.

There are many other factors which can influence the final result of engraving and so they should be taken into account if we want to create a really perfect and detailed simulation model. For example, the surrounding atmosphere during the engraving process itself belongs among such factors. Engraving could be provided in a protective atmosphere or in presence of air circulation. The circulation of the air can influence the direction of material particles cooling down during the laser engraving. They deposit around the pulse in the area of the transition ring and affect the shape of the pulse, especially the uniformity of the material depositing. Discussion of results engraved in ambient air and in vacuum can be found, for instance, in [Grig07].

Many other problems appear when we start engraving not only into a single point, but along some trajectory. The shape of the trajectory in the real samples is not accurate at the beginning and pulses are also engraved in different distances (the inaccuracies caused by starting the laser motion are shown in Fig. 11).

Because the simulation should reflect the real results as exactly as possible, all these problems should be taken into account.

2.2.2 Reasons for the Simulation

Reasons for simulating the laser engraving process are partly outlined in the introduction of this thesis. The whole laser engraving system should serve for miscellaneous scientific experiments. Results of these experiments are sometimes not fully deterministic and depend a lot on the engraving laser settings. In order to obtain an optimal result, experiments often need to be reoperated several times and various settings of the laser need to be tested to get the best results. Repeated engraving of the same experiment is expensive and time consuming. Moreover, some configurations of the laser device are inappropriate and so these engraving are made unnecessarily. That is why any software tool, which would eliminate the real engraving of incorrect experiments, would be very beneficial.

The simulation should provide experiments as quickly as possible. It should also enable optimization from different points of view (speed, accuracy, etc.) and help to eliminate the unreasonable experiments. All parts of the simulation should be automatic to the maximum extent so that the simulation can run independently of the user. Moreover, in contrast to real engraving, where each experiment requires servicing, simulation creates a possibility of batch-oriented experiments execution. After the simulation finishes and all gained results are described in some output files, the best results can be selected.

2.2.3 Technique of the Simulation

For the simulation, we have to explore the system that should be simulated and to find all important components and interconnections of the process. Also the settings of the system and its influence on the results are important. We also should specify reasons for the simulation and we should decide which simplifications of the real system are possible to perform in order to preserve the required accuracy of the simulation, because we do not want to lose the main features, which we want to obtain from the simulation. On the other hand, if we remove some features which have a little effect on the model accuracy, we can get a simpler simulation model that would be understandable and computable more easily. As described in [Robin04], an important and inseparable part of the simulation process is also data obtaining and description and final simulation model verification and validation.

Because we have not found any simulation interested exactly in the laser-engraving process, we have to use techniques for solving similar problems and than to decide which approach and simulation model to choose. During our decision-making, we also have to consider the possible cooperation with the real equipment for real data engraving and measuring and all the requirements important for the simulation usage.

Generally, we had to decide between two basic ways of simulation. It is possible to simulate the real situation on the basis of analytical methods or to create a simulation model using an application approach. Each approach has its advantages and disadvantages.

Simulation using an analytical approach comes out from the knowledge of physical equations, mathematical descriptions, procedures and dependencies describing the behavior of the material that is being heated by the laser beam. The simulated system has to be analyzed, its behavior should be investigated and all its parts have to be described using mathematical relations and equations, which can be solved.

The analytical approach is often used in practice and it could be a good way how to model thermal processes. Because the material is heated during the laser-engraving process, we could take an inspiration in methods for material heating simulation or other laser application, such as simulation of laser cutting described in [Dowd09]. As shown in [Wool99] or [Rami97], approaches to solve the heat conduction in various shapes of the material can be simulated. Some other problems, such as melting processes of the material can also be described this way (see, for example the Stefan problem [Alex93]).

Of course, the analytical methods can be discretized and results can be computed numerically. Simulation model obtained by this method could be general enough but for the case of concrete equipment it could be difficult to find the right combination of parameters and coefficients to describe it exactly. We believe that also lasers and their impact on the material surface changes during the engraving process could be modeled this way, but finally, we have decided to apply a different approach.

Because we would like to come out from the real engraving process and so to use the real laser engraved and measured data, we have decided to select another way to simulate laser engraving – the application approach. We want to start from real experiments and make use of knowledge of particular lasers and materials characteristics. From the real experiments a number of parameters describing the real results can be computed. These parameters can be further used for the simulation. Of course, neither the application approach can be used without some mathematical background. But the mathematical equations should not be used for the describing the whole process, but only for processing the parameters gained from the real experiments.

Because we use measured real data engraved by a specific type of laser into a given material, we could achieve more accurate results in comparison with the analytical methods mentioned above. The format of used data and the way of data sets acquisition are described in Sections 3.1 and 3.2.

2.3 Data Preprocessing Methods

As described in Section 1.3, we do not solve yet the whole simulation process, because of its breadth. We have decided to focus on the methodology for data preprocessing. To do that, we have to solve the problems of the sample parameterization and description and the problem of the automatic pulse detection first.

Each part of the data preprocessing operation has to be understood well to select the correct approaches and methods to obtain the best results. To increase the transparency of the processed parts, which we were dealing with during our research, we have decided to explain them in detail in the introduction of separate chapters. Each chapter describes a single problem, usable methods and our proposed methods for its solution. The sample parameterization and the artificial generation of the new sample surface according to the computed parameters are described in Sections 3.4 and 3.5. Approaches for the automatic pulse detection are shown in Chapter 5. In data preprocessing, methods for image processing or segmentation are used often. For the artificial generation of samples described by the set of parameters, we use various noise generation functions. All of them are described and referenced in corresponding chapters.

3 Parametric Pulse Description, Pulse Approximation

Because of our cooperation with the physicists, we can get data from the real experiments. The format of used data and the way of data acquisition are described in the following chapters. Our aim is to find a parametric description of samples and especially the area irradiated by the laser beam. These parameters could be further used for generating the sample surface (sample surface simulation) or for the comparison of samples. To parameterize the sample well, we have to explore it in detail first.

3.1 Data Acquisition

To get the data for the simulation input, real samples have to be engraved by an existing laser equipment into a real material and then to be measured. A set of samples is called an experiment. One experiment contains data for one particular laser device and one particular material. It means that for each combination of a laser device configuration and a material, which is used for the simulation, a special experiment has to be prepared. Each experiment consists of samples engraved by the laser into a single point in the material. The number of pulses goes in sequence, e.g. from 1 to 100 (in Fig. 12, each pulse from the sequence is engraved on a separate row).

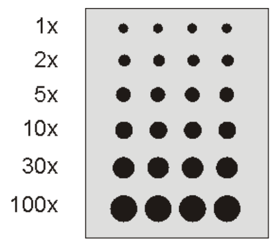

Fig. 12: Experiment layout.

After re-engraving the same pulse several times with keeping the same conditions, the results differ a little, so each pulse count is repeated several times in order to get an average result. These samples are placed side by side in a single row (one row in Fig. 12 corresponds to similar pulses). All data we use and which are shown in the following description was engraved by a laser device BLS-100 (Nd:YAG solid-material, lamp-pumped laser with wavelength of 1064nm) [SHTOnl], [Silf04] into steel and cermet (a composite material consisting of ceramics and materials). The parameters of engraving were as follows: laser power 100W, current 28A, width of the ray 0.01mm, diaphragm 1.8. For steel, we have obtained a complete engraved and measured experiment (sequence of samples with 1, 2, 5, 10, 20, 30 and so on up to 90, 100 laser samples engraved into a single point, each engraved five times) and so our data set is trustworthy. On the other hand, only several samples are available for cermet and acquired data does not represent the material quality sufficiently. An example of a sequence of samples engraved in steel into one point can be seen in Fig. 13. The number of laser pulses increases from 1 to 10.

a) b) c)

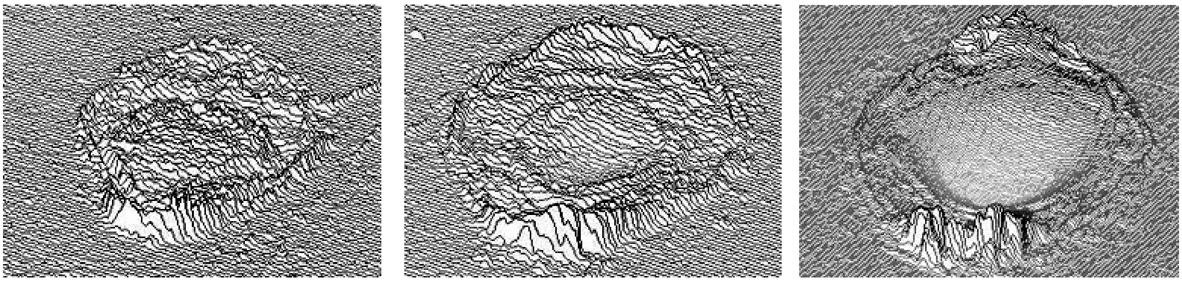

Fig. 13: 3D views on samples engraved with lamp-pumped laser BLS-100 into steal: a) 1; b) 5; c) 10 laser pulses engraved into a single point.

After the samples are engraved, they have to be measured. During the measurement, just a part of the material containing the engraved pulses is focused. A resolution and zoom are chosen, the material sample is scanned and the measured data set is saved. For the output from the confocal microscope, a text file (CSV) is used. The zoom is chosen according to the experience with the particular material. For the measurement, the confocal microscope Olympus LEXT OLS3100 [OlympOnl] was used in our data acquisition process.

Of course, the process of data receiving is costly and time consuming. The size of files with saved data in also not very small (in the case of several tens of measured samples for each material, the size of all measured samples of the experiment reaches several GB). We have to decide how many engravings have to be done to obtain a full-range and representative spectrum of pulses. Of course, we try not to do many unnecessary engravings. For different materials, the experiments can differ.

3.2 Data Description

The CSV file with the sample data description contains several head lines with descriptions of type of measured data, units for all three basic axes of the coordinate system and the step size that was used during the measurement. The head lines are followed by a matrix of real numbers which represents the sample surface. The values express the heights of intersection points in a uniform rectangular grid. This grid represents a height map which describes the surface of the sample. In Fig. 14, the 3D visualization of data from the confocal microscope is shown.

The majority of samples, which we use, have the same size as the sample in Fig. 14. Most of the sample surface is filled by the area that was affected by the laser beam engraving; the real dimensions of the sample are 256×192μm. The grid of the height map is really fine; the most common grid step in used data is 0.25μm. It means that the surface of such sample is described by 1024×768 values.

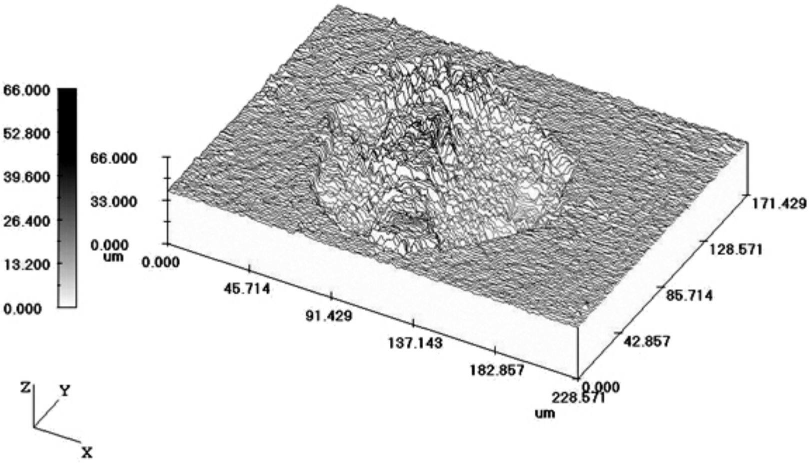

Fig. 14: Height map of a measured sample.

As described in Section 2.1, the shape of the pulse created during the engraving process on the surface of the material is caused by material ablation. If we want to parameterize samples, we have to explore the real samples first in order to see how the basic shape of pulse changes with the increasing number of laser pulses engraved into the material, how the roughness of the used material influences the sample surface or how the sample surface is affected by any other inaccuracies of the material. Let’s describe the sample surface in detail first. The roughness of the original surface depends on the used material. Examples of two different materials can be seen in Fig. 15a,b. The surface of steel (Fig. 15a) is quite smooth with any few local defects, which are irregularly spread across the surface. On the other hand, the roughness of the cermet is high and omnipresent. Moreover, some materials are susceptible to local defects – areas of a high roughness appearing occasionally on the surface. An example of local defects on a steel surface is shown in Fig. 15c.

a) b) c)

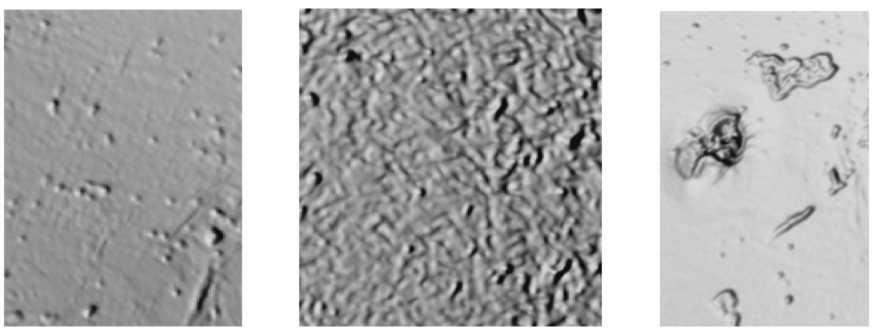

Fig. 15: Original unengraved surfaces of a) steel; b) cermet; c) local defects on the steel surface.

During the burning process, the laser beam affects the sample surface. In the following description, we will call the heat-affected area a pulse. Except for the roughness of the basic material surface, the quality of the material also differs. Thus the size of the pulse and its shape are influenced not only by the number and intensity of laser pulses engraved into the material, but also by the used material.

3.3 Basic Pulse Shape Description

To get information about the pulse shape, we use cross-section curves. A cross-section curve is created as the height relief of a selected row or column of the sample. A cross-section curve can also be generated along any line segment defined be two points of the sample.

We will start with comparing similar samples, i.e., samples with the same number of laser pulses engraved into the same material. Fig. 16 shows cross-section curves of four similar samples of steel with 100 pulses engraved into a single point. Also a rough dimension of the cross-sections is shown. It can be seen that even similar samples differ, but their shape is very similar, especially in the area of the pit. In Fig. 16b, the shape of the pit is damaged by a local defect in the material, but still the correct shape can be guessed well. The surface of the pulse in the pit is quite smooth and only a slight roughness is perceptible at the bottom. On the other hand, the border of the pulse – the transition ring, which is formed by the melted material – is different for each explored case.

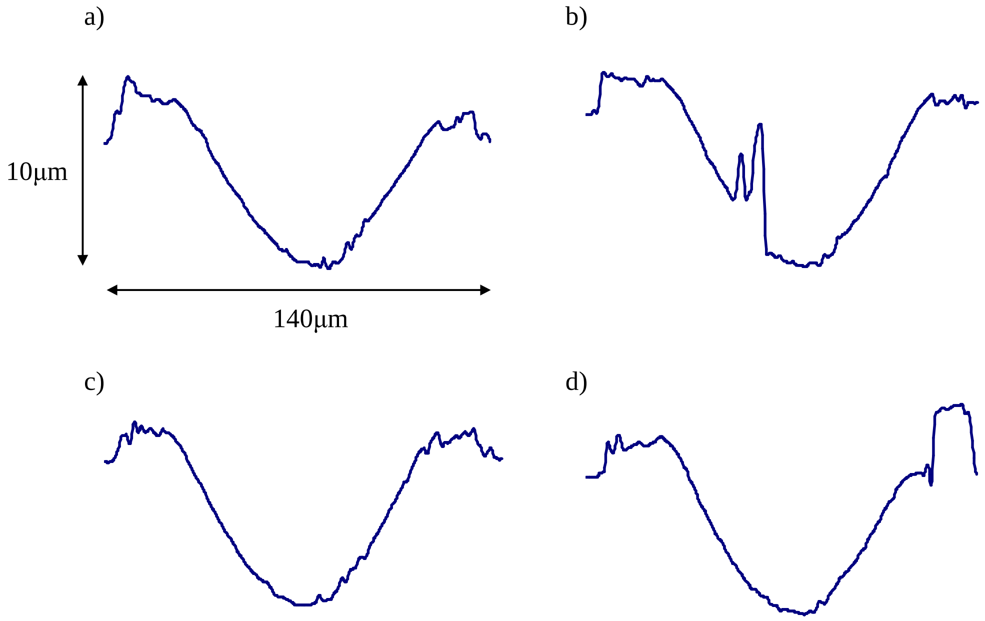

Fig. 16: Vertical cross-section reliefes of four similar samples – 100 laser pulses engraved into steel.

Real pulses are not symmetric and so we cannot use cross-sections measured only in one direction. However, our experiments show that cross-sections measured in two directions, in the broadest and the narrowest width of the pulse, are sufficient. Thanks to the character of pulses, the cross-sections are often orthogonal and correspond to cross-section parallel to *x* and *y* axis. For simplification, let's call them CS_X and CS_Y.

If we want to describe the pulse basic shape by some parameters, we should understand its single parts. In the simplified cross-section relief of the sample, we can detect several important points. Points $A[x_A, y_A]$ and $B[x_B, y_B]$ state the outer border of the pulse pit, $A'[x_{A'}, y_{A'}]$ and $B'[x_{B'}, y_{B'}]$ determine the outer border of the transition ring. Point $S[x_S, y_S]$ gives position of the bottom of the pit. All points are shown in Fig. 17. The symbols will also be used in the following computations.

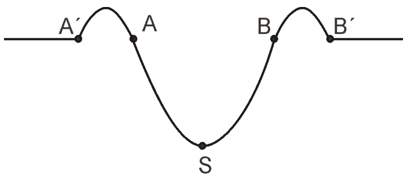

Fig. 17: Important points on the cross-section curve.

3.4 Pulse Basic Shape Approximation

Because both parts of the pulse (i.e., the pit and the ring) differ quite a lot, we have decided to approximate them separately by two different functions and most especially to differentiate the way of surface roughness description. Both generated surfaces are finally connected into the final shape. In following sections, the method for the pulse basic shape approximation is derived from [Rekt81], [Weiss99]. After the explanation of the whole method, the set of parameters for both basic pulse shape parts description is summarized. This topic is described also in [Háj09a].

3.4.1 Pit Approximation

After several experiments, it appears that the basic shape of the pit cross-section corresponds to the shape of the plot of a quadratic function. The cross-section can be approximated by a parabola having the equation shown in expression (3.1). The results of this parabolic approximation of the pulse pit can be seen in Fig. 18.

$$y = \frac{y_A - y_S}{(x_A - x_S)^2} . (x - x_S)^2 + y_S \tag{3.1}$$

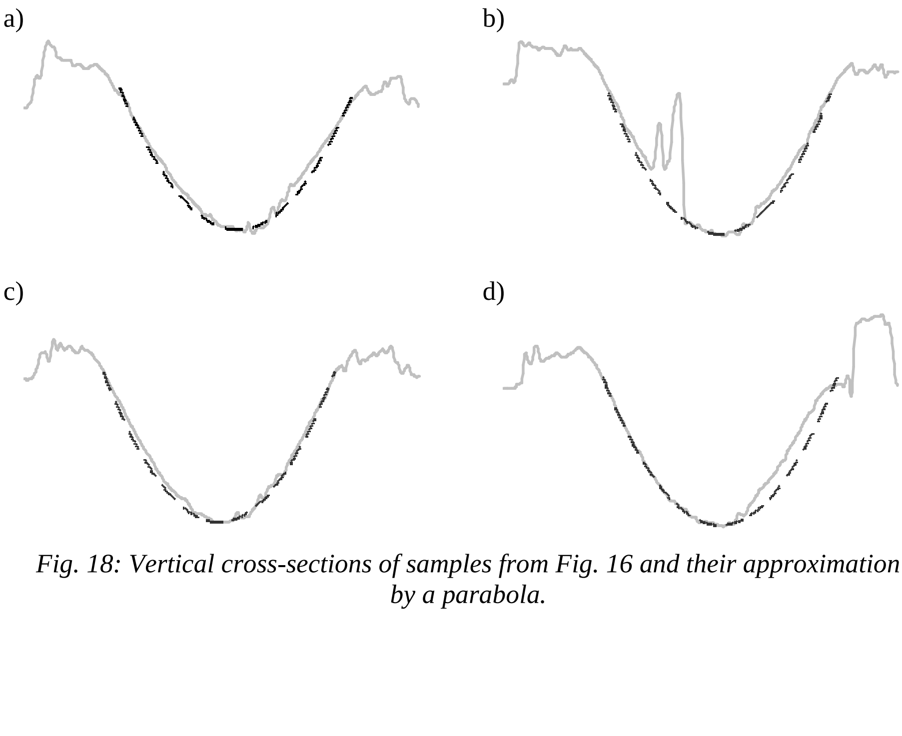

Fig. 18: Vertical cross-sections of samples from Fig. 16 and their approximation by a parabola.

As can be seen in Fig. 19, in the real samples of 10, 50 and 100 laser pulses engraved into steel, the pit has a circular or elliptical shape from the top view.

a) b) c)

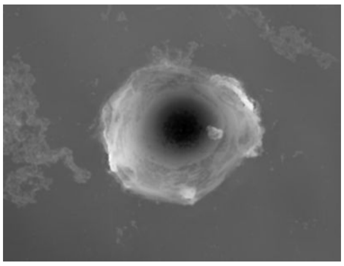

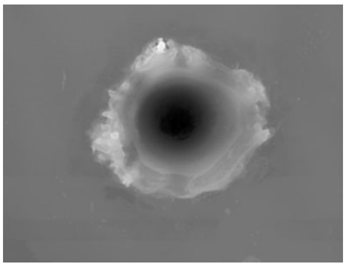

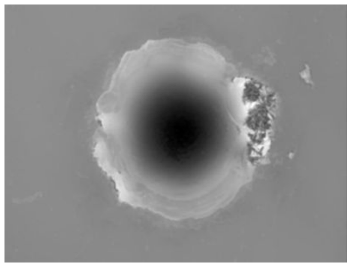

Fig. 19: Samples of 10, 50 and 100 laser pulses engraved into steel from the top view.

If the pulse pit can be approximated by the parabola in its each cross-section going through the center S, the whole pit can be approximated by an elliptical paraboloid. Because we need the paraboloid going through the top border of the pit, the equation representing it has to be modified as in (3.2). The origin of the solid lies in $S[x_0, y_0, z_0]$, h represents the depth of the paraboloid and a, b are axes of the ellipse. The elliptical paraboloid is shown in Fig. 20.

$$z = h * \left(\frac{(x - x_0)^2}{a^2} + \frac{(y - y_0)^2}{b^2} \right) + z_0 \qquad (3.2)$$

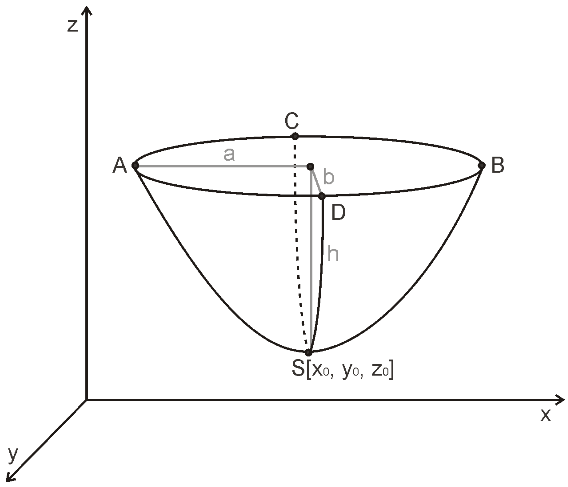

Fig. 20: Elliptical paraboloid and its parameters.

3.4.2 Ring Approximation

The approximation of the pulse transition ring area is much more problematic, because its shape is irregular and rough (as can be seen from samples in Fig. 16). The material surface is created during the engraving process by the expulsed melted and condensing ablated material that forms a ring on the border of the engraved pit. To find the approximating function, we have to simplify the shape and then to find a suitable way of random noise generation to get as realistic results as possible.

First, we have to find a suitable function that could be used for the approximation of the basic shape of the ring cross-section. We have decided once again to use a quadratic function. To find an appropriate parabola, we need several parameters to describe the ring. These are shown in Fig. 21 – the width of the ring and its maximal height and also the level of the basic material. The parabola is defined according to the equation (3.3).

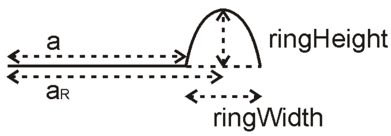

Fig. 21: Important parameters for the description of the ring cross-section.

$$y = \frac{ringHeight}{\left(\frac{ringWidth}{2}\right)^2} * (x - a_R)^2 + ringHeight + materialLevel \tag{3.3}$$

The whole ring should be approximated by a 3D function. It seems to be roughly similar to the top half of a torus. A torus is a surface of revolution generated by revolving a circle in three dimensional space about an axis coplanar with the circle, which does not touch the circle. A torus is shown in Fig. 22. Of course, for our purposes, it has to be modified.

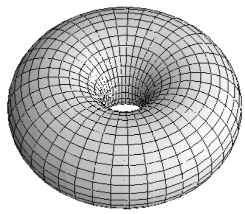

Fig. 22: A torus.

The ring has an elliptical shape from the top view and the shape of a parabola in the cross-section. Moreover, the parabola preserves the difference between the horizontal and vertical ring width. As it is shown in Fig. 23, the ring width should be computed for each direction separately (the value *ringWidth2* determines the half of the ring width). The solid representing the ring should be created as a surface of revolution generated by revolving a parabola along the elliptic trajectory in 3D space. The approximation of the whole ring can be done by the half of the parabolic elliptic torus. The ellipse and its axes are shown in Fig. 23.

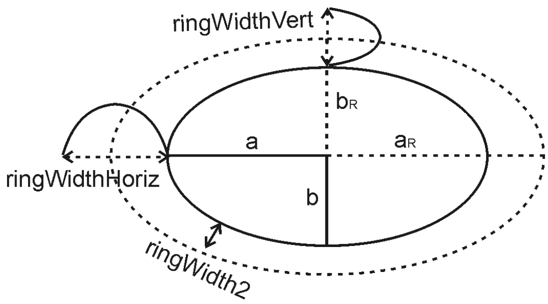

Fig. 23: Description of the ellipse axes

Now we have to describe it mathematically. The ellipse is generally defined as (3.4), where *u* and *v* are the axis of the ellipse.

$$1=\frac{(x-x_0)^2}{u^2}+\frac{(y-y_0)^2}{v^2} \tag{3.4}$$

The maximum of the parabola representing the ring has to be placed on this ellipse. We can define $u^2 = a_R$ and $v^2 = b_R$. For our case, we can use equation (3.5).

$$p=\frac{(x-x_0)^2}{a_R}+\frac{(y-y_0)^2}{b_R} \tag{3.5}$$

The various values of the variable *p* are outlined in Fig. 24. The value $p = 0$ represents the center of the ellipse, $p = 1$ defines the ellipse itself. If *p* varies from 0 to 1, it represents the area bordered by the ellipse and all values $p > 1$ points outside the ellipse.

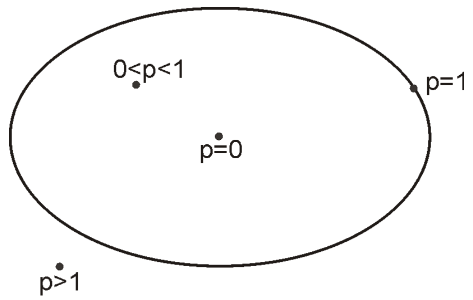

Fig. 24: Variants of values of parameter p *and position of the point in the ellipse.*

Next, we need an expression for computing the distance of two points. More specifically, we need to compute the distance of the processed point from the center $[x_0, y_0]$ during the surface generation. This distance has to be adjusted according to the ellipse and so for the next computation the value d_T will be used. The value computed according to equation (3.6) determines the distance of the parabola maximum from the center of the ellipse in a given direction (as can be seen in Fig. 25).

$$d_T=\frac{\sqrt{(x-x_0)^2+(y-y_0)^2}}{p} \tag{3.6}$$

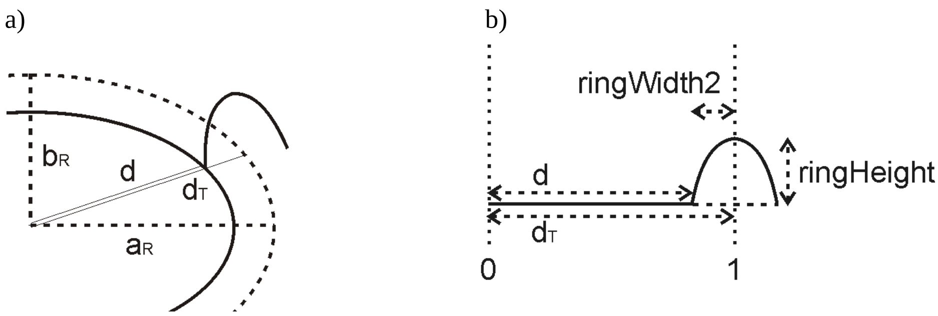

Fig. 25: Description of distances: a) from the top view, b) from the view of the ring cross-section.

To get the right shape of the parabola, we have to compute the parameter *k* that will determine the opening of the parabola (3.7). It depends on the maximal ring height and its width that has to be recalculated by d_T to get the ratio to the ellipse distance.

$$k = \frac{ringHeight}{\left(\frac{ringWidth2}{d_T}\right)^2} \tag{3.7}$$

Now we can substitute into the equation (3.3). Because we compute in recounted distance (in the interval <0, 1>) instead of the value a_R, we have to use the value 1. Finally, the torus is defined as (3.8). The constants *ringHeight* and *materialLevel* are added because of shifting the generated surface into the right height. Otherwise, it would be placed under the zero level.

$$z = -k * (p-1)^2 + ringHeight + materialLevel \tag{3.8}$$

As can be seen, the basic shape of the pulse can be described by a set of parameters. They are summarized in Table I. The names of parameters used in Table I are used also in all descriptions and computations.

pulse parts	**parameters description**	**parameters names**
basic material	height of basic material level	*materialLevel*
pulse pit	position of the pit bottom center	$S[x_0, y_0, z_0]$
	semimajor and semiminor axis of the ellipse	*a*, *b*
	ablation depth – depth of the pit	*h*
transition ring	width of the transition ring in the vertical and horizontal direction	*ringWidthVert*, *ringWidthHoriz*
	average ring height	*ringHeight*

Table I: Parameters for the pulse basic shape description.

If we want to get all parameters, all the important points in the vertical and horizontal cross-sections described in Fig. 17 have to be detected first. The level of basic material can be determined according to methods described in Section 5. The inner diameter of the ring corresponds to the diameter of the pit and the width of the transition ring is computed from the cross-sections. All values are computed in the vertical and horizontal directions. In the previous description also the value *ringWidth* or *ringWidth2=ringWidth/2* is used. The simplest way to get these values is to compute the distance of the inner and outer border of the transition ring from the center of the pulse in the given direction and to compute their difference.

More problematic task is to compute the maximal height of the ring (*ringHeight*), because the surface of real samples is in this area very irregular, so we cannot use only the maximal value from the ring cross-section. But if we discretize the quadratic function, we can compute the average value of the parabola. As can be seen in Fig. 26, where the average value is shown as a dashed line, the result depends on the sampling frequency.

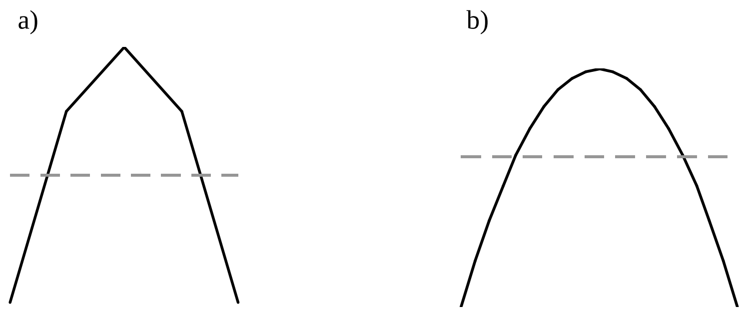

Fig. 26: The position of the average value in the parabola represented by a) 5 values; b) 21 values.

Because we need to compute the average height of the transition ring, we have to use the same frequency that was used previously for the cross-section of the pit. First, we compute the rate of the average value and the difference of the maximal and the minimal value (amplitude) in the discretized parabola and we get the relative position of the average value from the top of the parabola. This value is independent from the height multiplicator a of the parabola in the parabola definition ($f(x) = -ax^2$). That is why we can use the expression (3.9) to compute the amplitude (the height) of the transition ring of the pulse.

$$\frac{functionAverage}{functionAmplitude} = \frac{ringAverage}{ringHeight} \tag{3.9}$$

3.5 Generating Roughness

Real samples are measured in a very high level of detail and during a careful exploration, we can find bumps originating from the irregularity of the material surface. In addition to the roughness of the material, local defects in the material can also be detected here and there. Their size is variable and they are placed completely randomly.

As can be seen in Fig. 60 (see page 47), the mathematically generated sample described in Section 3.4 is too smooth in comparison with the real one. That is why it is necessary to modify the generated surface by some kind of artificial defects that would represent the granularity of the material and the roughness of different parts of a real sample.

When we want to explore samples engraved into steel, we can see that the central part of the pulse (i.e., the area irradiated by the laser beam) is quite smooth and the bottom of the pit is a little bit rougher (Fig. 27a). The most ragged surface part is the transition ring. The border of the ring is modulated by some concentric waves that are both regular and irregular (Fig. 27b). Sometimes, local defects with a considerable roughness can appear, especially at the outer border of the transition ring (Fig. 27c). At the outer border, the roughness declines slowly and fades into the roughness of the bulk material.

All these facts should be taken into account if we want to generate the surface of a pulse from its parameters. Samples engraved into the same material are similar and some characteristics of the engraved sample depend directly on the used material itself. We should design a set of parameters to describe the sample sufficiently. The set of sample parameters and their further usage are described in the following sections.

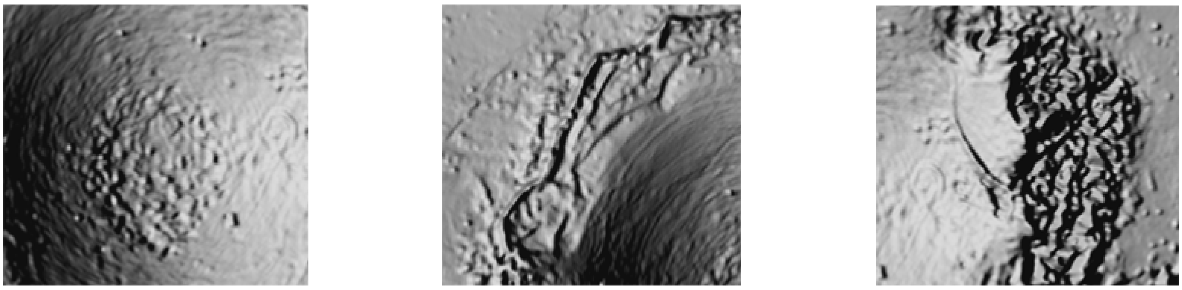

Fig. 27: Typical examples of roughness from different parts of a sample surface.

3.5.1 Perlin Noise Function

During increasing the lifelikeness of generated samples, we need to add global roughness to some parts of the sample. There are several possible solutions, e.g., fractal generation of the sample surface [Polack03], the Perlin noise function [Perlin85], [Perlin02], value-gradient noise, Ward's Hermite noise [Ebert03], etc.

Finally, we have decided to use the Perlin noise function because of its variability. It has a very wide range of application, not only in computer graphics, but also in many other areas where natural appearance is needed. In nature, many things have some fractal structure with various levels of details. Perlin noise is similar to fractals, with the only exception that it does not implement self-similarity. That is why it cannot be classified as a fractal [PerlinOnl]. It is widely used for generating textures in 2D and 3D. First, we will start with the 1D Perlin noise to explain the basics.

Perlin noise combines a noise function with an interpolating function. The noise function is based on a random generator that returns a number according to a parameter. For the same value of parameter, it always returns the same number. Prior to generating the sequence of numbers, we have to choose an amplitude that is defined as the difference between the minimal and maximal generated value. The noise is formed by randomly generated values, the distance of which is given by some frequency. This frequency is defined as 1/wavelength, where the wavelength represents the distance from one generated value to the next one (as can be seen in Fig. 28).

The generated values are interpolated using Hermit interpolation [Žára05] (Equation 3.10) to get a smooth interpolating curve (with given amplitude and frequency). The parameter *t* ranges in the interval <0,1>.

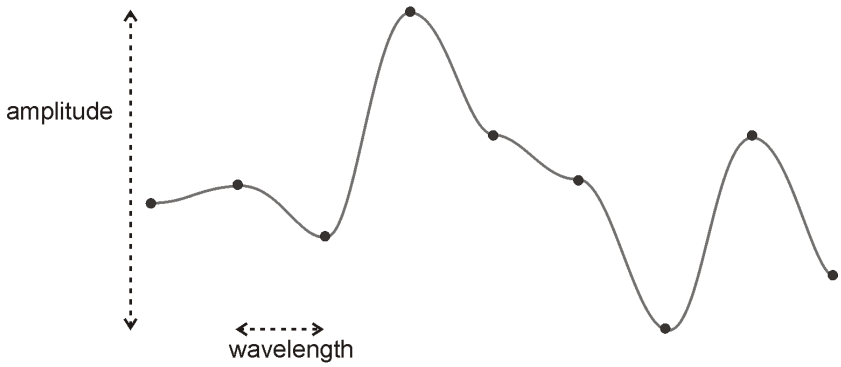

Fig. 28: Visualization of amplitude and wavelength definition.

$$H(t) = t^2(3-2t) \tag{3.10}$$

If we sum up several curves with various frequencies and amplitudes, we get the final Perlin noise function. The selection of frequencies and amplitudes affects the result. For simplification, a quantity value named persistence is used. The frequency and amplitude can be defined as in (Equation 3.11), where *i* represents the separate noise functions that are summed up. These functions are called octaves, because the frequency of each function is twice as the frequency of the previous one. An example of octaves can be seen in Fig. 29. The frequency ranges from 1 to 32, the amplitude is the same for all octaves.

$$frequency = 2^i \tag{3.11a}$$

$$amplitude = persistence^i \tag{3.11b}$$

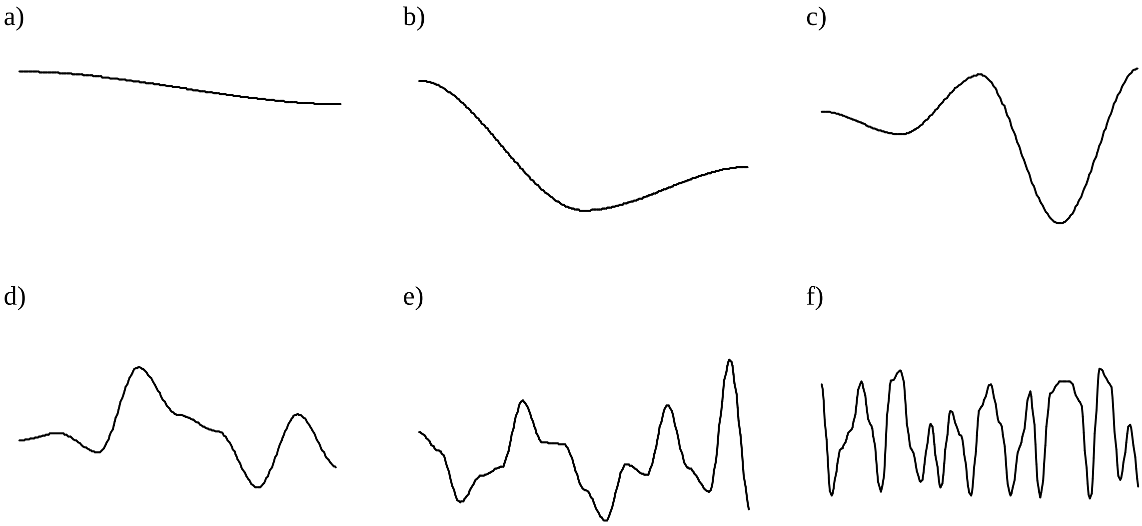

Fig. 29: Octaves that are added to the final 1D Perlin noise with the same amplitude and different frequencies: a) 1; b) 2; c) 4; d) 8; e) 16; f) 32.

The effect of persistence on the output of the final 1D Perlin noise can be seen in Fig. 30. We can use as much octaves as we want to. The upper limit is given by the smallest change that is registrable after adding the octave. Example of Perlin noise with 4, 6 and 8 added octaves can be seen in Fig. 31.

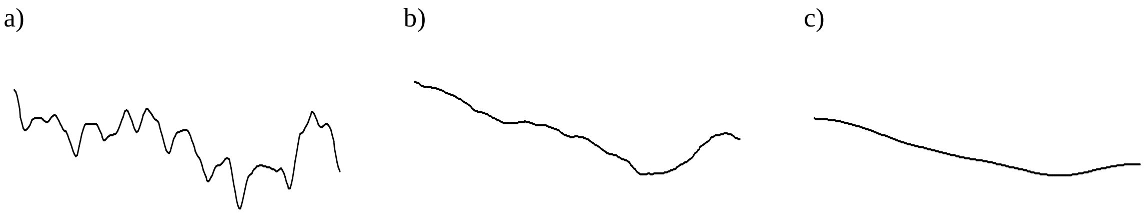

Fig. 30: 1D Perlin noise after summing up 6 noise functions and different persistence: a) 1; b) 0.5; c) 0.25.

a) b) c)

Fig. 31: 1D Perlin noise with persistence=1 and different number of octaves summed up: a) 4; b) 6; c) 8.

For the modification of the generated smooth material surface, we need a 2D Perlin noise function. To extend the noise generation into the second dimension, we have to use two-dimensional interpolation. Also in this case, Hermit interpolation (Equation 3.10) is used. At the beginning, points with the given frequency are randomized and the other points are interpolated as shown in Fig. 32. First, parameter u is used (in the Hermit interpolation $t = u$) and the points x_A and x_B are computed. From them, the resulting point in the Hermit interpolation ($t = v$) arises.

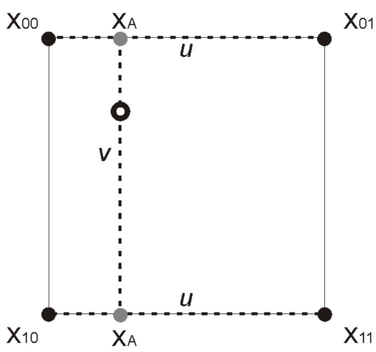

Fig. 32: Procedure of interpolation in 2D.

The results of 2D Perlin noise are shown in Fig. 33. The higher persistence is used, the rougher the generated surface is. To get a better imagination of roughness, the cross-section curves of all samples are also shown. These cross-sections were taken from the middle of the sample. The same persistence and the different number of octaves summed up were used for generation of the samples in Fig. 34.

a) b) c)

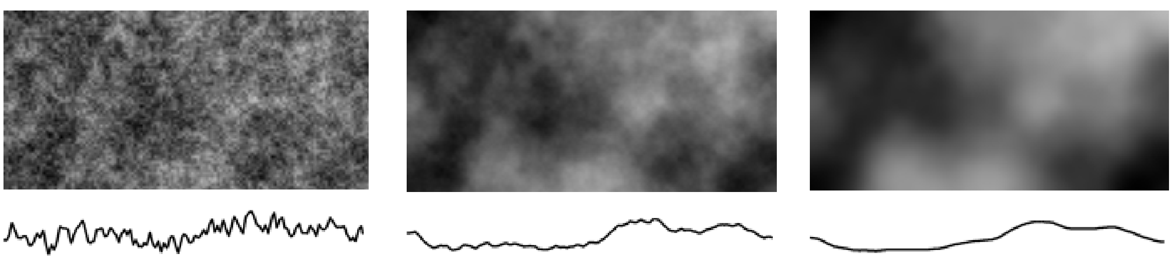

Fig. 33: 2D Perlin noise after summing up 6 noise functions and different persistence: a) 1; b) 0.5; c) 0.25.

So far, we were considering only octaves with amplitudes determined by (Equation 3.11). The result is that the octaves with a lower frequency influence the final Perlin noise more than the octaves with a higher frequency, which affects only the roughness of the resulting sample. We can also choose a little bit different approach and determine the amplitude for each octave separately, e.g. in the form of an amplitude vector. This way, we will be able to better control the shape of the final surface. The calculation of the frequency remains the same; the expression (3.11a) is used. The results of several experiments of this kind can be seen in Fig. 35. Each time, 6 octaves were summed up, but a different amplitude vector was used for each sample. For all the examples, the same starting values as before were used, only amplitudes were changed according to the amplitude vectors.

a) b) c)

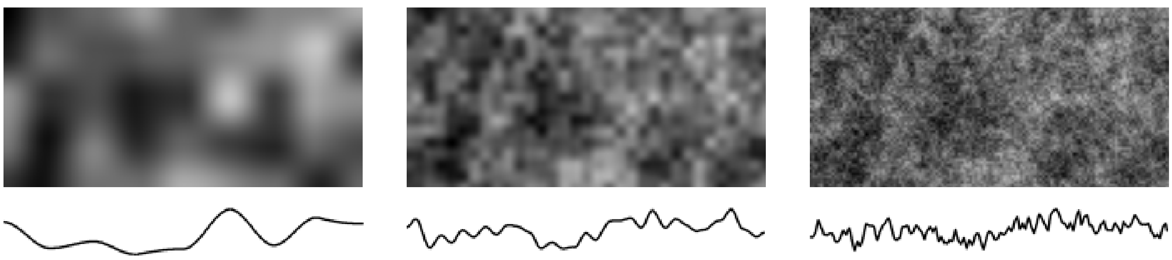

Fig. 34: 2D Perlin noise with persistence=1 and different number of octaves summed up: a) 2; b) 4; c) 6.

a) b) c)

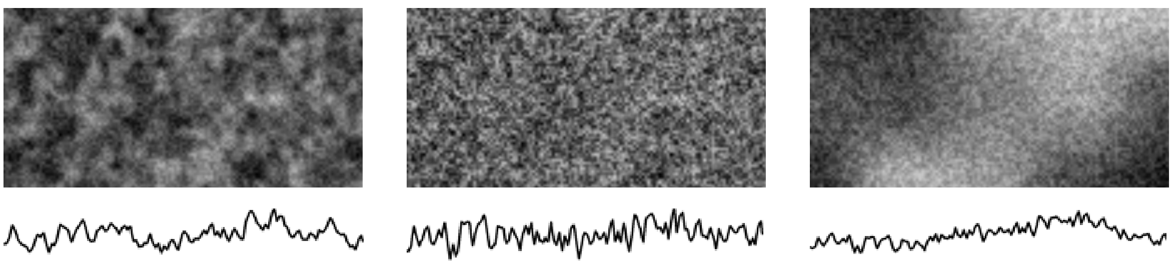

Fig. 35: 2D Perlin noises generated according to amplitude vectors: a) [0.25, 0.25, 1, 1, 0.5, 0.5]; b) [0.5, 0.5, 1, 1, 3, 3]; c) [2, 0, 0, 0, 0.5, 0.5].

It is evident that the variability of the Perlin noise function is high and so we can use it for generating the surface roughness to get realistically appearing samples. The result can be also modified by any other function, such as a quadratic one. In Fig. 36a, an example of surface generated by the Perlin noise with the amplitude vector [1, 1, 1, 4, 1, 3, 2, 2] can be seen in a 3D view. Fig. 36b shows a surface generated according to the same noise vector, where a quadrate of the final Perlin noise was used.

3.5.2 Usage of Perlin Noise Function

Perlin noise can be used several times during the process of pulse generation. The result depends on parameters which we use. Before using the Perlin noise function, we should normalize the parameters to get the amplitudes corresponding to the heights of the original surface. It means that the value of the Perlin noise function are not in the interval <0, max>, but they are in the interval <-max/2, max/2>.

a) b)

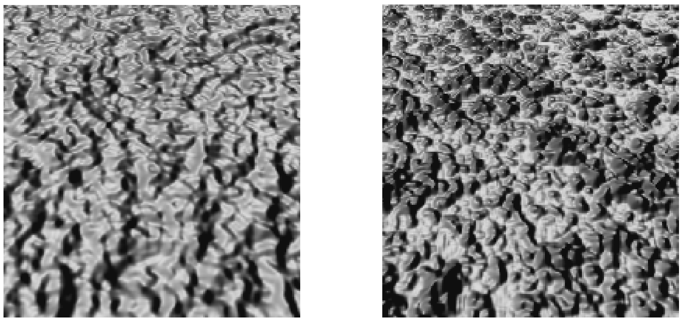

Fig. 36: a) 2D Perlin noise generated as heights of the surface; b) quadrate of the Perlin noise shown in a).

The first problem, where the Perlin noise can be used to solve it, is the generation of the roughness of the pit bottom. The roughness is generated according to a noise amplitude vector. A real sample (100 laser pulses engraved into steel) is shown in Fig. 37a, an example of the Perlin noise modulated surface of the ideal pit can be seen in Fig. 37b.

a) b)

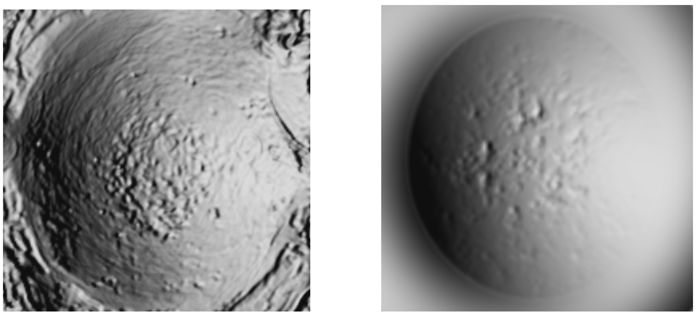

Fig. 37: a) The pit of a real sample; b) Perlin noise modulated on the surface of the ideal pit.

Another area where the usage of the Perlin noise is appropriate is generating the transition ring, or to be more precise, some local defects on it. To get a better imagination how the generated surface looks like in comparison to the real one, see Fig. 38. A 3D view on local defects in two real samples is shown in Fig. 38a,b. The surface generated by the Perlin noise can be seen in Fig. 38c.

For the sample generation, we need to form several smaller areas representing the local defects. For this purpose, we can also use the Perlin noise. At the beginning, we generate a mask of the transition ring (see Fig. 39a). The area of the ring is represented by the value of 1, the borders of the ring are a linear interpolation between the values of 0 and 1. Then, we generate another mask representing the basic shape of the thresholded Perlin noise. If we use only one threshold, the borders are too sharp, so we have decided to use two thresholds. The values of the Perlin noise greater than the first threshold are included fully, the values between both thresholds are included only from one half. In Fig. 39b, an example with thresholds 0.3 for the full value and 0.1 for the half value is shown. If we make an intersection of both masks, we get the result mask shown in Fig. 39c. This result mask serves for the modulation of the Perlin noise described above. The result of local defects final generation on the transition ring can be seen in Fig. 40.

a) b) c)

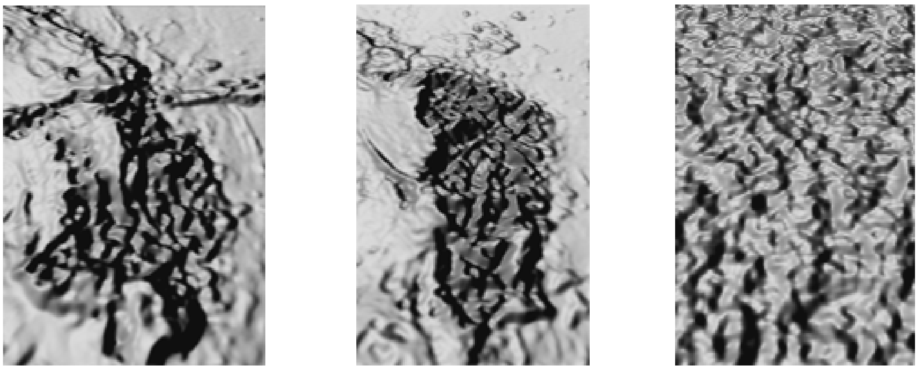

Fig. 38: a, b) Local defects in two different samples; c) surface generated by the Perlin noise.

a) b) c)

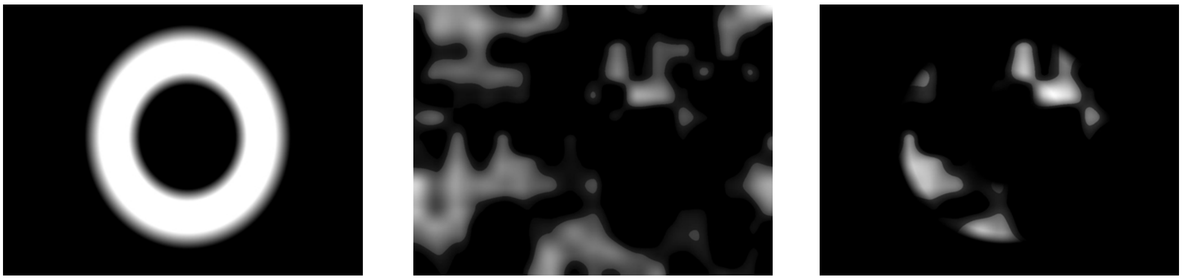

Fig. 39: a) Mask of the transition ring; b) mask of the local defect areas; c) intersection of both previous masks.

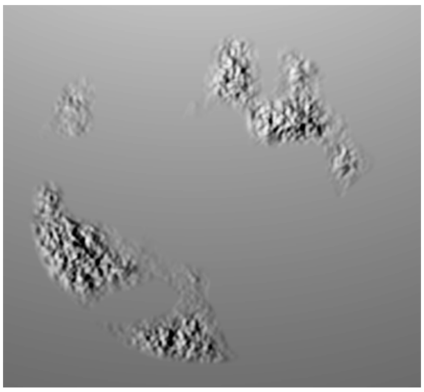

Fig. 40: Final result after the generation of local defects.

3.5.3 Waves Modulation

In the real samples, irregular concentric waves are visible in the area of the transition ring (as shown in Fig. 41b). These waves are especially noticeable on the outer border of the ring and they are relatively thin and sometimes even discontinuous. Their shape consists of a number of edges which approximately form an elliptical shape.

If we want to generate a wave, we have to know several parameters for its description – its shape and dimension. We have decided to represent each wave as a polyline with the given width and height, where the coordinates of vertices representing the polyline define the basic shape and size of the wave.

a) b)

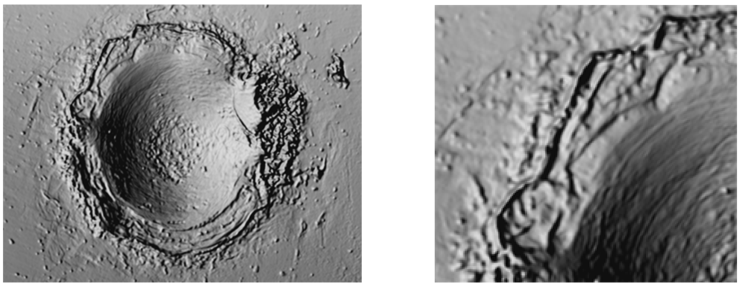

Fig. 41: 3D visualization of the sample with 100 laser pulses engraved into the steel: a) the whole sample; b) zoomed top-left part.

The diameter of the wave depends on the diameter of the transition ring. Because the wave should have an elliptical shape, the positions of vertices depend on the semimajor and semiminor axis of the transition ring. To preserve the irregularity of the wave shape, each vertex is randomly shifted from its original position to create the irregular shape of the final wave. The number of vertices determines the segmentation of the wave. If the continuous wave should be generated, the polyline is represented by all generated vertices, in the case of discontinuous wave the position of the wave segment beginning is selected and a number of points which should create the basic shape of the wave is reduced.

If the polyline vertices are generated (Fig. 43a), we have to compute the 3D shape of the wave, i.e. a height map representing the wave surface. Each couple of neighboring wave points forms a line segment. All line segments are converted to an arc plane during the wave generation. As shown in Fig. 42, for all points C from the surroundings of the line segment AB, the perpendicular distance to the line segment is computed. If the distance from the point to the line segment is smaller than width of the wave, the height of the surface in that given point is computed. The other points are ignored and the surface height in their position remains unchanged.

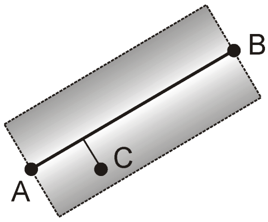

Fig. 42: The way of generation the line segment surroundings.

After this step, the wave surface is formed by several discontinuous segments (Fig. 43b). To connect the segments together, we have to compute the surroundings of the points using the same algorithm as in the case of line segments (Fig. 43c). The final result of the generated wave is shown in Fig. 43d.

In the real samples, more than one wave can often be recognized. Sometimes, they even overlap each other. The heights and widths of the waves differ less. Examples of 20 and 30 waves modulated on the smooth sample surface can be seen in Fig. 44.

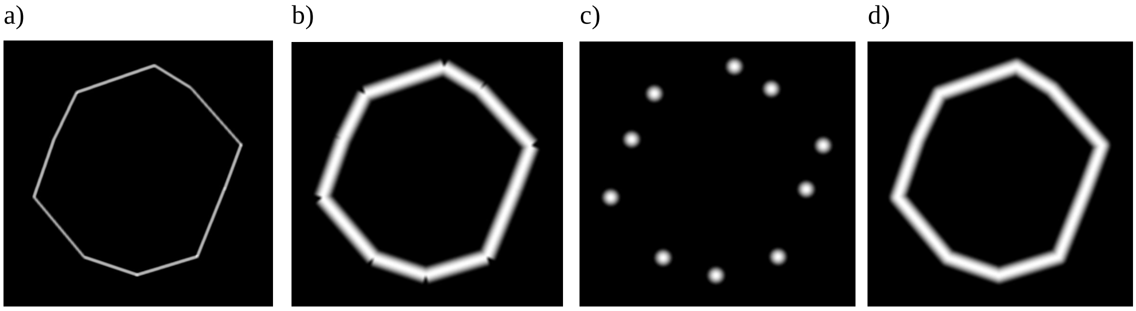

Fig. 43: a) Generated polyline; b) heights generated in the surrounding of the line segments; c) heights generated in the surrounding of the wave points; d) final surface of the generated wave surface.

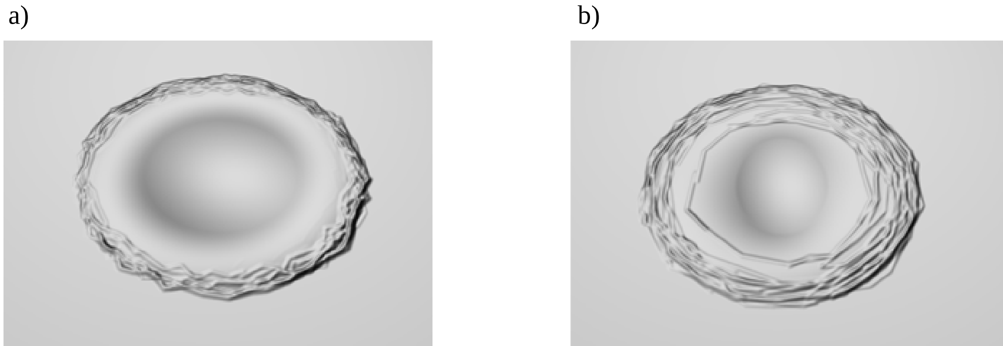

Fig. 44: Examples of a) 20 and b) 30 waves modulated on the smooth sample surface.

In some cases, the surface of the real sample (especially the outer border of the transition ring) has the irregular shape of the wave, but the profile of the wave cannot be detected, because in its inner border it turns smoothly to the surface of the ring (as shown in Fig. 45). That is why not only profile of the wave, but also the filled area in the shape of the wave, should be sometimes used for the surface modulation.

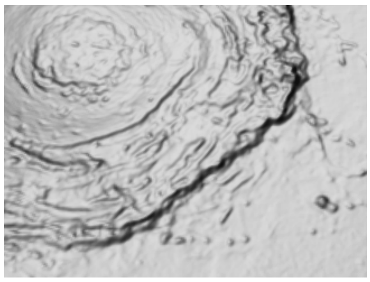

Fig. 45: Part of a sample, on the outer border of the transition ring a full wave border is visible.

To compute the full wave, we have to return to its polyline representation. For the filled wave computation, only continuous waves are used, and so each polyline creates a polygonal shape. The polygon can be divided into a set of triangles (as outlined in Fig. 46). If we want to compute the surface of the polygonal full wave effectively, we can find points in the neighborhood of each triangle and test which points lie inside the triangle. In dependence on the distance of the point P laying in the triangle from the wave center S_W, the actual height of the wave surface is computed.

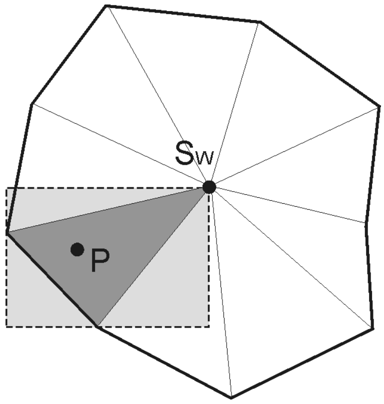

Fig. 46: Full wave divided into the set of triangles. Dashed rectangle indicates the neighborhood of selected triangle.

The height of the wave is biggest exactly at the polyline representing the wave. From the maximum, it is linearly decreasing in the direction to the wave center. Profile of the full wave with the center S_W is shown in Fig. 47a. The computed heights are shown in Fig. 47b as the gray scale shading of the triangle.

a) b)

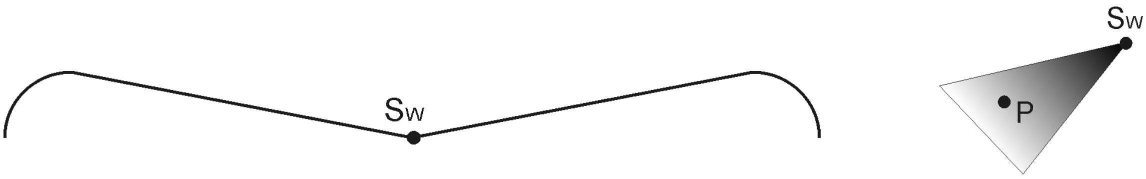

Fig. 47: a) Profile of the full wave. b) Heights generated for one triangle represented as a gray scale shading.

The full wave computed according to the previous description and modulated on the smooth mathematically generated basic shape of the sample is shown in Fig. 48.

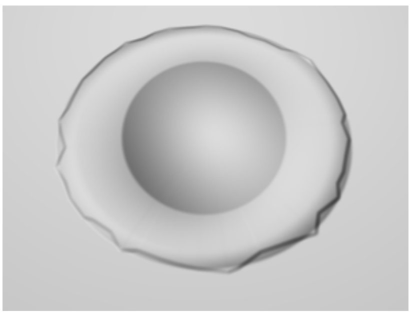

Fig. 48: Full wave generated according to the described algorithm.

3.5.4 Distortion

Another surface modulation that could be used is distortion. It can be used for both for the deformation of the basic smooth shape and for the distortion of waves or masks used for the noise generation. Usage of the distortion can improve the realisticity of the shape.

The simplest form of distortion is computed according to a line. The line is determined by two points and this kind of distortion changes the shape of the distorted object in the direction orthogonal to the line. An example can be seen in Fig. 49. The original image (Fig. 49a) is distorted by the vertical distortion according to two different lines (Fig. 49b,c).

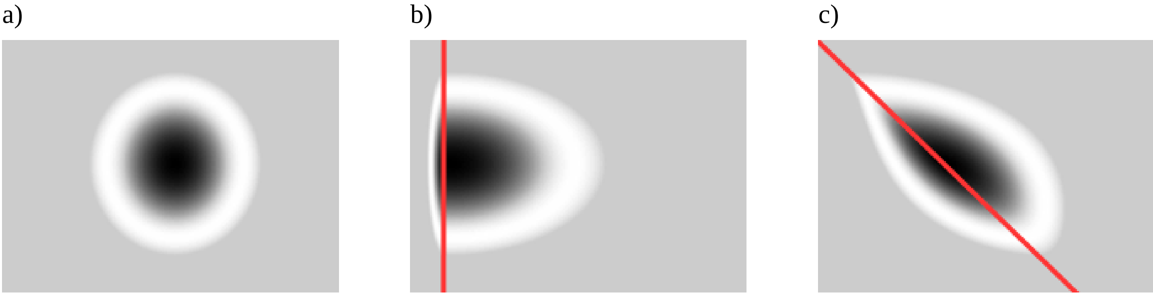

Fig. 49: a) The original image; b-c) images after the vertical distortion according to a line.

We can distinguish vertical and horizontal distortion. It depends on the direction of the basic line we use. The computation is not very complicated and it will be explained on the case of vertical distortion. During the distortion, the original image (Fig. 50a) is transformed into the new one (Fig. 50b). For the transformation we have to set the basic direction and the distortion line which determines the final distortion.

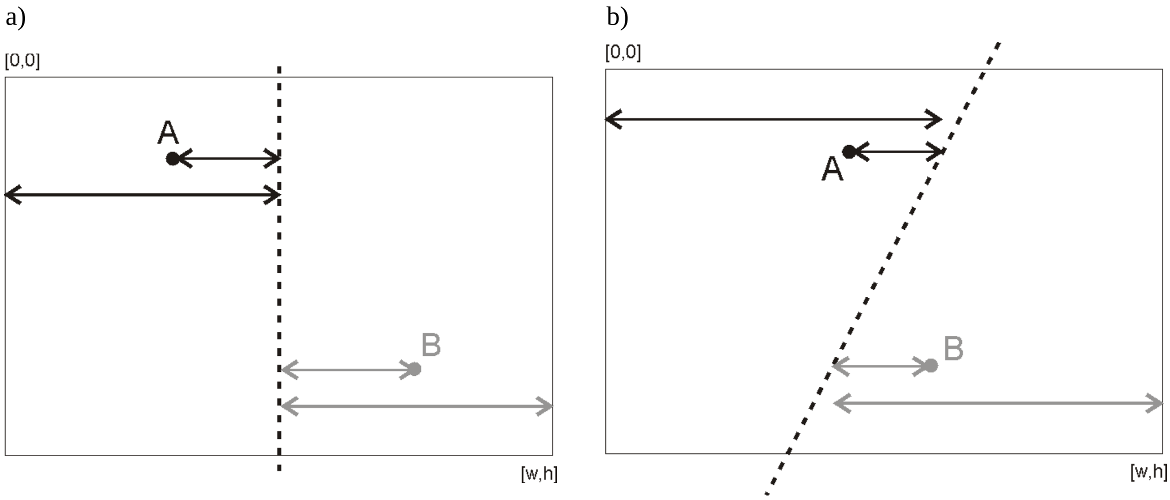

Fig. 50: a) Position of two points in the original image, the basic line of the vertical direction is shown; b) position of both pixels after the vertical distortion to the dashed line.

According to the distance of the distorted point from the basic line in a given row, the original point is shifted either to the left or to the right. During the computation, a new image is created and, for each pixel of the new image, the most fitting pixel in the same row from the source image is searched. If the result is computed between two points, their average is used. For the calculation we have to distinguish points on the left from the distortion line (in Fig. 50 point A) from the pixels placed on the right (in Fig. 50 point B). For the first case the relation (3.12) is valid and for the computation of the corresponding pixel we use the equation (3.13).

$$\frac{xOrig}{xLineOrig} = \frac{x}{xLine} \tag{3.12}$$

$$xOrig = \frac{x(xLineOrig)}{xLine} \tag{3.13}$$

For the computation of the other pixels, the relation (3.14) is applicable and so equation (3.15) is used.

$$\frac{xOrig - xLineOrig}{w - xLineOrig} = \frac{x - xLine}{w - xLine} \tag{3.14}$$

$$xOrig = \frac{(x - xLine)(w - xLineOrig)}{w - xLine} + xLineOrig \tag{3.15}$$

The horizontal distortion works analogously, only the horizontal basic line is used and instead of the width of the image, its height is included. Vertical and horizontal distortion can be used independently or they can be combined. Fig. 51a, b show the simple vertical and horizontal distortion to the line which is highlighted in the images.

a) b)

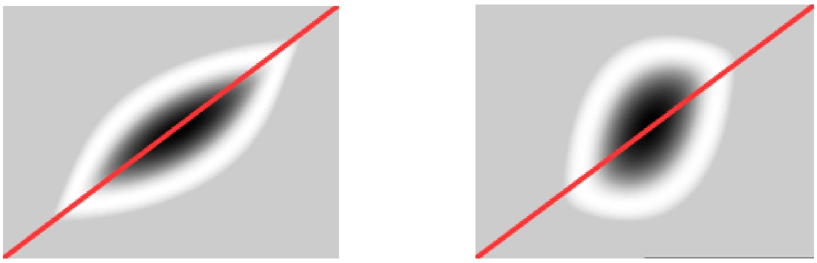

Fig. 51: a) Vertical distortion to the line; b) horizontal distortion to the line.

Of course, the potential usage of any global distortion (not only vertical or horizontal one) could be discussed. But because the actual tests are looking promisingly, we have postponed it so far to the future plans.

The distortion shifts all points of the processed sample in vertical or horizontal direction nearer to the distortion line. If the distortion is used on the basic shape of the pulse, the center of the pulse pit is shifted. An example is shown in Fig. 52. The original smooth pulse basic shape is shown in Fig. 52a, the same shape after the vertical distortion to the solid line can be seen in Fig. 52b. In both images, the center of the sample is highlighted by a solid line. If we want to keep the position of the pulse center, we have to recompute position of the smooth surface and shift it in the opposite direction than the distortion modified it.

3.5.5 Basic Sample Surface

The inseparable part of the sample is the surface of the basic material. As it was mentioned in the previous sections, the real samples are measured in a very high detail. The size of the irregularities depends on the used material. The roughness of the material affects the surface of the final sample and that is why we cannot ignore it. To get the most realistic results we have decided to use several samples of real material measured surface and to use them as a basic material for the pulse generation.

a) b)

Fig. 52: An example of the smooth surface of the pulse basic shape: a) the original one; b) the original shape after the vertical distortion.

3.5.6 Roughness Parameterization

Several methods for increasing the lifelikeness of the generated sample were described. To use them, we have to get any parameters to know, where to use them and how intensively should they modify the sample surface.

Some parameters depend on the quality of the used material; they can be detected for the material itself and then used for all samples engraved into the same material. The other parameters depend on the number of laser beam pulses, which had to be engraved into the material to create the real sample. Moreover, it would be possible to find any dependence of some parameters on the number of engraved pulses and then, the value of unengraved samples could be computed according to any relation. In Table II, parameters, which we have defined and which are used for the roughness generation, are summarized. The topic of roughness parameterization is described also in [Háj09b].

pulse parts	**parameters description**	
pulse pit	roughness of the pit bottom	
pulse transition ring	waves description	waves count
		diameter
		segmentation
		maximal height
		wave width
		plain wave × full wave
	parameters for local defects	local defects density
		roughness of local defects
pulse shape distortion	points specifying the distortion line	
	type of distortion – distortion of the whole shape × distortion of some parts of the pulse (waves, masks, etc.)	
	direction of the distortion – horizontal × vertical distortion	

Table II: Parameters for the pulse roughness description.

As mentioned in the previous section, the roughness of the basic material is not generated artificially. The material surface is loaded from randomly selected real measured material surface of the used material.

The roughness of individual parts of the generated sample (e.g., pit bottom or local defect roughness) is generated by the Perlin noise function. As parameters for this function mostly amplitude vertices (described in Section 3.5.1) are used. Because also the local defect density is described by the Perlin noise function, its amplitude vector has to be determined. Majority of these qualities seems to be dependent on the material itself more than on the number of laser pulses engraved into the material.

Dimensions of waves that modulate the transition ring area are computed according to the dimension of the outer border of the real sample. Our experiments show best results when the axes representing the main shape of the wave are computed in dependence on the diameter of the transition ring with adding a random component. The first wave has the maximal possible size and each following wave is also a little bit smaller. The heights and widths for each wave can be also computed randomly from a small interval. The intervals for the height and width, segmentation, number of waves and their type (if the plain or the full wave should be used) are at this time set experimentally. All parameters describing the concentric waves change with the number of laser pulses engraved into the material. It can be seen also in the sample approximation results in Fig. 60.

The distortion process can be used for the modification of shape of the whole pulse, or only some parts of the roughness generation can be changed (for example, the waves, masks for the roughness generation, etc.). It also has to be decided if the vertical or horizontal distortion should be used and, finally, the points of the distortion line have to be determined. For the basic shape distortion, these points could be possibly guessed from the irregularity of the real sample, but it is also not trivial. The distortion direction, type and points definition are, similarly to the other parameters for description of sample roughness, also set according to our experiments.

Of course, we would like to improve the system and extend its capabilities for the automatic detection of all possible parameters, so that the real samples could be processed, parameterized and generated automatically. Some of our plans are described as a part of Chapter 10.

4 Pulse Parameterization and Approximation Results

If we are able to form all described features, we can put them together and create the new complete artificially generated sample. First, from the set of parameters the basic smooth shape of the new sample is computed, then other features are generated – waves, noises etc.

For the simpler combining all parts together into the result pulse, we have decided to use various masks. An example of using the mask is described in Section 3.5.2 for the local defects generation. Each important part of the pulse is described by a mask (a pit, a transition ring, a distribution of local defects, etc.) and used in the sample finalization. Some masks contains only two values (0 and 1). The value 1 determines places which are taken into account during the result computation, the other points marked with 0 are ignored. The majority of masks contain values from the interval <0, 1>. Values in the mask express the proportions with those the masked feature is included into the result. All masks should be generated during the computation of the basic shape.

4.1 Evaluation of Real Samples

As a part of the parameterization process, we have to explore the real samples carefully. As written in Section 3.1, the same number of laser pulses engraved into the same material several times under the same conditions does not give the same results. That is why each pulse count engraving is repeated several times. First, we need to know how much the similar samples differ. To show concrete numbers, were summarized the basic parameters computed for five similar samples with 50 and 100 laser pulses engraved into steel in Table III and Table IV. Moreover, the average values and the mean relative error for each single parameter were computed.

Measured values representing the area of the pulse pit of both explored cases do not differ a lot. The mean relative errors computed for the semimajor and semiminor axes of the ellipse and the ablation depth of the pulse for both examined cases oscillates between 4 and 8%. It can be seen that average values could be used for description of the pulse pit of similar samples.

On the other hand, description of the transition ring is really difficult. The roughness of material is high. There are more reasons for this. The first one is the irregularity of the basic shape of the pulse, concretely the shape of the transition ring. As can be seen in Fig. 53, the irregularity of some pulses can be very appreciable. The second problem is the problematic detection of outer borders of the pulse transition ring, especially if they are detected automatically (for more information about the automatic detection, see Chapter 5).

real sample	***a***	***b***	***pit depth***	***ring height***	***ring horizontal width***	***ring vertical width***
A	144.50	129.50	6.46	2.17	116.00	100.00
B	142.50	131.50	6.24	2.22	234.50	125.00
C	138.00	130.50	5.91	4.17	114.00	104.00
D	131.00	115.50	5.35	3.19	121.50	109.00
E	124.00	123.00	7.06	3.19	120.50	111.00
average	136.00	126.00	6.20	2.99	141.30	109.80
MRE	5%	4%	7%	21%	26%	6%

Table III: Basic parameters of five similar samples (50 laser pulses engraved into the single point into steel) [μm].

real sample	***a***	***b***	***pit depth***	***ring height***	***ring horizontal width***	***ring vertical width***
A	155,00	170,50	8,71	2,72	112,00	85,00
B	153,50	174,00	9,89	1,96	122,00	75,00
C	160,00	178,00	8,83	1,87	106,50	93,00
D	192,50	152,00	8,42	1,82	67,50	144,00
E	177,00	177,50	9,42	3,45	89,50	106,00
average	167,60	170,40	9,05	2,36	99,50	100,60
MRE	8%	4%	5%	24%	17%	19%

Table IV: Basic parameters of five similar samples (100 laser pulses engraved into the single point into steel) [μm].

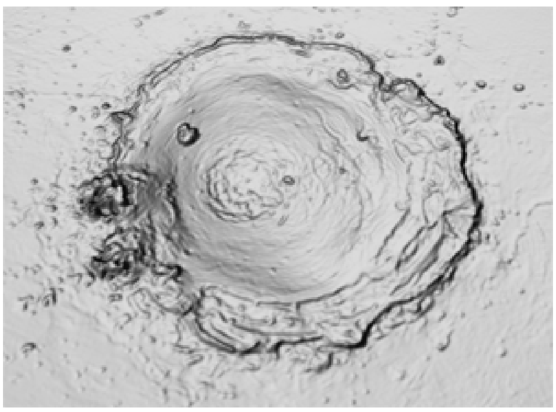

Fig. 53: A sample with an irregular shape of the transition ring.

Although the similar samples differ, we can use some parameters to describe the basic shape of the heat affected area. The average values can serve for the basic shape generation of the pulse pit and the transition ring that is further modified to get a more realistic shape. Our second aim is to get the information if there is any dependence between the number of laser pulses engraved into the material and the shape of the sample. The knowledge of any computable dependence could be used for getting parameters also for unmeasured samples. We can have a look at the real values again. The computed parameters for the set of samples with 10, 20, 30 and so on up to 100 laser pulses engraved into steel are shown in Table V. In the table, average values are used. To get better imagination about the trend of the measured values, they are compared in three separate plots.

	a	***b***	***pit depth***	***ring height***	***ring horizontal width***	***ring vertical width***
10	85.38	82.50	3.45	2.30	198.25	171.00
20	79.00	93.40	3.36	2.41	235.10	175.60
30	88.30	86.10	3.27	2.06	244.40	209.60
40	100.50	99.83	3.86	2.50	177.83	149.67
50	130.40	119.00	5.43	3.20	116.00	134.00
60	126.20	135.20	6.28	2.75	132.60	103.00
70	148.13	144.13	8.59	2.81	147.25	92.25
80	159.00	149.40	8.50	1.79	119.50	87.40
90	162.70	163.80	7.49	2.23	95.90	85.00
100	166.80	165.00	9.13	2.37	99.20	88.80

Table V: Basic parameters of the set of samples [μm].

Fig. 54 shows dependence of semimajor and semiminor axes of the ellipse representing inner border of the pulse pit. This trend seems to be predictable and single values differ from the potential approximation curve that could be computed just a little. The more laser pulses engraved into a single place of the material, the larger pit is created in the material surface. The measured values have an approximately logarithmic progress.

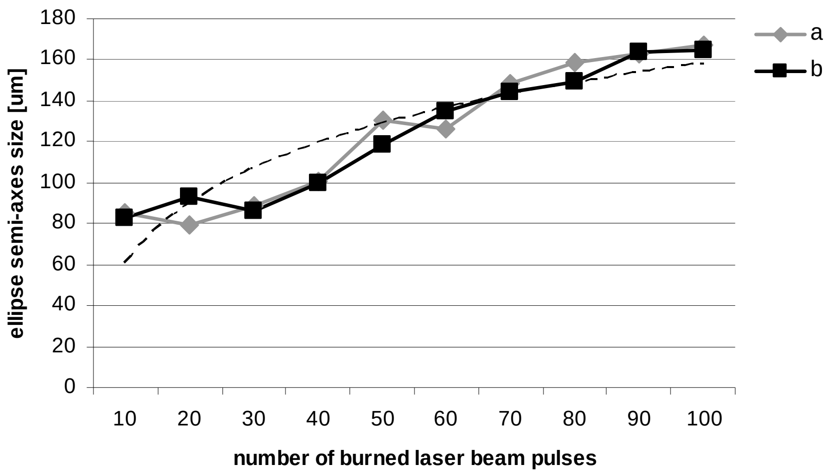

Fig. 54: Dependence plot of ellipse semi-axes a *and* b.

Dependence of the pulse pit depth and transition ring height is shown in Fig. 55. The depth of the pit increases considerably with growing number of engraved laser pulses.

From one experiment, the trend is hardly to find out, it seems to correspond to logarithmic or quadratic function. The second plotted value represents the maximal height of the transition ring. It seems to be independent of the number of laser pulses. The fluctuation of measured values from the constant value is probably caused by the high roughness of the transition ring. The same reasons caused high value of mean relative error described in Table III and Table IV.

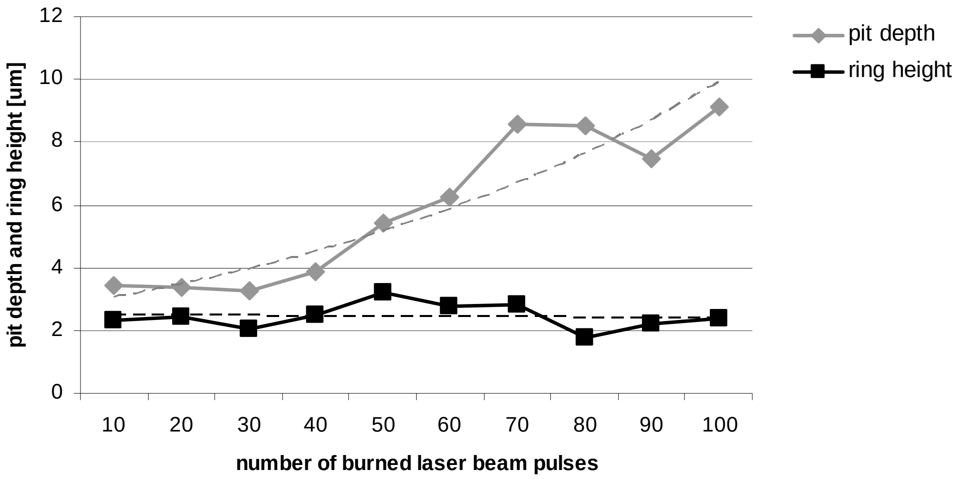

Fig. 55: Dependence plot of pulse pit depth and transition ring height.

The last plot (Fig. 56) shows the dependence of the transition vertical and horizontal width on the number of laser pulses engraved into the material surface. Reasons for this are also described in the comments to Table III and Table IV and an example of a problematic sample is shown in Fig. 53. For all that, also in this case, we can try to guess the trend as the logarithmic one.

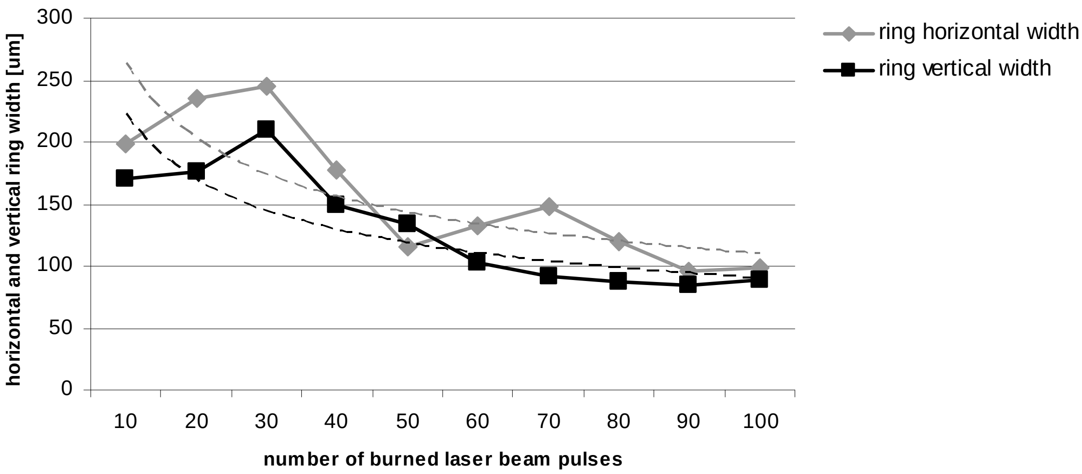

Fig. 56: Dependence plot of transition vertical and horizontal width.

It is evident that finding any precise computable dependence or approximation of measured samples and their parameter will not be a simple task. So far, we can use the simplified trends represented in the previous plots as dashed curves. But in this case, we can hardly estimate the precision of the computed parameters. To get accurate parameters description trends, we should evaluate more experiments. Possible future work on this problem is described in the Chapter 10.

4.2 Pulse Approximation

The pulse approximation was tested on various samples. Results for the area of the pit are very successful. More problematic is the area of the transition ring, where the roughness of the sample surface is high.

First, we decided to compare results of approximation the sample with 100 laser pulses engraved into steel by the smooth surface generated according to the method described in Section 3.4 with the real engraved sample. Results of this comparison can be seen in Fig. 57. Black curves represent cross-section reliefs of the real sample, gray curves show the smooth generated sample surface. Cross-sections in the horizontal direction are shown in Fig. 57a-c; vertical cross-sections can be seen in Fig. 57d-f. The first cross-section from each triplet represents the middle of the pulse in the given direction, the others move more to the margin of the pulse.

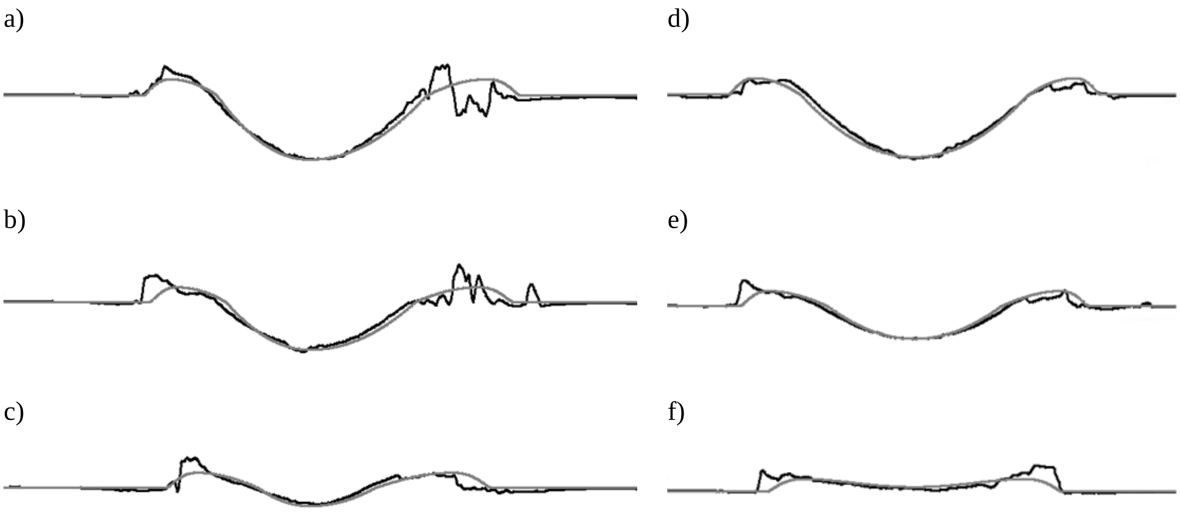

Fig. 57: Approximation of sample with 100 laser pulses engraved into steel by the smooth surface – cross-section reliefes.

To compare the results in 3D view, see Fig. 58. The original samples are placed in the top row and the smooth surfaces generated according to the parametric description are shown in the bottom row. For the comparison, samples with 10 (Fig. 58a), 50 (Fig. 58b), and 100 pulses (Fig. 58c) engraved into steel were chosen. All samples are watched from the same distance and direction.

In the following case (see Fig. 59), the same sample as in the previous case was approximated by the smooth surface and then all possible artificial defects were generated. The roughness of the surface was added by the Perlin noise function, the increase of the transition ring surface lifelikeness was reached by generating the concentric waves.

To compare the real and artificially generated samples, we have used methods described in Section 8.1. These evaluating methods show the basic similarities and differences of both samples in the form of overlaid cross-section curves and as the 3D views on all samples. The rate of samples similarity is expressed as the mean square error value.

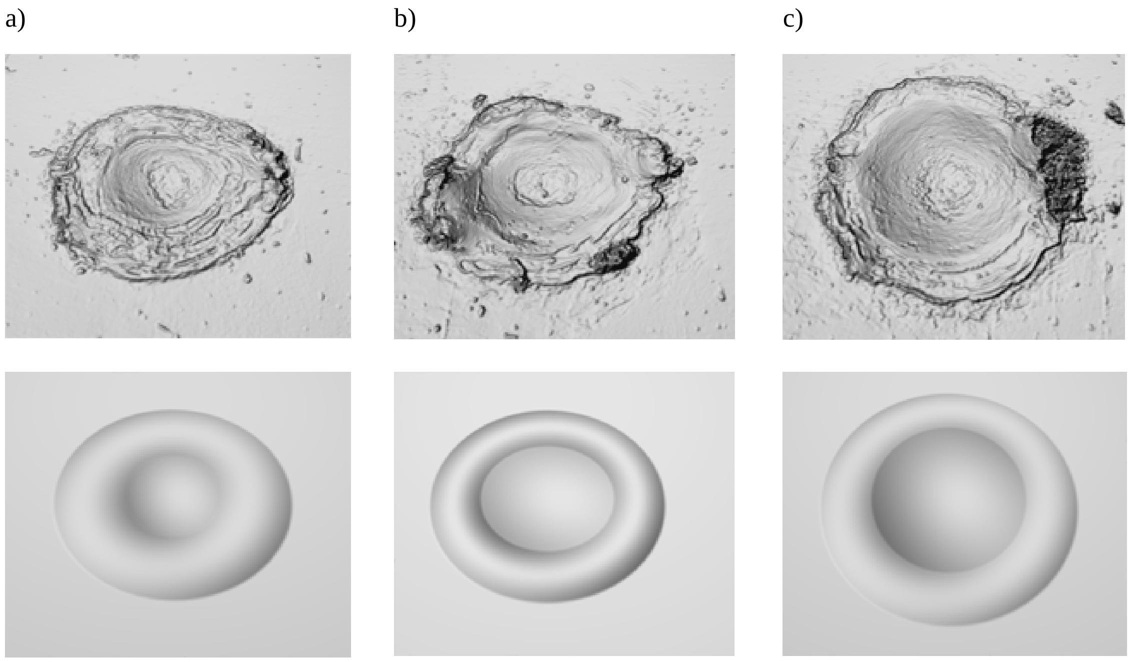

Fig. 58: 3D views at the original samples (top row) and smooth surfaces approximating the samples (bottom row) of a) 10; b) 50; c) 100 pulses engraved into steel.

First, we can compare the original and the newly generated sample in their cross-section curves. Black curves represent cross-section reliefes of the real sample and gray curves show the generated sample surface. Cross-sections in the horizontal direction are shown in Fig. 59a-c; vertical cross-sections can be seen in Fig. 59d-f. The positions of the cross-sections in the sample are the same as in the previous example.

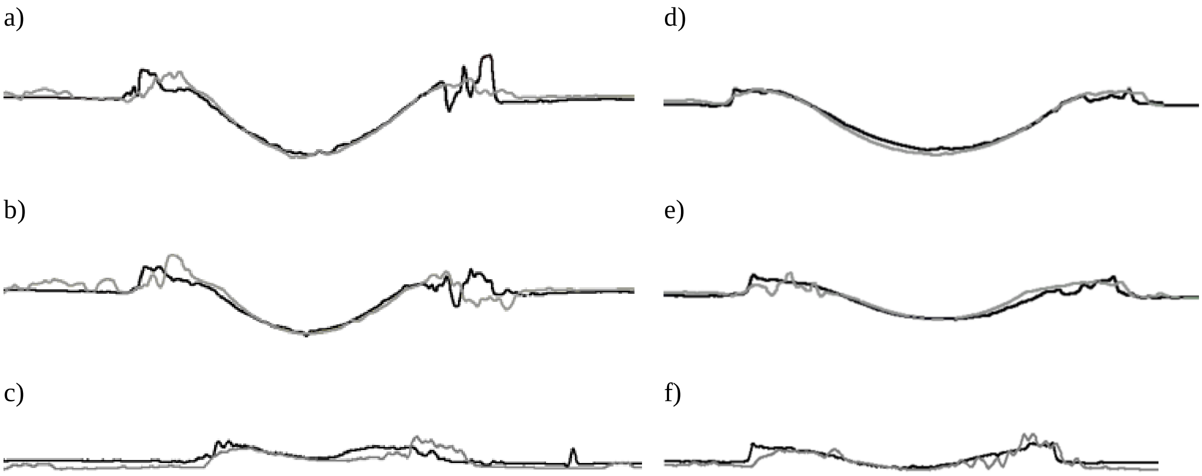

Fig. 59: Complete approximation of sample with 100 laser pulses engraved into steel – cross-section reliefes. Black curves represent cross-section reliefes of the real sample and gray curves show the generated sample surface.

To compare the final results in 3D view, see Fig. 60. The top row shows the same samples those were described in Fig. 58. The complete fully artificially generated samples can be seen in the bottom row. For the comparison, samples with 10, 50, and 100 pulses engraved into steel were used again.

Results seem well and so we can try to evaluate them in a different way. The similarity of both samples is numerically expressed as the mean square error (MSE) and the results are also shown in Fig. 60. As outlined in Section 8.1.1 (where also the way of computing the MSE is explained), values calculated for our testing samples, especially the samples in the column a) and c), correspond to the results of similar samples comparison.

a) b) c)

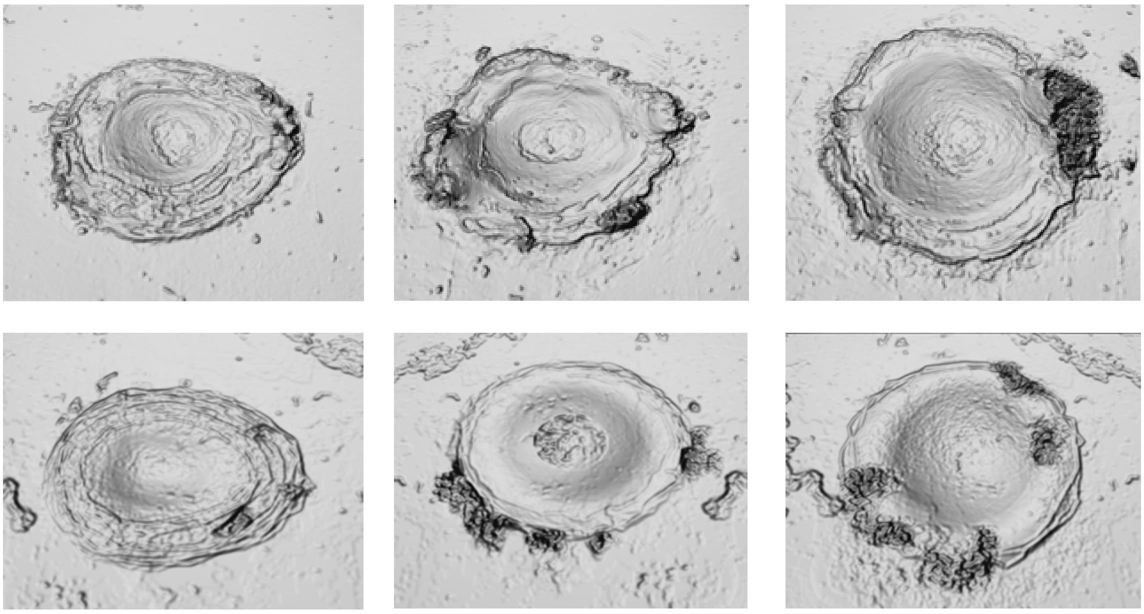

MSE = 0.871 MSE = 2.269 MSE = 0.945

Fig. 60: 3D views at the original samples, smooth surfaces approximating the samples and generated samples of a) 10; b) 50; c) 100 pulses engraved into steel.

5 Automatic Pulse Detection

Pulse detection should be used several times during the process of the laser-engraved samples simulation.

The main task of the detection is to define the area of the material surface, which was affected by the laser beam during the engraving process, as exactly as possible. It is used both during the data preprocessing and parameterization and during the process of result verification, where two samples are compared. In the data preprocessing phase, the detection has one more task – to detect one vertical and one horizontal cross-section those could be used for the pulse basic shape parameterization (described in Section 3.3).

Pulse detection can be done manually, but if we want to use it as a part of the whole process, the manual usage slows it down and prevents automation of data preprocessing. So, for speedup and simplification of the whole preparation process, the system has to be maximal self-sufficient. But the precision and accuracy has to be preserved as well with the process automation.

The main problem during the process of automatic detection is the basic material surface roughness. As mentioned above and as can be seen also in Fig. 61, the surface of some materials is quite smooth (such as the surface of steel in Fig. 61a). Another situation comes in the case of cermet (Fig. 61b), where the roughness on the material surface is more noticeable. Moreover, on the surface of some materials, local defects can also appear. Such defects do not need to be visible on the material surface by a naked eye, but because of the high resolution of real sample scanning, they are included in the description of the sample and they are the source of problems during the automatic pulse detection. Local defect roughness can be seen in Fig. 61a on the top side of the sample.

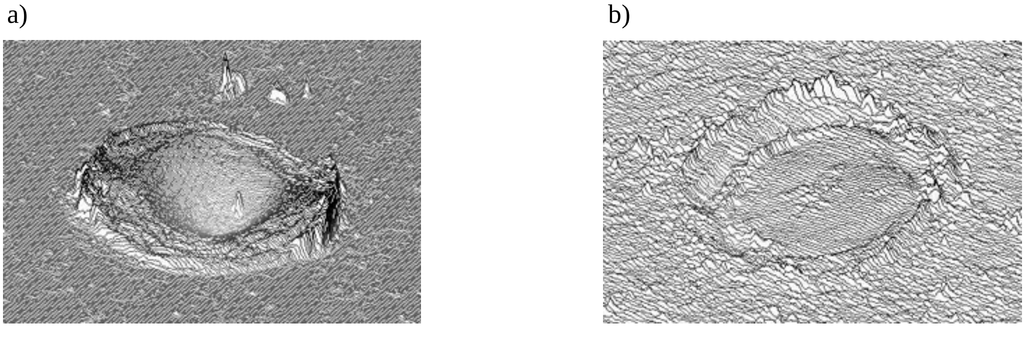

Fig. 61: a) Surface of steel with relatively smooth surface; local defect can bee seen on the top side of the sample; b) surface of cermet sample with globally higher roughness of the surface.

The user is able to distinguish roughness or defects in the material during the manual pulse detection well, but for the automatic method it is very difficult to differentiate these inaccuracies from the outer border of the pulse. Designed methods (described in Section 5.2) for the pulse detection have to be precise enough to give the best results. To get quick and reliable method, we have to create a new method designed right for this task. To detect the pulse area, some methods need to find a starting point at first, and then, from this position to search borders of the detected area. The other methods use different approach.

5.1 Starting Point Computation

The starting point is a position of the surface sample from which the algorithm detecting the heat affected area of the sample should start. A proper starting point is placed in the area of pulse that should be detected. The starting point can be used also for the detection of the cross-section lines position. This usage of starting point is outlined in Section 5.3.1.

To demonstrate the usability of both methods for starting point detection, we decided to show results on the same set of samples that is used for testing the automatic pulse detection methods. These samples and reasons for their selection are introduced in the beginning of Chapter 6.

5.1.1 Minimal Height Position

This method searches positions of minimal height in the sample surface. During the engraving process, laser beam engraves several pulses into the material surface and so, in the place of laser beam impact, some material vaporizes. The height of the sample surface decreases in this area. That is why, a point with the minimal height is supposed to be placed in the area of the engraved pulse that should be detected. In an ideal case, the minimal value of the sample surface will be found in the centre of the pulse pit. But the reality is not optimal, and so the starting point position would be most probably computed somehow shifted. Results of this approach are shown in Fig. 62.

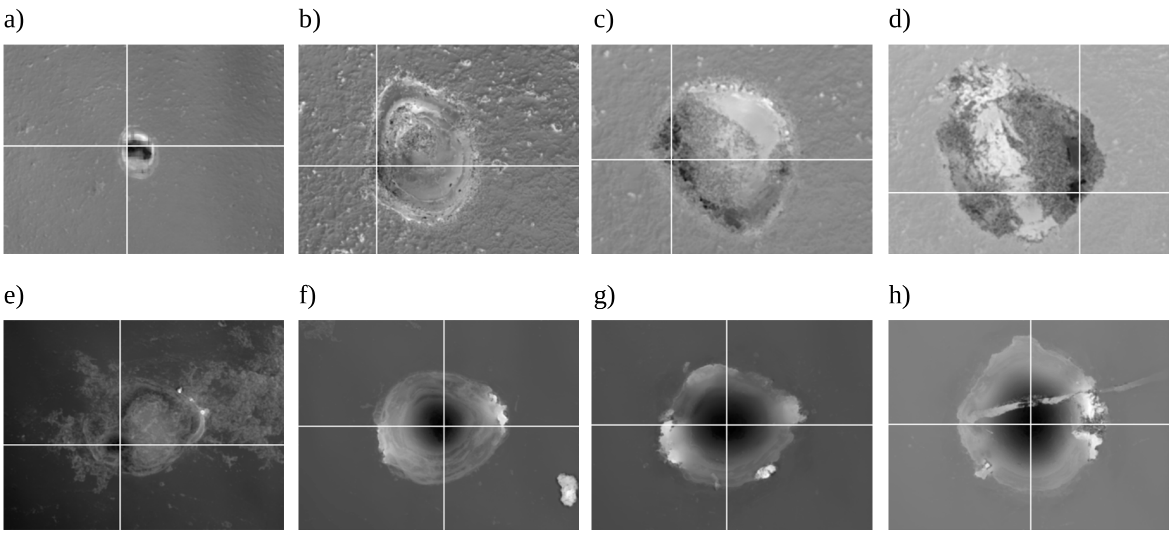

Fig. 62: Results of the starting point detection as the sample surface minimum value.

As can be seen in computed examples, this method returns good results for samples with the typical shape of the heat affected area. This can be seen on samples engraved into steel in Fig. 62e-h. The shape of samples engraved into cermet (Fig. 62a-d) is very irregular and the minimal value is placed very often nearly at the outer border of the pulse.

5.1.2 Centre of Mass Position

Another way how to get the starting point for automatic pulse detection is finding the position of centre of mass in the sample. The tandard procedure of the center of mass computation has to be adapted for the sample representation. The basic equation for calculating the center of mass x_c of a system of particles is defined as the average of the particle positions x_i, weighted by their masses m_i (Equation 5.1).

$$x_c = \frac{\sum m_i . x_i}{\sum m_i} \tag{5.1}$$

Let us label the point of the sample as $f_i = f[x, y]$. Because the whole sample is represented by positive values (the values representing the material level in the sample are given by the height of the material sample into which the sample was engraved), we could define $m_i = f_i$. The simplified cross-section curve of the sample can be seen in Fig. 63a. The result is shown in Fig. 64a. If the pulse does not take the majority space of the sample and the pulse is not placed in the centre of the sample, the rest of the surface overbalances the pulse area and the centre of mass is moved from the centre of the pulse partly to the side of plain surface (as in the case shown in Fig. 64a).

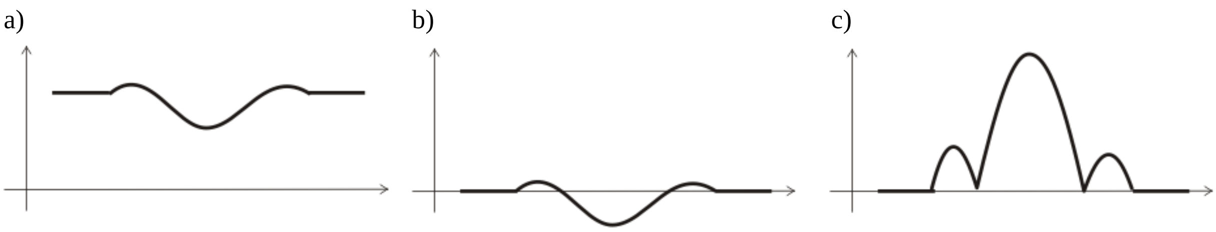

Fig. 63: Simplified cross-sections of the sample in all three phases of computation; a) the original sample; b) the situation after shifting material surface to the zero level; c) the sample after application of power function.

That is why it is necessary to shift the whole sample in a vertical way so that the material level would be represented as zero value (see Fig. 63b). After this shifting, some parts of the sample are represented by negative values. Such sample cannot be used for the center of mass computation and so the negative values have to be converted to positive ones. That can be done by using power function with even and positive exponent. To stress values of the pulse from small values in the neighborhood of the zero level, we have decided to use exponent of 4 (Fig. 63c). Finally the weights for center of mass computation are defined as in the equation (5.2), where *materialLevel* represents the height of the basic material. The result of such calculation can be seen in Fig. 64b.

$$m_i = \left(f_i - materialLevel\right)^4 \tag{5.2}$$

a) b)

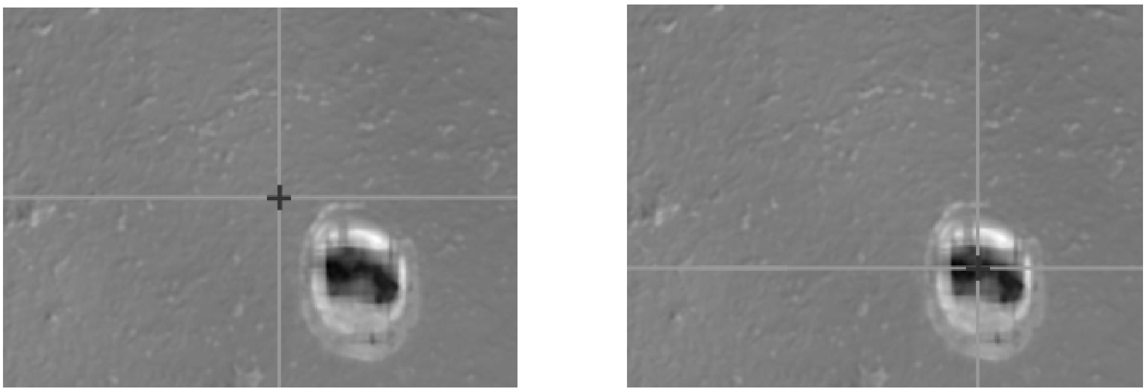

Fig. 64: The result of center of mass computation with the weight a) $m_i = f_i$;
b) $m_i = (f_i\text{-basicLevel})^4$.

This method returns the starting position which is placed in the area of engraved pulse and is affected by local material defect in a minimal way. The results can be seen in Fig. 65.

a) b) c) d)
e) f) g) h)

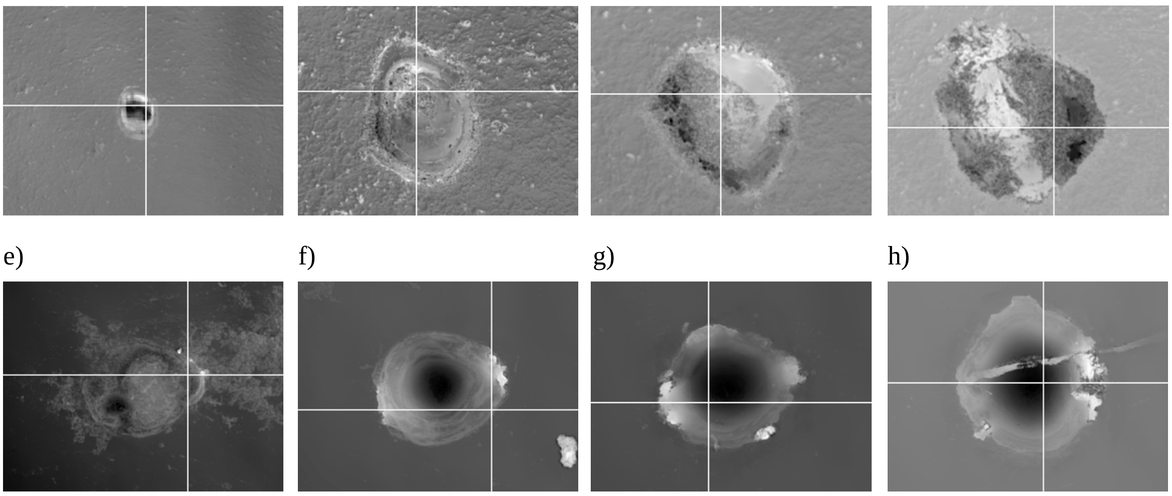

Fig. 65: Results of the starting point detection as the center of mass.

As can be seen, starting points for samples engraved into steel (samples Fig. 65e-h) are not detected as precisely as by the previous method. On the other hand, the position of starting point for samples engraved into cermet (Fig. 65a-d) is detected more to the center of the heat affected area. This feature is caused by the sensitivity of the computation to the height irregularity of the shape. It means that especially the irregular height of the transition ring can cause shifting of the position of the computed point.

5.2 Methods of Pulse Area Detection

Methods described in this section should be used for the most precise detection of the processed sample heat affected area. As results of computation we get values representing the position and dimension of the heat affected area. Some methods start from one point computed as a starting point, the others use completely different approach. Several methods described in the following sections are also described in [Háj08c].

5.2.1 Clipping Method

This detection algorithm goes from unmodified sample surface. The procedure is in a simplified way shown in Fig. 66. The algorithm can start from point computed according to any algorithm described in Section 5.1. From its position, columns of the height map to the left and to the right side are inspected and the height difference of points in each single column (it means the difference between the maximal and minimal value in the column) is computed. If the value does not exceed given height limit, an inspection in the direction is finished and columns behind these left and right borders are clipped. After clipping the columns on the left and right side of the heat affected area, the same process of border searching is started for rows. From the position of the starting point, the method goes throw rows and looks for the first line above and under the pulse for which the height difference is lower then the value of given height difference limit. Horizontal borders (showed as horizontal lines) are appointed, the other rows are clipped.

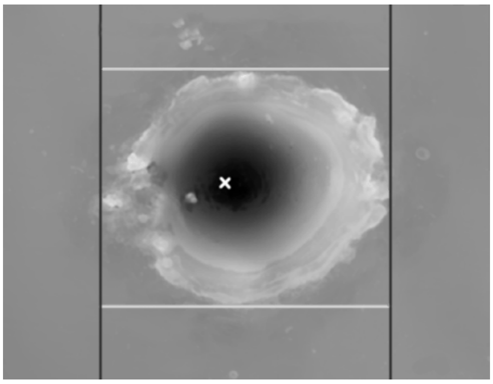

Fig. 66: Borders determined during the algorithm of pulse detection. White cross represents the starting point.

There is a question, how to gain the value of difference height limit. If we do not want to set the constant manually, we have to explore the sample automatically, for example during its loading into the system. We can suppose that the borders of the sample are not modified during the laser engraving and so, they represent the original material surface. The difference constant can be, for the most samples computed for example as the minimal height difference of several border columns or rows. But this approach may not work well if the used border of the sample is damaged by any local defect of the material. In such case, the difference constant is computed too big.

5.2.2 Spiral Method

If we are able to find the starting point reliably we can try to use another approach to determine the borders of the pulse. We can start in the starting point and then inspect the surroundings up to find the basic level of the material.

In the ideal case, the pulse has a circular or an ellipsoidal shape and the starting point is placed exactly in the centre of the pulse. For such pulse we can find the bounding rectangle simply. If we put through the starting point two lines parallel with axis *x* and *y* (as can be seen in Fig. 67a), we can make cross-sections of the sample along these lines (the vertical and the horizontal one). The cross-section curve is in an ideal case more diverted in the area of the pulse than in the part of the unengraved material. That is why we can determine two points of the curve, where the pulse finishes and to define borders there (Fig. 67b).

a) b)

Fig. 67: a) Sample with nearly circular shape, lines parallel with axis x and y going through the starting point; b) cross-section curve with defined borders.

Searching for the border values starts at the beginning and at the end of the curve and continues in the direction to the starting point. First, we are in the area of unengraved material and so values of the curve do not differ from the average material height a lot. When the values start to differ more, we have found the border of the pulse. By this approach we get left and right border of the pulse from the horizontal cross-section curve and the top and bottom border from the vertical cross-section curve.

In the real cases the method described above is not sufficient, because the shape of the heat affected area is mostly irregular. If the shape of the pulse is irregular, the starting point is shifted from the middle of the pulse. Moreover, the irregularity of the pulse from the top view deflects the borders (as in Fig. 68). It is the reason why the previous procedure gives only a rectangle that borders a part of the pulse. However, we can use its result as a starting state for the next processing.

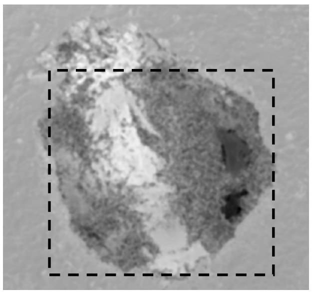

Fig. 68: Asymmetrical pulse shape with the detected area bordered by the dashed rectangle.

The final borders are searched in a spiral way. All borders are periodically tested if it is possible to move them for one row or one column further from the starting point. In each step for each single border (left, bottom, right and top), the height difference between the minimal and the maximal value in the shifted position is computed and compared with the difference limit for the processed sample. The difference is computed only in the interval of existing borders, e.g., if we test the left border, we move one column left and compute the height difference in the interval between top and bottom border. The sequence of borders is preserved through the whole computation (it means borders are rotating during the algorithm). If any border can not be moved, it is used no more in the next steps.

5.2.3 Statistical Method

To get other alternatives in the automatic detection process, we were searching for various approaches to find the most reliable method for detection of the heat affected area in any sample. That is why we have decided to try using statistics. We can try to compute any statistical qualities of the sample surface and to utilize this knowledge for the pulse area recognition. This approach is also described in [Háj09c].

The whole sample height map can be divided into the regular rectangular grid and for each cell of the grid, a representing value can be computed. By this operation, we get the simplification of the height map representation that can be further processed. We have to solve two basic problems – determining size of the statistical grid cell and computing the cell representing value. Both topics will be discussed in the following description together with its influence on the computed results.

The size of the statistical grid cell is bordered from the top by the number of values representing the processed sample. In this case, the whole sample would be represented as one cell. From this representation, we would probably get no beneficial results, because it would cause an oversimplification of the sample. The cell size is bordered also from the bottom; the smallest cell would have the size of one height map representing value (pixel of the grayscale image). Also this case is not the proper one, because we do not get any simplification, as each value of the sample height map would be computed separately. That is why we have to find a suitable value to be able to get the appropriate information about the part of the sample and not to simplify it too much. In Fig. 69a, the sample divided into a too large cells is shown, in Fig. 69b, cells of the statistical grid are too small, Fig. 69c shows the optimal choice of the cell size.

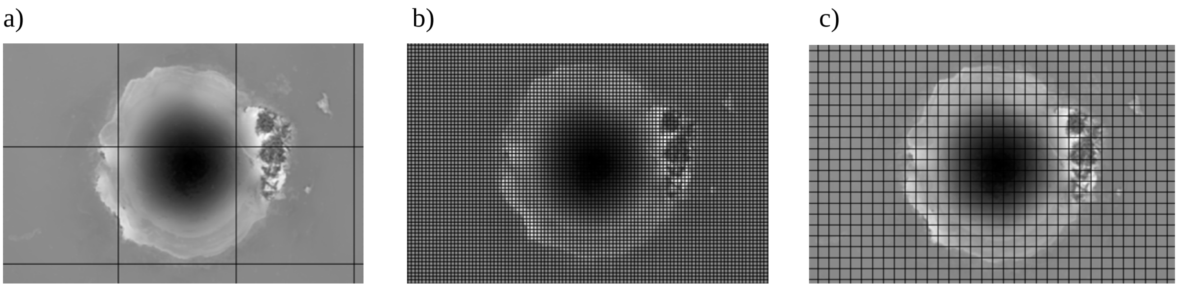

Fig. 69: Sample with statistical grid with different cell size, which is: a) to large; b) too small; c) optimal.

The second problem to be solved is the computation of value representing the statistical grid cell. We have tested three different alternatives. All of them are shown on two samples engraved into both tested materials. In the left column (samples a), all three approaches are tested on the sample engraved into steel and results for the sample engraved into cermet are shown in the right column (samples b). In the first case (Fig. 70), we have computed the difference between the minimal and the maximal value of the height map in each cell. Second (Fig. 71), the median of each cell was calculated. The third method (Fig. 72) uses the average height value of the cell. To eliminate irregularities of the surface, values are truncated to integers. In each cell of shown figures, the computed values are shown, to get a better imagination about the results of the used approaches.

The first used method computes the difference between the minimal and the maximal value of the height map in each cell. If we explore values of the grid of the smoother material in Fig. 70a, we can see that for the heat affected area of the pulse the computed values in the grid are not zero, while the basic material level of the sample is represented by the zero difference. Non-zero values appear also in places with any larger local defect (an example can be found in the top right part of the sample). The situation for the other sample with the rougher material surface (Fig. 70b) is a little bit worse, but still acceptable. The values representing the border of the transition ring are bigger by an order of magnitude than the values representing the basic material. The difference could be further made bigger by for example raising the results to a higher power.

a) b)

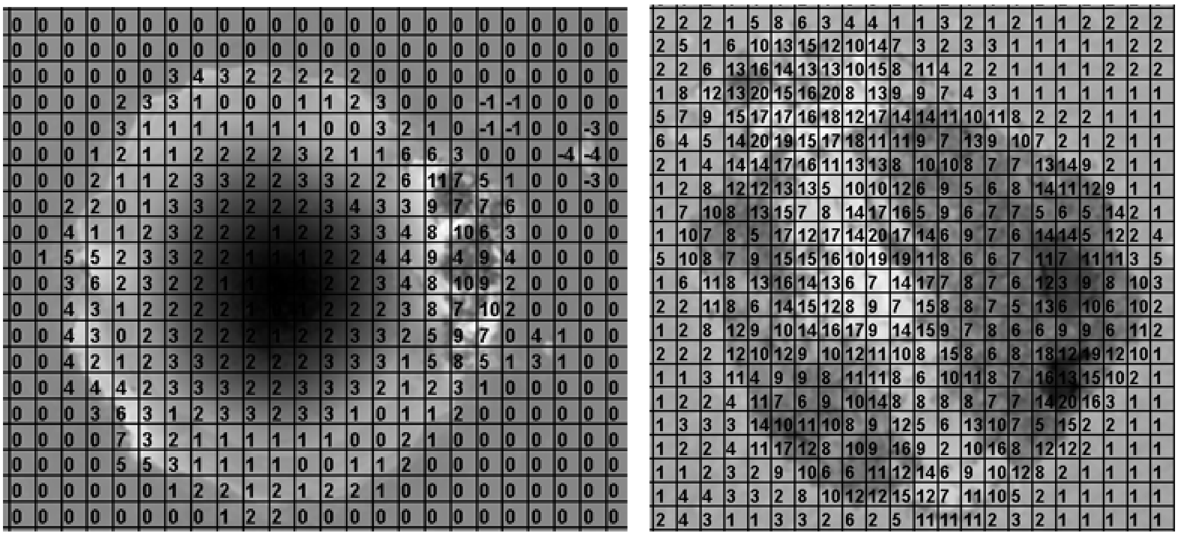

Fig. 70: Samples engraved into a) steel and b) cermet; for each grid cell, its representing value is computed as a difference of the minimal and maximal height in the cell.

In the second case, we have computed a median of each cell. Local defects are in this case, in comparison with the previous approach, more covered. On the other hand, irregularities of the grid can be found e.g. in the top left corner of Fig. 71a. They are caused most probably by the global height irregularity of the used sample. For the second sample (Fig. 71b) this approach is completely unusable. While the height differences have differentiated the basic surface from the heat affected area well, values of medians cannot give any kind of information we need to get about the surface. This approach seems not to have any use for our purpose.

As can be seen in Fig. 72, results for the last method are very similar to the results of the second one. Neither median, nor the average value of the cell seems to get any results usable for the differentiation of the pulse area from the basic material. That is why we will further use the difference of minimal and maximal height in the statistical grid cell as the representing value of the cell for our future computations.

a) b)

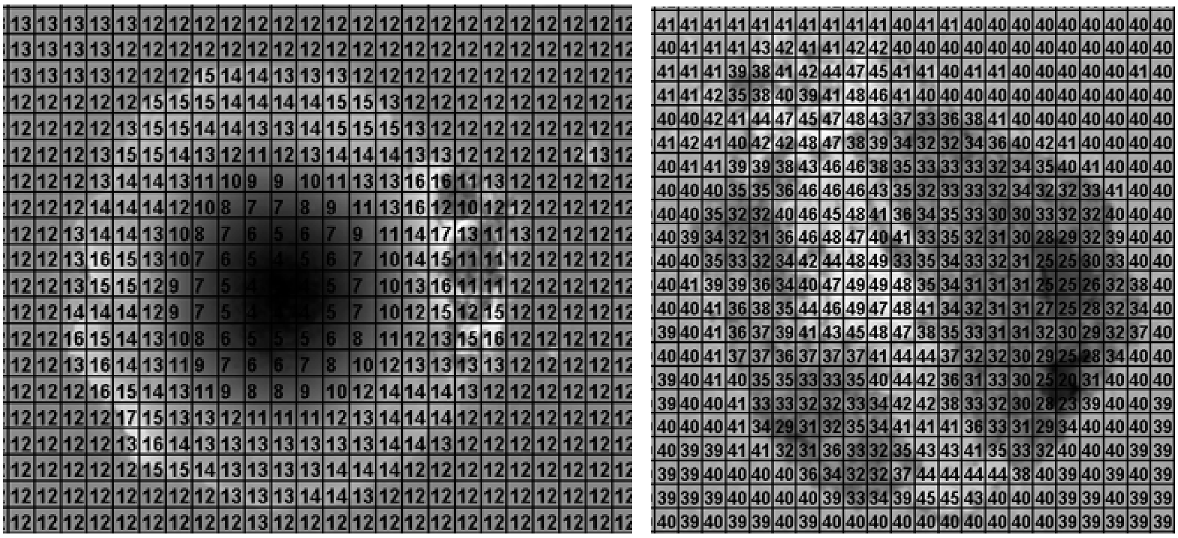

Fig. 71: Samples engraved into a) steel and b) cermet; for each grid cell, its representing value is computed as a median of the cell.

a) b)

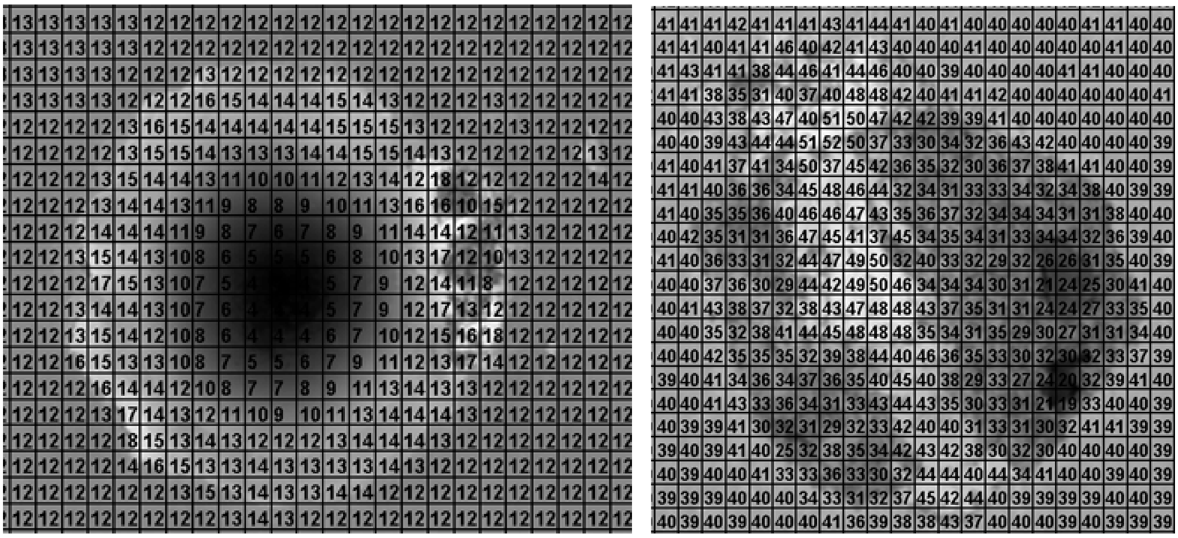

Fig. 72: Samples engraved into a) steel and b) cermet; for each grid cell, its representing value is computed as an average height of the cell.

Now, to detect the pulse area, we have do decide which values of the statistical grid should be included as representing the pulse and which should not. If the value representing the pulse area and basic material can be distinguished well (as shown in Fig. 70), we can use, for example, thresholding for this purpose. All values under the threshold are masked as zero (not a pulse) and the others are in the mask indicated by the value of 1. After this step, we are in the situation shown in Fig. 73. Cells marked as pulse (with the value of 1 in the mask) are highlighted with the color.

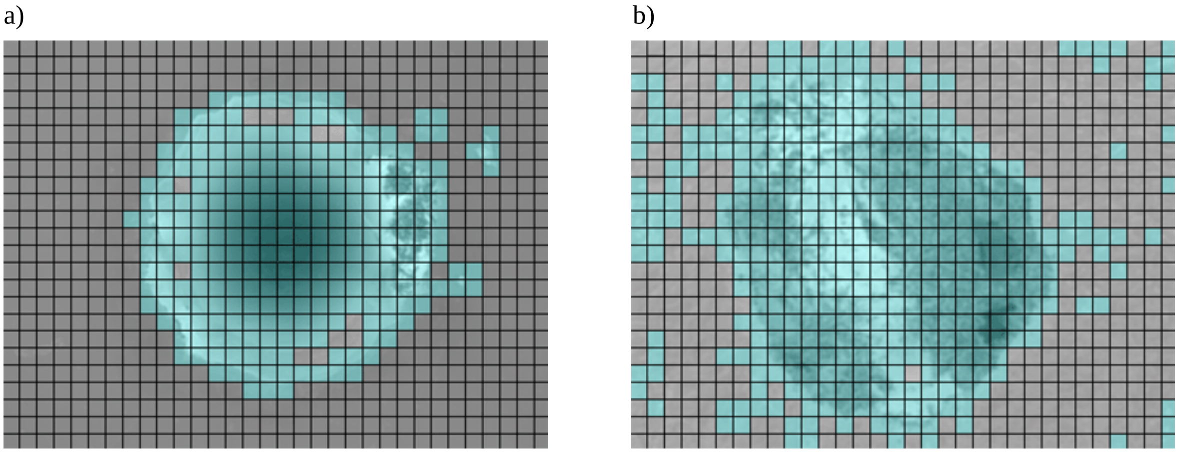

Fig. 73: Both samples described in the previous example with the highlighted mask computed over the statistical grid.

As shown, not only area of the pulse is highlighted sometimes. The grid cell representing value is computed as the difference of minimal and maximal height in the cell. If there is any local defect on the material surface, the value of the difference is computed higher than for a basic material and the cell can be simple thresholded as an area of the pulse. Because we want to detect the heat affected area as exactly as possible, we have to remove local defects and other irregularities. We can suppose that the heat affected area is the largest continuous area marked in the mask with the value of 1. And so, we should provide the segmentation of the result. Various methods of segmentation are described, e.g., in [Sonka07] or [Achry05]. Image segmentation is the process of partitioning a digital image into multiple segments (sets of pixels). For the image segmentation, various methods can be used, e.g., clustering methods, histogram-based methods, region growing methods, and many others.

The best fitting algorithm for our purpose seems to be the algorithm of binary image segmentation described, e.g., in [Haral92] or [Shap01], namely the connected component labeling. There are a number of different algorithms for this method, for example a recursive labeling algorithm or a row-by-row algorithm. We have decided to use a modified row-by-row labeling algorithm. During this process, each separate segment of the image (in our case each separate object in the mask) is labeled with the consecutive natural number. The biggest number determines the number of identified segments. This segmentation algorithm is a sequential process. We have to go through the image (mask) row by row and process each single pixel (cell) that is marked as object (in our case the value of the processed mask cell has to be 1). The others pixels (cells) are ignored, because they belong to the background.

The algorithm makes two passes over the mask. In the first one, each cell representing the object area is labeled with a positive integer according to its neighbors. Cells are processed from the top left corner along rows, it means that as neighbouring cell only such on the left or top border of the processed cell are taken into account, because the others will be processed later and so they are already not labeled.

During the labeling process we can reach one of three situations. If in the neighborhood of the processed cell no labeled cell is found, it is labeled as a new segment (as in Fig. 74a). If any neighboring cell or both cells neighboring with the processed cell are labeled with the same number, also the processed cell is labeled with the same integer (Fig. 74b). The last case is the most complicated one. If more neighboring cells are labeled with different numbers (as shown in Fig. 74c), the processed cell is labeled with the biggest of them and the collision has to be registered into a local equivalence table. Processed cells for the each single of three described cases are highlighted in examples shown in Fig. 74.

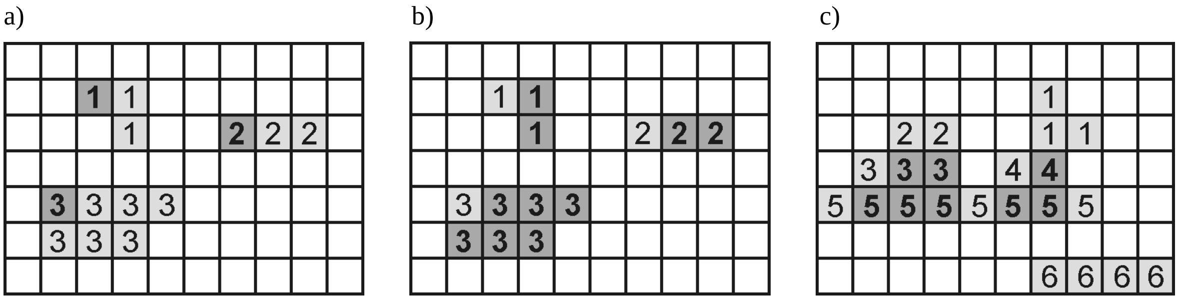

Fig. 74: Mask cells labeled with the natural numbers according to the top and left neighboring cells: a) no labeled cell yet; b) one or both cells labeled with the same number; c) each cell labeled with another integer.

Finally, the whole mask (in the original algorithm the whole image) has to be processed once more to solve collisions. Each object has to be represented only by one positive integer. During the second pass, objects are relabeled according to the equivalence table so that the same number is used to represent objects with colliding numbers. If we want to prevent the sequence of natural numbers, we have to recompute the majority of objects. In this case, the maximal number determines the number of objects. An example can be seen in Fig. 75b. For our purpose, it is sufficient to unite colors for each single object and so, we can mark all cells of the same object with the maximal value as shown in Fig. 75a. In both cases, the relabeled cells are highlighted. The same mask as in Fig. 74c was used.

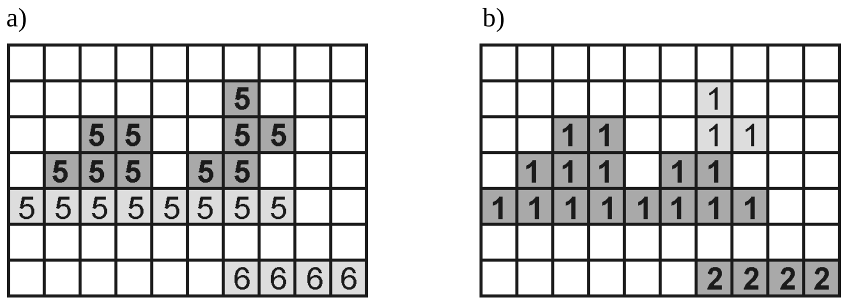

Fig. 75: The situation after final processing, where cells of each object are labeled with the same natural number: a) the maximal value; b) numbers recomputed for all objects to prevent the numbers sequence.

Finally, we get the largest labeled area (the area with the highest number of cells of the mask) that is declared as a pulse. The other objects detected by the segmentation are ignored and for the only segment remaining in the mask, the bordering rectangle is computed. Results of the automatic pulse detection by the statistical method can be found in Section 6.1.3.

A very important part of this algorithm is the correct choice of the statistical grid cell size. In Fig. 76, two different cell sizes are used. All colored cells are in the mask marked as 1, the turquoise cells are detected as a pulse. The violet cells are ignored after the mask coloring. In the first case, the grid cells are too large and a local defect is included into the detected pulse area. The cell size in Fig. 76b is determined better.

a) b)

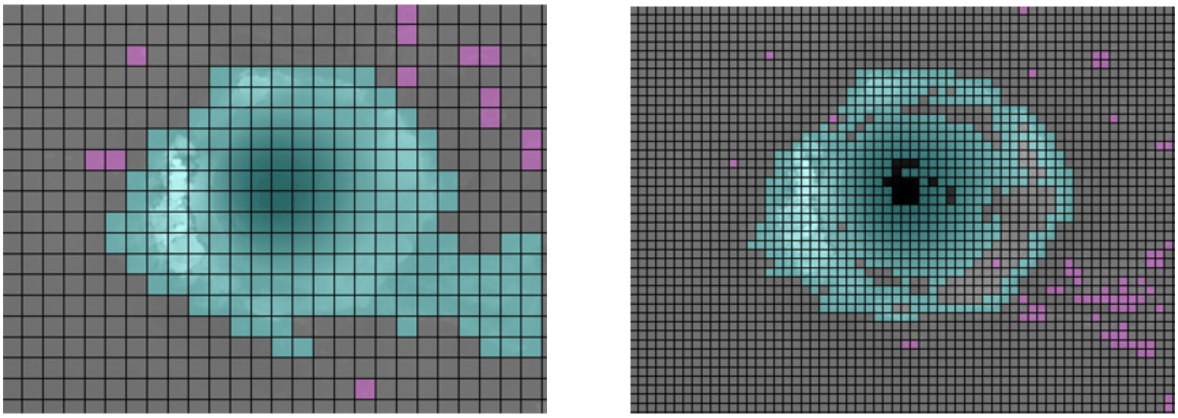

Fig. 76: Mask computed above the statistical grid with the sizes of cell that was determined a) incorrectly; b) optimally.

As can be seen in Fig. 77, incorrectly determined value of the grid size can also cause separation of the area representing the pulse. Only the largest part is labeled as a pulse, and so the whole pulse is not detected correctly. To solve this problem, we can compute more masks for different sizes of statistical grid cell and search the final pulse area in their intersection.

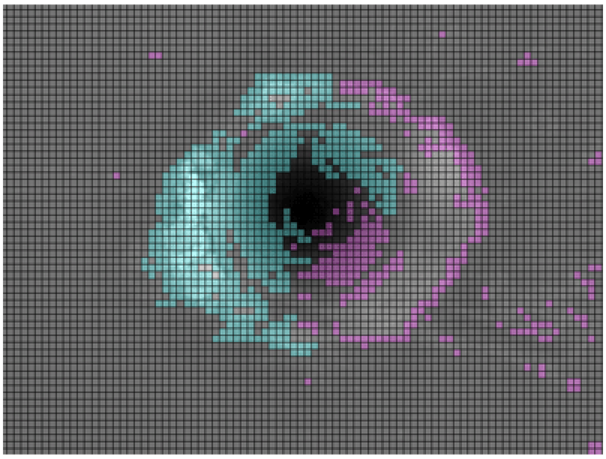

Fig. 77: An example of wrong pulse area detection because of discontinuous mask.

5.2.4 Image Processing Methods Application

Methods for pulse detection described above use similar principles (especially computation of height differences) and so they face the similar problems. So we have decided to try to test another approaches. One of the tested alternatives are methods used for image processing and recognition such as thresholding, erosion, dilatation, edge detection, pattern recognition, various types of image filtration etc. [Hlav93], [Hlav01], [Klette04] or various sequential operations in image processing [Rosen66]. Methods could be used in combination with different variants of resampling the image. The main problem of these methods is the automation of setting the detection process parameters.

So far we have tested two approaches. The first one uses thresholding together with image resampling and compression. In Fig. 78, the results of thresholding applied on the sample with 60 pulses engraved into the same point into cermet are shown. First, the original image was thresholded by two thresholds, so the image was converted into three colors: white for points above the material surface, gray for the material itself and black for points under the material basic level. Fig. 78c-d show the same sample modified by the maximal JPEG compression [Blell01] before and after thresholding. The compression is used to remove high frequencies, which causes roughness of the material and the discrete cosine transformation used by the compression ensures that.

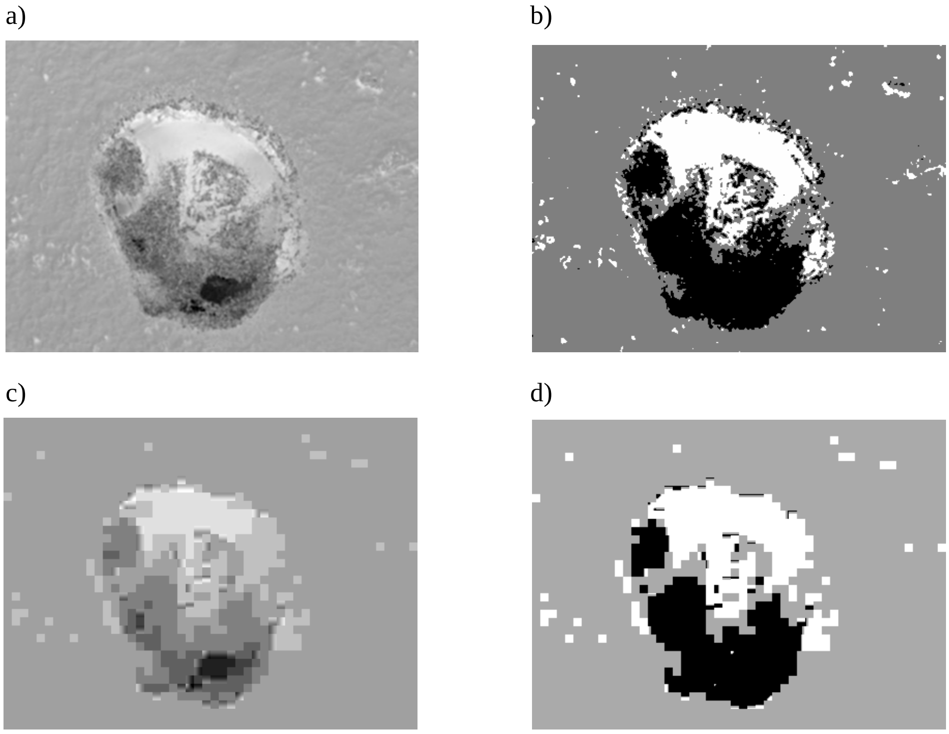

Fig. 78: a) Original sample – 60 pulses engraved into cermet; b) the sample thresholded by two thresholds; c) the original sample resampled by the JPEG compression; d) the resampled image after application of two thresholds.

The second way for automatic pulse detection using the image processing methods might be the methods using any kind of filtration in the combination with isolines searching. This approach has resulted from our cooperation with the Department of Mathematics, which was mentioned in Section 1.1. First, the surface of the material had to be filtered. For the filtration, the fast Fourier transform [Brigh88], [Hogg06], [Rich06] can be used. After the filtration, the surface of the material is smoothed out. In Fig. 79, the original and filtered sample can be seen. The smoothed image is clipped because of the filtration.

After the smoothing the surface we start searching isolines. They are created by the values tightly above and under the basic material level which are connected into the continuous curve. Finally, the isolines are smoothed out. An example can be seen in Fig.

80. The blue line shows the isoline tightly under the basic material level, the red one represents the isoline above the unengraved material surface. In Fig. 80a, isolines in the smoothed image are shown, in Fig. 80b, isolines are transferred into the original image. Our current results of these methods can be found in Section 6.1.4.

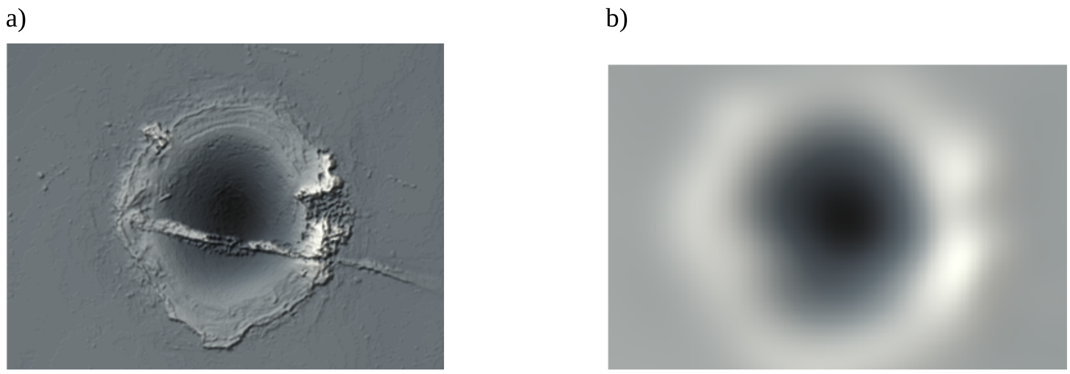

Fig. 79: Images representing the sample surface: a) the original one; b) image after the filtration.

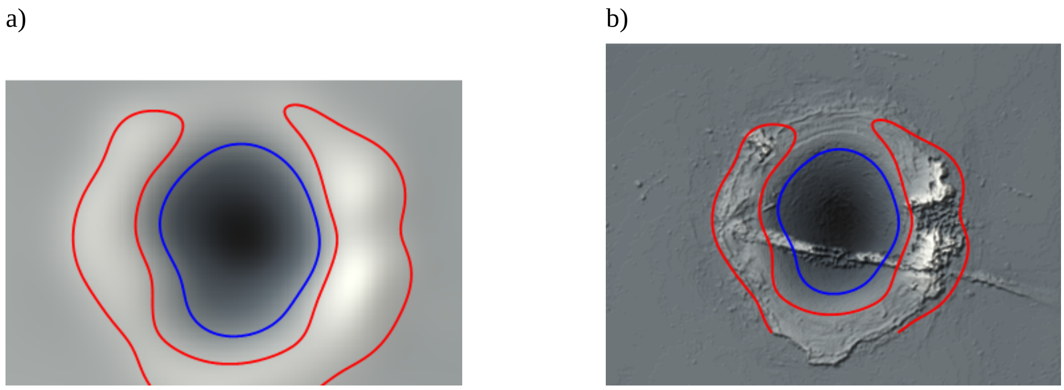

Fig. 80: a) The smoothed and b) the original images representing the sample surface with computed isolines.

5.3 Methods for Cross-Sections Detection

In Section 3.4, the algorithm for the pulse basic shape approximation is described. This algorithm comes out from the shapes of the vertical and horizontal cross-section relief curve. To parameterize the pulse shape as exactly as possible, cross-sections in the broadest parts of the pulse in the vertical and horizontal direction that are going throw the middle of the pulse pit center should be used.

The position of cross-section line determining the row or the column of the sample, which is visualized as the relief curve, can be set manually. But this approach is inappropriate for the automatic sample parameterization. That is why we have to find some proper algorithm to find the cross-section lines positions.

5.3.1 Starting Point Methods

We can search for the inspiration in methods for automatic pulse detection. Especially, we can concentrate on algorithms for the starting point searching. Two alternatives were described – position of the minimal height in the processed sample surface and computing the centre of mass of the sample. Both methods for starting point computation are described in Section 5.1. We can use these computation approaches and use the results as the cross-section lines positions.

5.3.2 Detected Area Center Method

Algorithms for automatic pulse detection work well and so we can try to use them for detection of cross-section positions for samples, where the previous methods do not give optimal results.

We can determine the cross-section lines position as the centre of the detected area. This approach uses the precondition of sufficiently regular shape of the pulse and exact pulse area detection. Then, the middle of the pulse pit is placed in the middle of the detected area. Results of this approach are outlined in Section 6.2.

6 Results of Automatic Pulse Detection

6.1 Pulse Area Detection

In this section, results from each method are shown and described and problematic samples are discussed. For the pulse detection, various samples engraved into steel and cermet were used to test the stability of the algorithms with respect to the roughness of different materials and irregularity of the pulses shape.

In the previous sections, several methods for pulse detection were described. They differ in precision and reliability. Some of them were implemented in our system and some methods were so far tested in Wolfram Mathematica® [WolfOnl]. All methods were tested on the same samples which were chosen because of any specific feature. The task of the algorithm was to detect the pulse in the most perfect way.

Tested samples are shown in Fig. 81. Some of them are engraved into cermet (Fig. 81a-d), where the high roughness of the material influences the detection process and some are engraved into steel (Fig. 81f-h) which has much smoother surface. Samples with various numbers of laser pulses engraved into one point of the material were chosen. Into the testing set we have included samples with 1, 2, 70 and 100 laser pulses engraved into cermet and samples with 1, 10, 50 and 100 laser pulses engraved into steel. All samples except the first one were measured with the same scale. Surfaces of several samples are influenced by the local defects in the material and shapes of pulses are in some cases more and in some less asymmetric. An areal local defect can be recognized in the surface of the sample in Fig. 81e. It influence both the surface of the heat affected area and also its surrounding. Another local defect affecting the area of pulse that should be detected can be found in Fig. 81h. These types of local defects affect the detection together with the roughness of the sample surface most. In Fig. 81f, another type of local defect is shown. This defect does not influence the results of detection algorithms. The samples are in the following text for the simplification labeled by letters A-H.

As can be seen in the following sections, several samples can be well detected with the majority of methods. On the other hand, there is a set of samples problematically detectable by all methods. To describe the category of unproblematic samples is not very complicated. Such pulses are well bordered, no defects occur on the material surface and the roughness of the material is minor.

a) b) c) d) e) f) g) h)

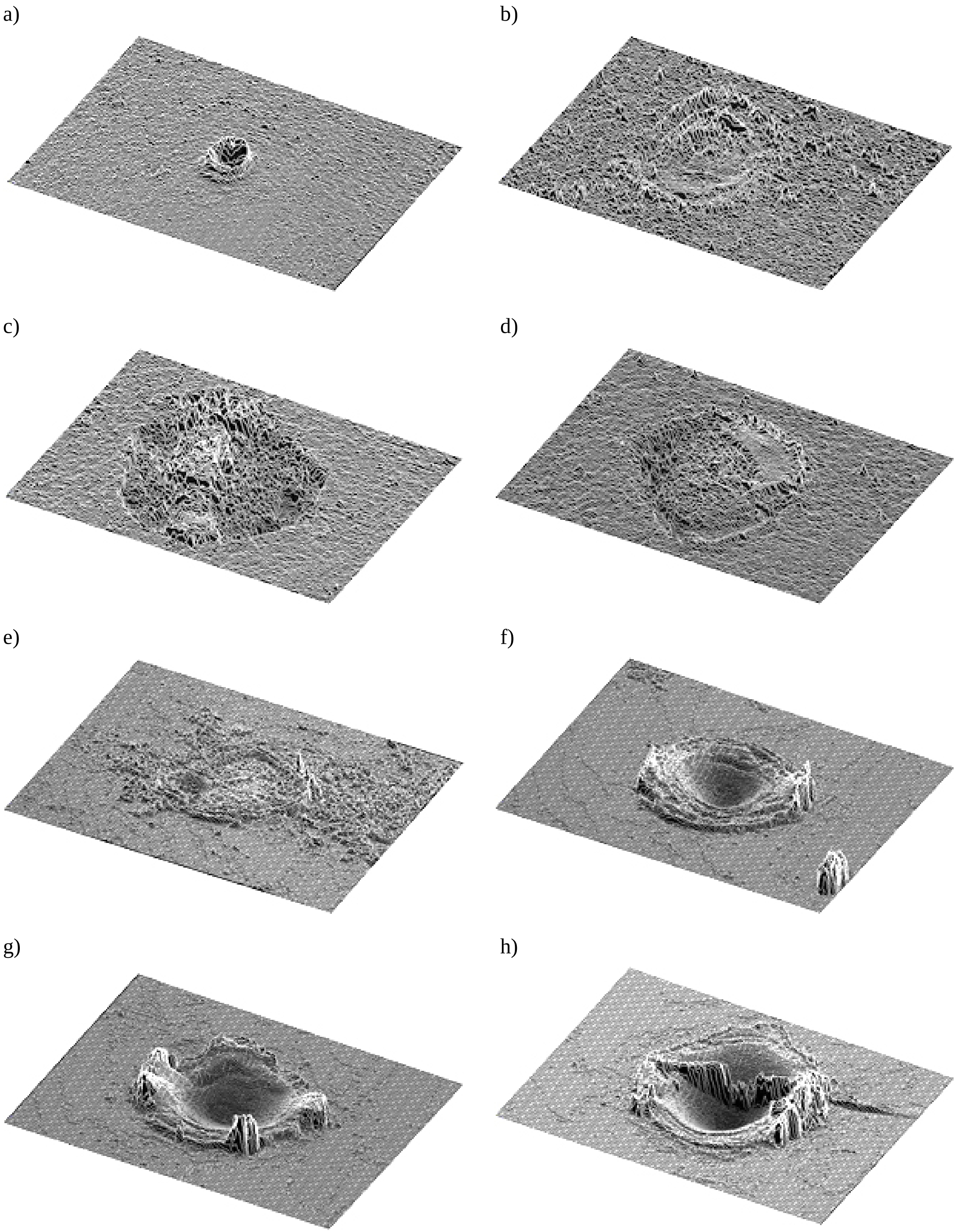

Fig. 81: Samples used for testing pulse detection algorithms (material of the samples: a-d cermet, e-h steel). a) 1 pulse measured in smaller zoom; b) 2 pulses where the area of pulse is not strictly bounded; c) 70 pulses and d) 100 pulses with the non-symmetric shape of the pulse; e) 1 pulse with the areal local defect of the material surface; f) 10 pulses with the local defect in which the global height maximum is located; g) 50 pulses; h) 100 pulses with a defect in the area of pulse.

6.1.1 Clipping Method

A feature problematical for this method (as well as for the Spiral method) is determining the height difference limit. The way of the minimal height difference computation from several border columns or rows works quite well for samples without any areal local defect in the material surface. But the areal defect around the pulse can produce incorrect pulse detection (as in Fig. 82e). Even other local defects can influence the result as in the case of Fig. 82h. The other samples are detected correctly (see Fig. 82).

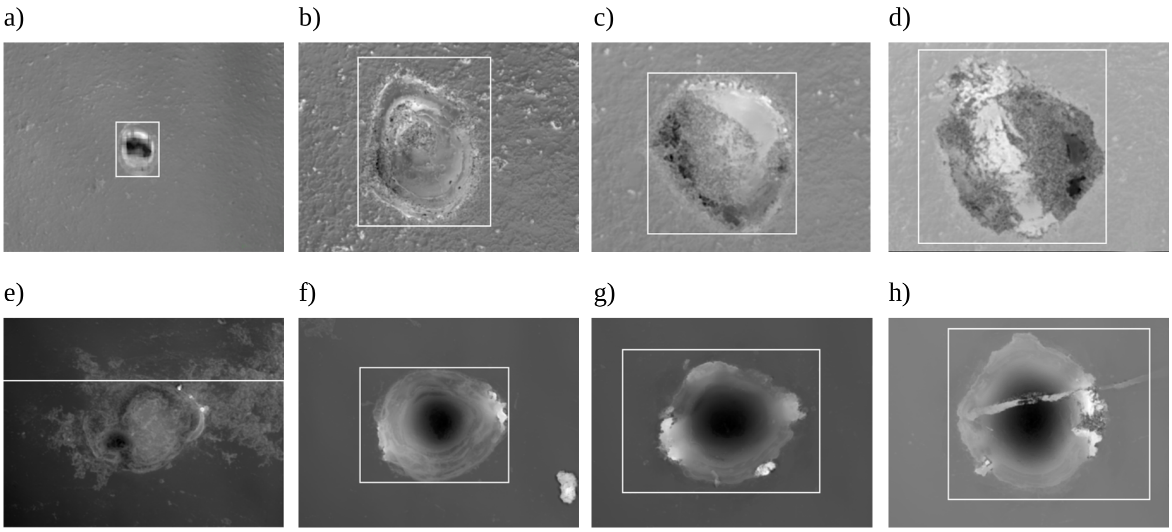

Fig. 82: Results of the pulse detection by the clipping method.

6.1.2 Spiral Method

As can be seen in Fig. 83, the most pulses are detected correctly except for three samples. The reasons for the inaccurate detections are the high material roughness and local defects. The material of sample B is very rough and so, the bordering rectangle is computed too wide (see Fig. 83b). Also samples E and H are detected incorrectly as in the previous case.

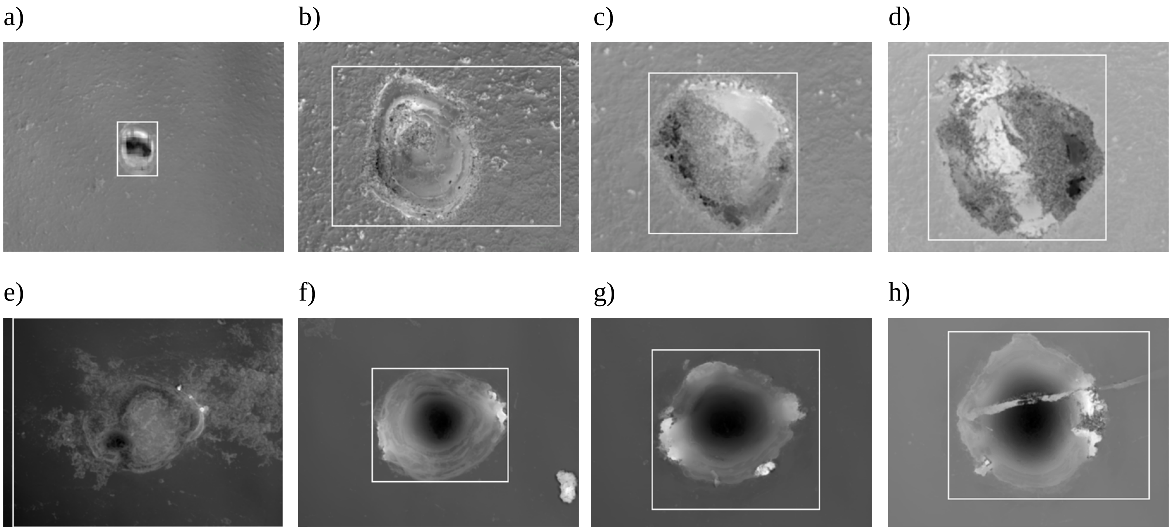

Fig. 83: Results of the pulse detection by the spiral method.

6.1.3 Statistical Method

As described in Section 5.2.3 and as can be seen in Fig. 84, the most important precondition for the correct detection of the heat affected area is the optimal choice of the statistical grid cell size. If it is used too large (Fig. 84a) or too small (Fig. 84c), the pulse is not detected well. On the other hand, the optimal selection of its value can provide the correct detection even in the case of the problematic sample A. The right choice of the grid cell size is discussed at the end of this section.

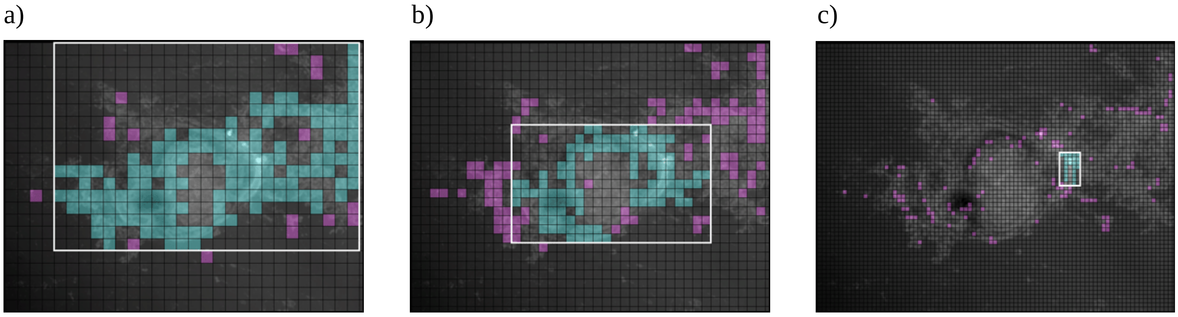

Fig. 84: Results of the statistical method detection with changing the statistical grid cell size that is a) too large; b) optimal; c) too small.

We have also tested this method on our set of testing samples. Results can be seen in Fig. 85. The optimal size of statistical grid cell changes according to used material and also in dependence on the precision that was used during the real sample measurement. During our tests, we were looking for the optimal cell size experimentally. For sample A the size had to be decreased to detect changes on the relatively small area of the pulse. The other samples were measured with the same resolution, and so the optimal size differs only in dependence on the used material. Our tests show that for the rougher material, such as cermet (Fig. 85b-d), the grid cell size has to be determined smaller than for the smoother material, such as steel (Fig. 85e-h). For all testing samples engraved with the same precision into the same material (B-D and E-H), the same size of the grid size was used.

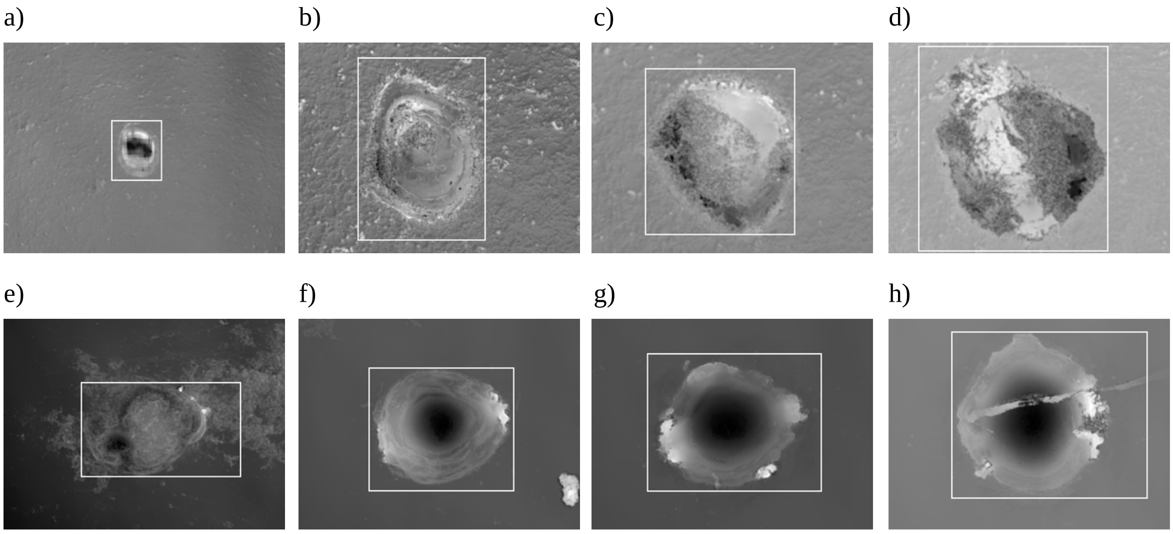

Fig. 85: Results of the pulse detection by the statistical method.

All testing samples were, unlike the previously described methods, detected correctly. So, this method seems to be the right way. In spite of that, also this method has some problems to be solved if the detection should be provided automatically. As described in Section 5.2.3, the method is, thanks to the usage of statistical grid, able to distinguish the heat affected area from the original basic surface. From Fig. 70b, it is obvious, that the basic material does not have to be represented by the value of 0. Because the values representing the original material surface do not differ a lot, we just have to explore representing values of cells on the border of the statistical grid and to determine the value of the basic material level.

The second problem is the choice of the grid cell size. As shown on our testing samples, the size can be experimentally precomputed. The precomputed value should be determined particularly according to the most problematic samples. For the testing samples engraved into steel, the size was found for the sample E first, and than used without any changes for the other samples. If the method of the grid cell size precomputation is not sufficient, several masks for different cell sizes could be computed and the results intersected to detect the pulse area best.

6.1.4 Image Processing Methods Application

Another method tested as a possibility for the pulse detection is thresholding. In Fig. 86, the results of thresholding by two thresholds are shown. All samples have been processed manually, to get the best results. As can be seen, this method is not appropriate for materials with very rough material (such as cermet). This was the main reason, why we decided not to use this approach for our future research.

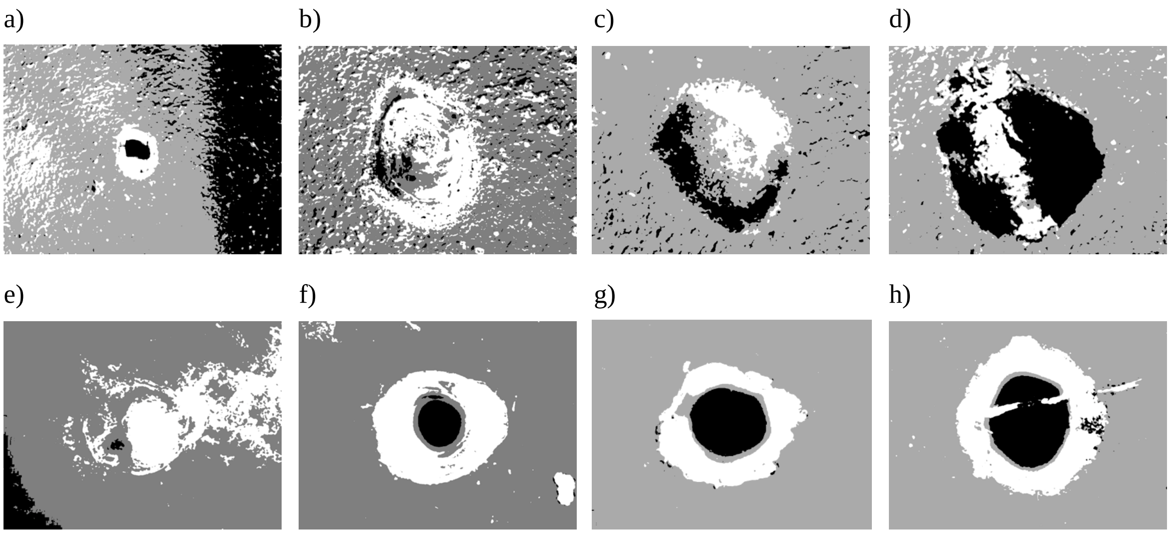

Fig. 86: Results of the manually thresholding by two threshes.

The other approach using image processing methods is filtration of the sample surface together with isoline searching. For speeding-up the testing process we have decided to test the method in the Wolfram Mathematica® [WolfOnl] computational environment. Thereafter, we were able to apply predefined functions of the Mathematica system to form the algorithm.

The successfulness of the algorithm depends on several conditions. One important standpoint is the choice of parameters (the size of the filter mask or the difference between the basic material level and the level of each single isoline). The sample surface itself also plays a significant role. Very important is the height symmetry of the pulse, especially its outer border.

The size of the filter and the value of difference, which gives the level of the isoline above and under the basic material level, have to be determined. The filter size has to be set to smooth the roughness of the material well, but not to smooth out the whole pulse too much. In Fig. 87 the results of using different size of filter masks are shown. Sample B was used because of its high material roughness. In Fig. 87a, the mask is too small, in Fig. 87b it is quite optimal and in Fig. 87c it is too large and in the filtered image, hardly anything can be detected.

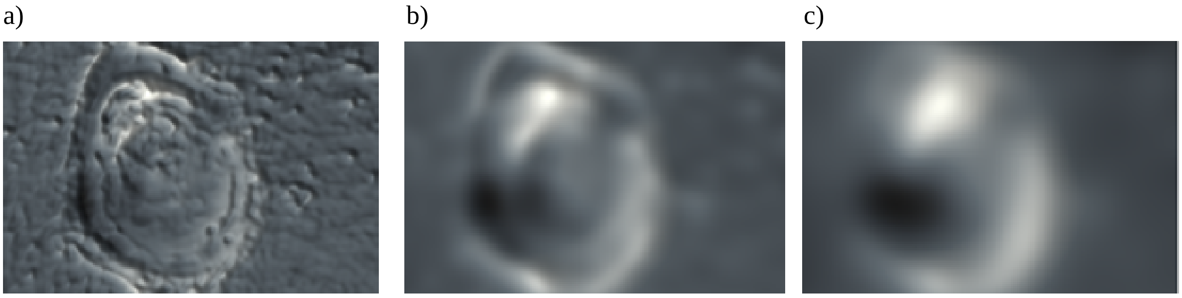

Fig. 87: The results of using different size of filter masks for filtration the sample B: a) too small filter mask, b) optimal filter mask, c) too large filter mask.

If the material is melted around the pulse pit irregularly, the filtration is affected by the height difference of the material surface and the upper isoline is not found completely. Moreover, the filtration clips the image by the size of the filtration mask. Because the area of the laser-engraved pulse takes the majority of the sample related especially to the sample height, the isolines are not computed for the upper and bottom part of the pulse very often. This problem could be solved by the individual adaptation of the sample surface filtration.

After the filtration the isolines are searched. Another important parameter for this method is the difference between the basic material level and the level of isoline. In Fig. 88, the same filter size (the optimal one) was used for the sample G. The difference between the basic material level and the level of isoline was increasing. In Fig. 88a, the isoline was found directly on the basic material level. The result looks well, but there is a space between the isoline and the outer border of the pulse. In Fig. 88b, the difference was increased (the isolines were searched a little bit more above and under the basic material level). The isoline was founded more tightly to the pulse. Finally, if the difference was increased more again, in Fig. 88c, the upper isoline is separated into several parts which border the highest places in the pulse.

As mentioned, this method seems to give good results, but its main problem is a complicated automatic parameters setting. As can be seen in Fig. 89, for this method the pulse detection of samples B (Fig. 6b) and E (Fig. 6e) is problematic. Moreover, many other samples were detected incorrectly, when the parameters were not individually adapted. The detected areas are discontinuous and they border only parts of the heat affected area. On the other hand, if we border isolines with a rectangle, the detection of the majority samples gives good results.

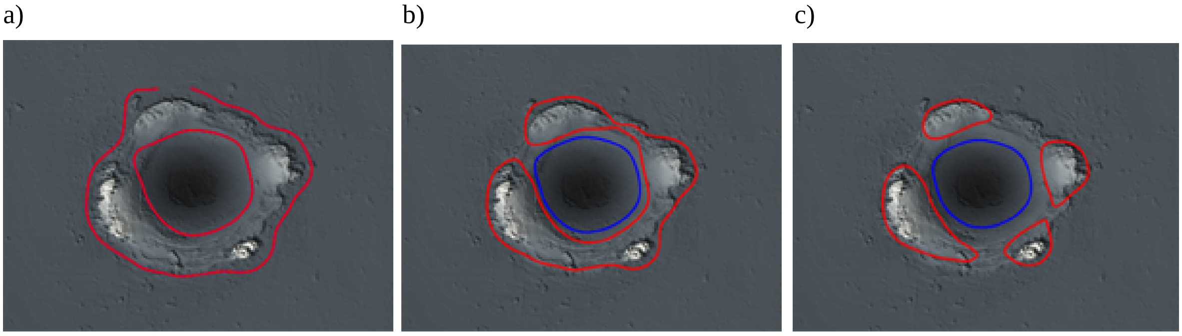

Fig. 88: Results of isoline searching with the same filter, the difference between the basic material level and the level of isolines was changing. a) isoline directly on the basic material level, b-c) increasing value of difference.

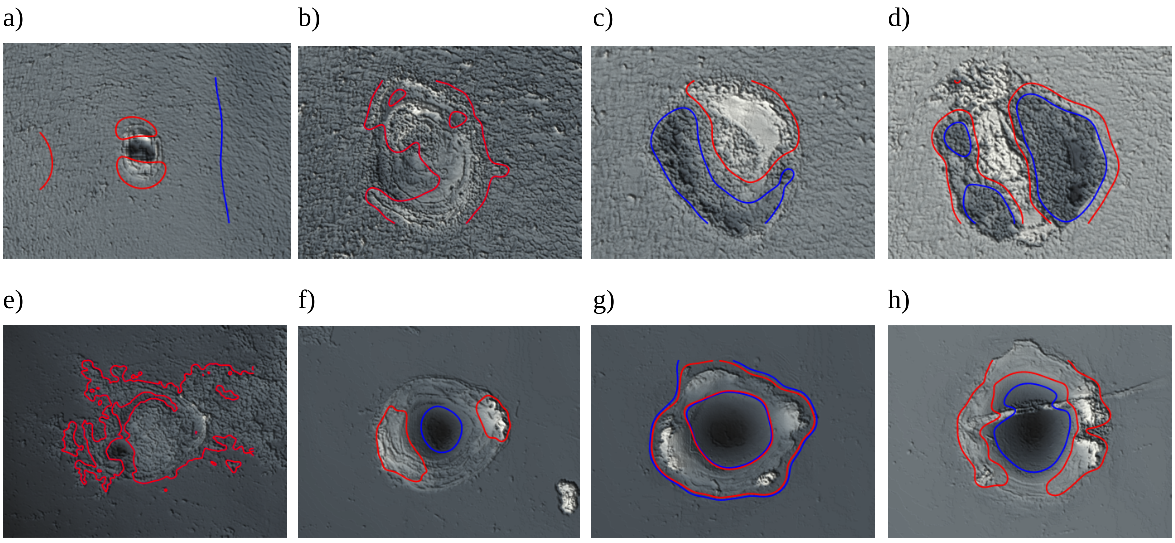

Fig. 89: Results of the pulse detection by the isolines searching.

Unfortunately, this method is also very slow especially because of the sample surface filtration. The speed has been partly increased by resampling the original sample to the size 400×300 pixels, but it is still not optimal. The next speeding-up of the computation could be reached for example by the decreasing the isoline shape accuracy.

Although the approach of surface smoothing and isolines searching is not the optimal solution yet, it gives us another point of view on the sample and its processing. Except the automatic pulse detection, this method seems to be a good way to get more detailed description of the sample which would enable to compute better statistics over the sample or to compare them from the different point of view. In this approach also linear and non-linear filtering described, e.g., in [Nishi06] or [Mitra01] could be used. This could be investigated in the future research.

6.2 Cross-Sections Detection

As can be seen in Fig. 62 and Fig. 65, if we put two lines through the starting point computed by methods describe in Sections 5.1.1 and 5.1.2, we can get vertical and horizontal cross-sections. For each material, different method gives best results.

In the case of samples engraved into steel, where the pulse shape is more similar to the ideal pulse shape, the center of pulse pit corresponds to the minimal height value position. The starting point position is the right position for the cross-section curves extraction. If we want to compute the center of mass for this sample, the local defects on the transition ring cause shifting the starting point from the optimal position.

Samples engraved into cermet have mostly more irregular shape, but on the other hand, the surface heights are not affected by local defect a lot as in the case of samples engraved into steel. For this reason, the method for the centre of mass computation gives for samples engraved into cermet better, but unfortunately still not optimal results.

The last method for cross-section position detection is described in Section 5.3.2. For the heat affected area detection, the slipping method described in Section 5.2.1 was used to show dependence of the result on the detection method successfulness. Results of this approach are shown in Fig. 90. For all samples, except for the sample E and partly sample H, positions for cross-section lines were detected well. The results could be further improved by using a better detection algorithm (such as the statistical method described in Section 5.2.3).

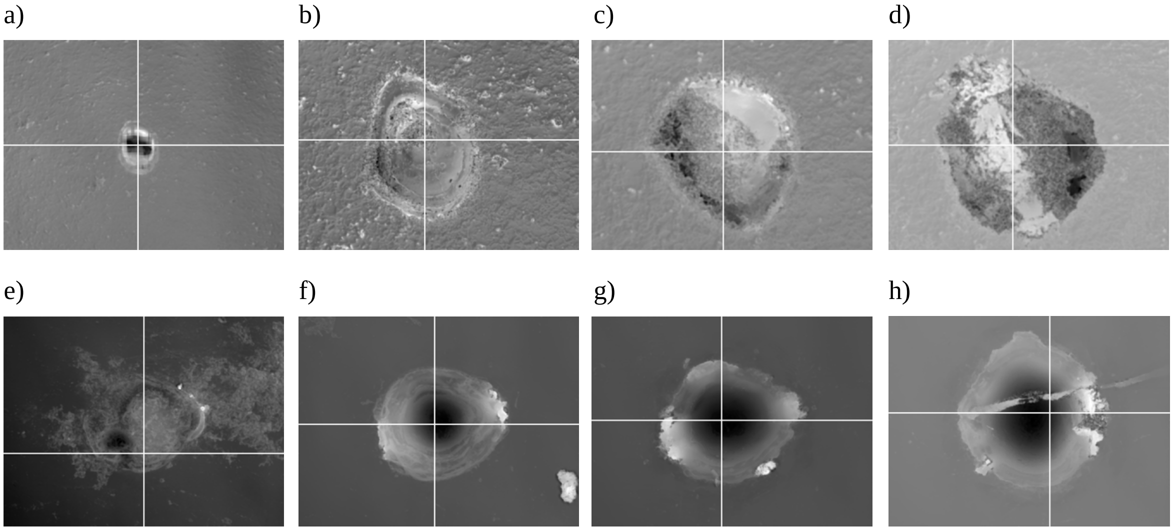

Fig. 90: Results of the cross-section position detection.

For highlighting the difference, samples B (Fig. 91) and F (Fig. 92) are compared. Cross-section lines are interleaved through the points detected as minimums (a), through the centre of mass (b) and through the center of detected area (c).

If we use a reliable method for the heat affected area detection, the best approach of determination the cross-section lines position is the detected area center method described in Section 5.3.2. It is independent of the used material and so it can be used generally. If we need to process only samples engraved into one specified material, we can choose another approach suitable in particular for this material. As an example, we can bring the minimal height computation method (5.1.1) and usage of its results as a cross-section lines position for samples engraved into steel.

a) b) c)

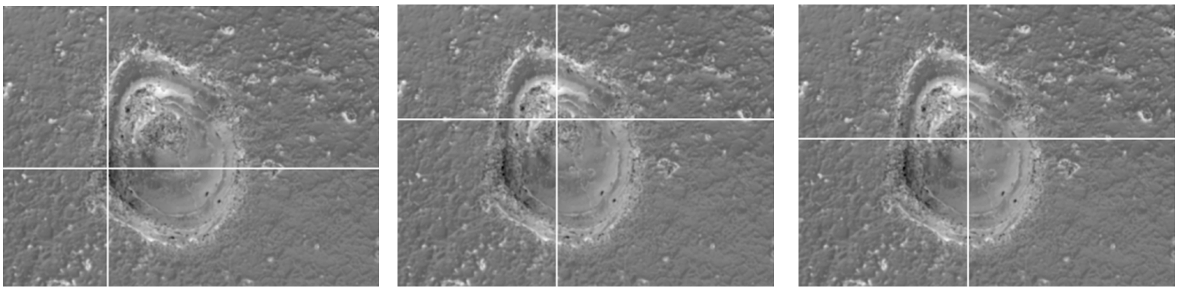

Fig. 91: The cross-section lines positions computation as a) the minimal height; b) a centre of mass; c) a centre of detected pulse area for sample B.

a) b) c)

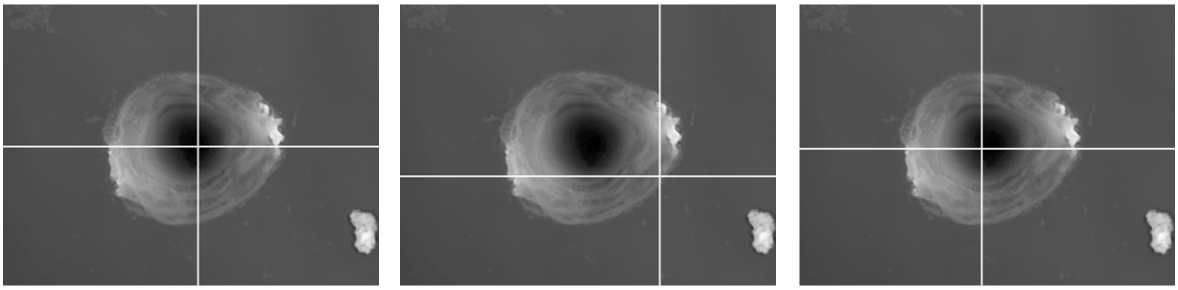

Fig. 92: The cross-section lines positions computation as a) the minimal height; b) a centre of mass; c) a centre of detected pulse area for sample F.

7 Experimental Verification by the Simulation Tool

Reasons which lead us to create the simulation are outlined in Section 2.2.2, possible approaches in general are discussed in Section 2.2.3. Development of approaches and concrete techniques and methods which could be used for the simulation is described in the following sections. Although the simulation itself was not the main aim of this thesis, we had to test all the designed methods described in Chapters 3 and 5 and so we have prepared an exploration and simulation tool. Its main functions are summarized in detail in Chapter 9. Both simulation techniques outlined in the following sections are implemented into the tool. These simulation models are simplified in comparison to the complete simulation described in Section 1.1, but for all that they show convincingly, that the designed algorithms work well.

As it was described in [Háj08a], originally, we have planned to use a simulation technique based on the pulse extraction and its further progressive application on the surface of the sample. But as it was discussed in Chapter 1, the simulation itself should not be solved as a main part of this thesis and only methodology for the automatic heat area detection and sample parameterization should be handled. That is why we were further not interested in the simulation a lot and the designed simulation method is not worked up more in detail. Its main idea is summarized in Section 7.1.

During the sample parameterization, several methods for the laser-engraved samples generation were designed. During testing these methods, we have found out that our results look very promisingly and realistically (for concrete results, see Chapter 4). That is why we are convinced of possible usage of this method in our future approach. Basic suggestions of this technique are outlined in Section 7.2. Possible future extensions of the simulation method are described in Chapter 10.

7.1 Simulation Method Based on the Pulse Extraction

All the time, we have worked with real measured data. An input data set is explored and processed. Also this approach to the laser engraving simulation uses processed real data as input.

In Section 5.2, methods for the heat affected area detection are described. These methods can be used also as a part of the simulation input data preparation. If the area of the pulse is detected, the bordered part of the sample can be selected, further recomputed and saved separately. We call this process a pulse extraction. To enable simulation for various materials and lasers, pulses are extracted from input data for each combination of used material and laser setting that should be used for the simulation.

The selected pulse has to be recomputed and saved in a proper format. As a representation of the extracted pulse surface, the height map seems to be optimal. Moreover, the values describing the pulse surface should enable the pulse to be used for the engraving simulation in the simplest way. After several experiments, it seems to be a good choice to represent the level of the material by the value of zero. All points of the pulse height map have to be recomputed during pulse extraction and saved as a difference of the basic material value and their original height. It means that the final saved pulse consists of positive and negative real values. The positive values represent material above the basic material level, the negative values represent material that has vaporized during the engraving process. An example of a pulse can be seen in Fig. 93. The white color represents basic material zero level, red parts of the pulse are positive values and blue parts represent negative values. The higher is the distance of the value from zero, the brighter is the color. The format of the height map is exact enough, but its disadvantage is constituted by the amount of data which have to be saved for various pulses for different materials.

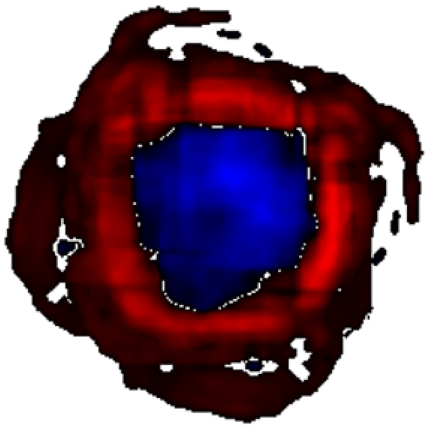

Fig. 93: A pulse representation – white color represents basic material zero level, red parts of the pulse are positive values and blue parts represent negative values.

The basic technique of simulation of samples engraving is to place adequate pulses gained from input data on the right place of the unengraved material surface. The matrix of the pulse height map is simply added to the height map of the surface in a given point during the simulation. Pulses can be placed also over each other to simulate engraving of a different number of laser pulses engraved into the material surface. As described above, format of the pulse is designed for the simplest usage and so it can be directly applied on the material surface. Negative values representing the removed material in the pulse pit are subtracted and positive values of the material on the transition ring are added to the original surface (as can be seen in Fig. 94).

This simple technique is not able to catch the changes in results caused by changing the quality of the material because of material heating during the repeated engraving into one point on the material surface. These processes are described in Section 2.1. That is why not only the real measured samples with one engraved pulse, but also samples with more laser pulses engraved into a single point should be used and combined.

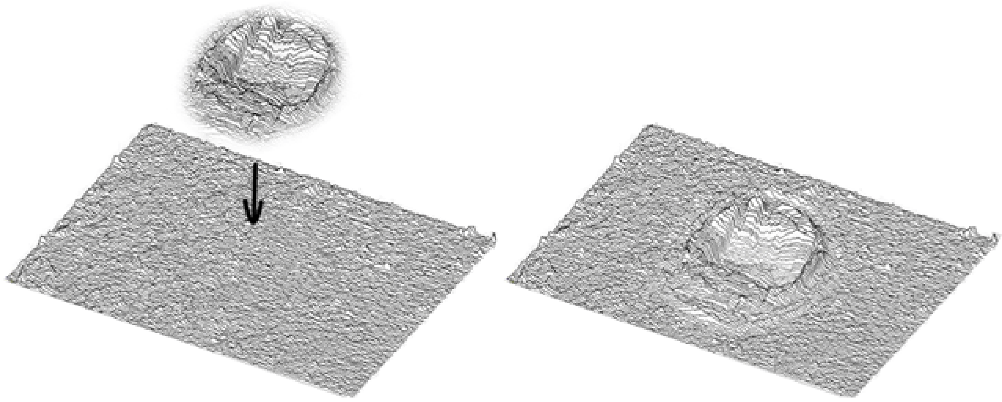

Fig. 94: Material surface before and after simulation engraving of the selected pulse.

Using various input samples leads to more realistic simulation. For example, if a pulse with 10 pulses and subsequently a pulse with 5 pulses is used for the simulation, it corresponds more to the situation where the engraved material is heated after engraving of 10 laser pulses then it cools down and 5 laser pulses are engraved. Of course, the real 15 laser pulses are engraved without any pause, but for the simulation, it can help us to approximate the result better.

Let’s assume a task of engraving a sample with 15 laser pulses into a single point. We can use real measured data for 1, 2, 5, 10 and 20 laser pulses and we have to choose the best way to simulate the engraving process result. There are many possibilities how to combine the input data, e.g. 5 + 5 + 5, 10 + 5, or 5 + 10. The order of pulse engraving is important because the operation of adding pulses is not commutative. The simulation has to accept it and to include it into its computations.

Described basics of simulation method do not deal with the problem of randomly appearing local defects, it solves only the simulation of the heat affected area shape. It also does not handle with the differences of similar samples and others features existing in the real engraving process. They should be discussed in its potential further development.

7.2 Simulation Based on the Sample Parameterization

The main idea of this approach has arisen as a side product of the methodology of pulse parameterization and their further usage for the sample surface artificial generation, which was one of our main aims till now. Because all methods, which we have designed up to now, are described in Sections 3.4 and 3.5, the process of sample generation will not be described here in detail yet. We will just sum up the process shortly. We need to get the real sample description as a set of parameters. These are gained from the real engraved and measured samples in the process of sample parameterization. From the parameters, the smooth sample surface of the sample is generated according to the mathematically described basic shape. To get a real appearance of the generated sample surface, we have to modify the smooth surface with noise and other artificially generated irregularities.

After that, we get a new sample surface, a simulation of the real one. Results of our methods can be seen in Section 4.2.

This approach can be taken as the starting point for the whole simulation technique. First, the simulation model has to be prepared from parameters of the real measured data sets. Let us suppose that we are able to compute the parameters for the real samples automatically. As it was already mentioned in the previous sections, we can also find the trend of parameters in dependence on the number of pulses engraved into the sample surface and on the material used for the engraving simulation. We could improve our methods and design some additional ones, which will be able to form a newly generated sample surface from the set of parameters for any material and any properly described experiment. For all the sets of computed parameters, we can generate a new sample surface and compare it with the real samples, which will be engraved not as the input sample, but just for the purpose of simulation verification.

After validation of the simulation model for pulses engraved into a single point, we can try to deal with engraving pulses next to each other and to search sample engraving modifications for such areas of the sample surface, where two or more pulse parts overlap each other. If we are able to simulate the real shape of several overlapping samples, we can extend it to simulate engraving along any trajectory or, what is more, engraving a continuous area, as it is shown in Fig. 10. We can search for the right description also for other (especially physical) experiments, so that the simulation could be used for the purpose planned in the project, i.e., simulation of an arbitrary described experiment. Of course, all the processes should be fully automatic and reliable before the simulation could be used in the real technological process.

8 System Verification and its Results

To ensure correct function of the simulation system, it needs to be verified. During the verification, engraved samples are compared with the real ones. The real samples for verification are gained by the same method as described in Section 3.1. We can compare and evaluate results one by one visually, but the application has to enable evaluating results automatically.

The manual evaluation is used for single samples. The selected sample is “engraved” by the simulation and compared with another one that is really engraved into the material and measured by the confocal microscope. Depending on the result of the comparison, the simulation can be adjusted.

To test and evaluate the system in a more global way a broad range of samples has to be simulated and compared. An automatic verification is used for speeding the process up. In this phase, whole experiments designed for verification can be evaluated at once. For each single case, several comparison parameters are computed and, based on these parameters, the results can be marked as accurate or problematic. Problematic sample has to be re-operated or the simulation can be further adjusted to get better results.

Because always two samples are compared, the described approaches can be used also for the comparison of two real samples to find out their similarities and differences. We can take advantage of this during the real samples exploration process. A question arises, which parameters to use to represent the difference of both compared samples well enough. Possible methods and approaches are described in the following sections. These methods are also outlined in [Háj08d].

8.1 Samples Comparison

During the verification, two samples are compared. At the beginning, we should discuss possible variants of samples and location of the pulse in the sample. Pulses can be shifted against each other, they can be scaled or they can have even a different shape. Several basic possibilities are shown in Fig. 95 from the top view and in Fig. 96 from the side view as simplified cross-section curves. In both figures the first sample (a) is compared with the others. The second compared sample can be, for example, shifted (b), scaled (c) or can differ from the first one in its shape (d). Of course, all these differences can be combined together. We have to decide, which one of the simulated pulses is more similar to the real one and what pulse characteristics influence the difference at most.

Now it is a good time to think about which of the described modifications are the most problematic. The most uncomplicated situation is in the case of vertical shift (Fig. 96b). Both samples can be aligned to the same height by recomputing the surface of the basic material into the same level. Solving of the horizontal shift (Fig. 95b) is a little bit more complicated, but it can be solved by samples overlapping, which is described in Section 8.2. The problem of the scaled sample or pulse in the sample has to be solved by the simulation modification. The worst situation arises in the case, when pulses differ in the shape as visible in Fig. 95d and Fig. 96d. This could be solved partly by changing the input experiment used for the sample parameterization and also by modifying the simulation (or sample generation) itself.

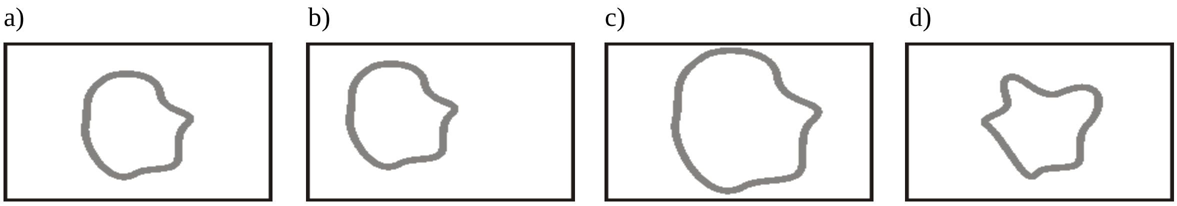

Fig. 95: Possibilities how can a sample (a) differ from another one which: b) is shifted; c) is scaled; or d) has different shape of pulse. All variants are examined from the top view.

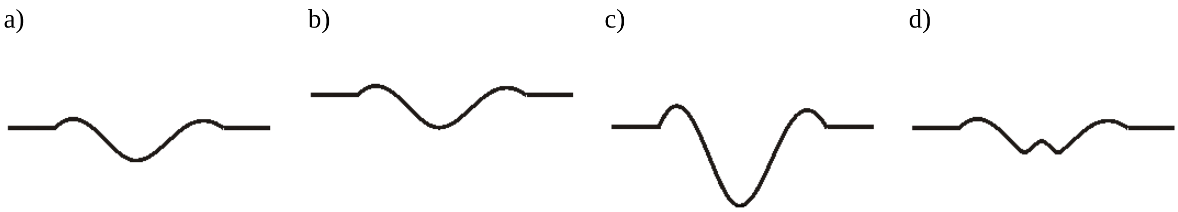

Fig. 96: Possibilities how can a sample (a) differ from another one which: b) is shifted; c) is scaled; or d) has different shape of pulse. All variants are in the form of cross-section curve examined from the side view.

Of course, to get correct comparison results, samples must be saved in the same precision and resolution or they have to be recomputed before the comparison begins. The recomputation is also done in the case when basic material levels of both materials are not in the same height (e.g., because of different thickness of the sample) or if the heat affected areas of both compared samples have to be overlapped. Using these operations, we eliminate shifting of both samples.

On the surface of the sample, the roughness of the original material is visible. Also local defect of the material can change the original surface unpredictably. That is why we would not get a zero difference after comparing two real samples of the unchanged material (samples without any pulses) measured in different places. It shows the fact that even more samples of the same basic material will differ. There can be seen that the roughness of surrounding material can increase rate of inaccuracy of compared samples. This happens also in the case of samples in which the pulse fills the majority of the sample surface. To increase the precision, we should try to evaluate only the area of engraved pulses and their closest surroundings. For this purpose, the methods and techniques used for automatic pulse detection in the sample described in Section 5.2 can be used successfully.

Another question is what to do in the case of different dimensions of the samples (Fig. 95c). If the sample sizes differ, but the whole engraved areas are correctly detected, they can be resized and compared.

Let's suppose that we have detected engraved areas successfully in both samples and we want to compare them. Even though we expect only minimal space around the engraved area it is necessary to overlap both samples over each other, so that we really compare only engraved areas. Usable methods, possibilities and problems of samples overlapping are described in Section 8.2.

Samples are represented as height maps and so the problem is about to compare two surfaces described in the form of uniform rectangular grid. This representation can be transferred into the format of grayscale image. It is the reason, why the problem of two engraved samples comparison can be solved by methods and algorithms applicable for image comparing [Zapl07]. Methods based on image comparison are not the only possible way how to solve the problem of sample comparing. The usage of the Principal Component Analysis, which is outlined in Section 8.1.4, seems to be a promising approach.

We have to decide which information to get as the result of the samples comparison. Some methods return one value, which expresses a total difference of both samples. Such methods are suitable for automatic verification. Another group of methods shows difference as the whole image (or image part) and enables better localization of problematic parts. However, they are unsuitable for automatic processing.

In the following three sections, the methods used for images comparison, which can be after some modifications used for samples comparing, are described and their usage is demonstrated on concrete samples. However, because methods for the samples comparison were not the main topic of this Ph.D. research, not all possible solutions were discussed, but only some of them, which were sufficient for the simulation system verification and real data exploration.

8.1.1 MSE

This method computes the mean square error (MSE) of both samples. It is defined as the difference of pixel heights of samples squared for error highlighting. Differences for all pixels are summed and divided by the sample surface dimension. The resulting value expresses the average error of each pixel. The computation is given by Equation (8.1), where *W* and *H* represent the width and height of the samples, *sampleAl(i, j)* and *sampleB(i, j)* indicate single points at the given position in the sample height map grid.

$$MSE = \frac{1}{W \times H} \sum_{i=0}^{W-1} \sum_{j=0}^{H-1} \left(sampleA(i,j) - sampleB(i,j) \right)^2 \qquad (8.1)$$

It is easy to see that the more identical samples, the lower result of MSE method is computed. Let us compare two real engraved and measured samples with the same pulse counts from the real experiment (5 pulses engraved into one point into steel; shown in Fig. 97a,b). Samples are very similar, but nevertheless they differ a little. The MSE for this case reached the value of 0.385. In the other case, we compare two absolutely different samples (sample with 5 and 50 pulses engraved into one point into steel; shown in Fig. 97b,c); MSE = 4.186.

a) b) c)

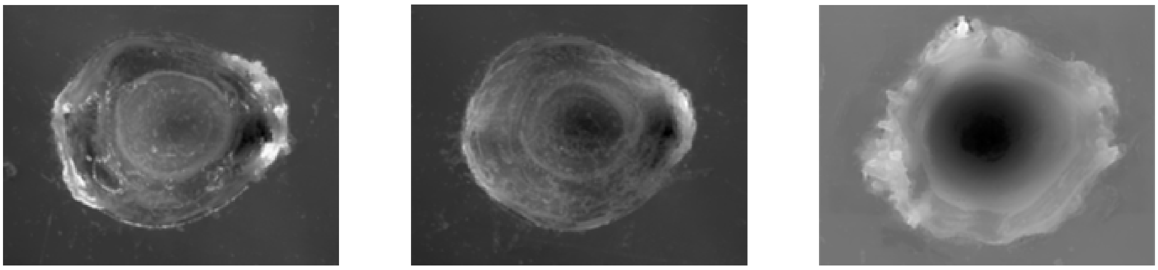

Fig. 97: a-b) Two similar samples with 5 pulses engraved into steel; c) sample with 50 pulses engraved into steel.

Results of MSE computation for the sample height maps are much smaller than in the case of grayscale images. The reason is simple, gray scale images consist of values in the interval <0, 255> while values representing the sample surface reach the maximal values of about a few tens. Moreover, before the computation itself, basic levels of both samples are shifted to the same height, and so the differences among values of both samples come more near. After the sum of individual differences is divided by the total dimension of the sample, the result ranges typically between 0 and 10.

During the MSE computation for the whole sample a computational error arises. It results from the number of points on the basic material level, which do not neighbor the pulse area directly, but where the zero difference is computed. These points do not add any increment into the total sum, but they are included into the sample dimension and so they distort the result. That is why to get the most accurate results it is important to compute the MSE only in the area of pulse. For the purpose of the automatic pulse detection algorithm described in Section 5.2 can be used.

8.1.2 Difference Image

Difference image is in its principle a visualization of the MSE. The color of a pixel is defined as the difference of heights of both samples at the corresponding position recomputed to the grayscale interval. The relationship can be simply described by expression (8.2), where *min* and *max* represent minimal and maximal values of difference. The method differs a little from the typical difference image computation, where the absolute value of difference is used. By this modification we preserve information about the order of sample heights (we can find out from the image which sample has the higher value representing the surface in the given pixel).

$$dif[i,j] = 255 * \frac{(sampleA(i,j) - sampleB(i,j)) - \min}{\max - \min} \tag{8.2}$$

The color of the basic material level represents the level of zero difference; all points which are darker are the places, where the sample B surface was higher than the surface of the sample A. In the opposite cases, where sample B does not reach heights of sample A, the pixel is lighter. The points with biggest difference have white (sample A is higher) and black (sample B is higher) color.

The results of comparison of the samples described in the previous section are shown in the following images. Two different samples with 5 pulses engraved into one point were compared and its result can be seen in the left column of images. The comparison of sample with 5 pulses and the sample with 50 pulses are placed in the right column. All samples are engraved in steel. Difference images are shown in Fig. 98a. Together with difference images, the horizontal cross-section curves going throw middle of the samples are also shown. In Fig. 98b, cross-sections of difference images are visualized and in Fig. 98c cross-sections of both simulated (black curve) and real (gray curve) sample are presented.

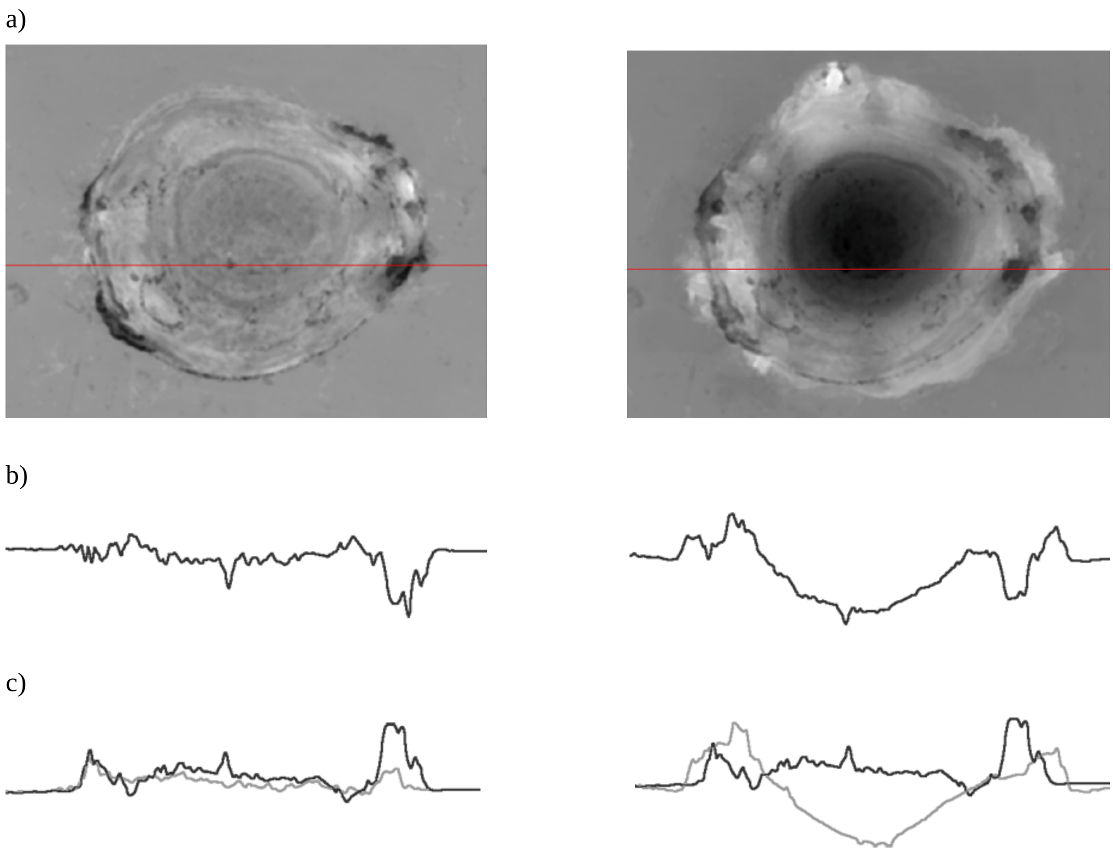

Fig. 98: Difference images of two similar samples comparison (the left column) and two very different samples (the right column): a) difference images; b) horizontal cross-sections of difference images; c) horizontal cross-sections with curves for both simulated (black curve) and real (gray curve) sample.

8.1.3 Logarithm Operator Adaptation of Difference Image

For difference images with a broad range of values, small differences can not be distinguished well, because they are represented by very similar or even the same gray color in the image. If we are interested in these small differences, we have to highlight them. It is possible to do so using the logarithm operator [LogOnl]. The logarithmic function is used as a mapping function for modifying the difference image. It means that during this operation each pixel value is replaced with its logarithm.

The Equation (8.3) is typically used for logarithmic modification of images. It expresses a logarithm operator mapped on the standard difference image with the absolute value of difference. The basis of logarithm does not influence the result; there can be used for example natural logarithm or the base of 2 or 10 logarithm. The multiplicative constant of the expression ensures scaling to values in the interval <0, 255> representing shades of gray. Because the logarithmic function is not defined for 0, the value of 1 is added to the parameters of logarithmic function used in the expression.

$$difLog[i, j] = \frac{255}{\log(1+255)} * \log(1 + Abs(sampleA(i, j) - sampleB(i, j))) \tag{8.3}$$

As described in the previous section, the modified algorithm for the difference image computation is used for the samples comparison. That is why also logarithm operator has to be used in a modified way. We have to distinguish points, where the height of sample B is higher than the surface of sample A (such points are in the difference image placed under the zero level) from the opposite case. So, we have to apply logarithmic operator separately on the points above and under the zero level.

The modified Equation (8.4) goes from the value *dif[i,j]* computed by the Equation (8.2). The value *M* is computed for each case separately as a number of gray colors between the material basic level and maximal difference in the relevant direction. For example, if the basic material level is represented by the gray color with intensity 160, all pixels above the material are spread into 95 levels. The other values are recomputed into the interval <0, 159>. The value of the fraction at the beginning of the expression on the right side of the equation differs for converting the points above and under the level of the original material.

$$difLog[i, j] = \frac{M}{\log(1+M)} * \log(1 + dif[i, j]) \tag{8.4}$$

The results can be seen in the following images; in Fig. 99a, the original difference image is shown; in Fig. 99b, the difference image modified with the logarithmic operator can be seen. The difference of both images is visible well. The original difference image defines the color equally in dependence on the displayed color. From this representation we can get good imagination of heights distribution. On the other hand, from the logarithmically modified image, we can find out small differences in the neighborhood of the material level better.

a) b)

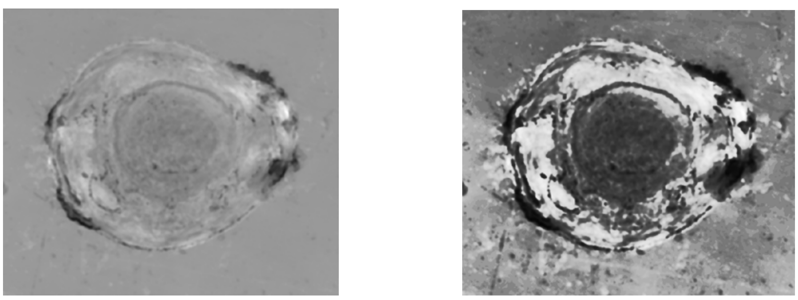

Fig. 99: Difference images of two compared samples a) the original difference image; b) difference image adapted by the logarithm operator.

8.1.4 Principal Components Analysis

Principal Components Analysis (PCA) can be used as a powerful tool for data analysis. It bases on computation of the eigenvectors and eigenvalues which help to identify patterns in data. The data set is expressed in such a way that similarities or differences are highlighted. PCA seems to be a promising approach for the comparison of samples. All peaces of information for this section were gained from [Smith02], where the whole method is explained in a very understandable way. That is why we will not describe here the whole method in detail, but just several main features will be outlined.

The method runs in several steps. At the beginning, data has to be loaded. An example of the original data set is visible in Fig. 100a. To get a data set with the mean value of zero (which are used in PCA), all values have to be shifted in each dimension by the mean value (by subtracting the average in all dimensions). An example can be seen in Fig. 100b. From the n-dimensional data set, the covariance matrix of dimension $n \times n$ is calculated and n eigenvectors and eigenvalues are computed. All eigenvectors are orthonormal (i.e. they are perpendicular to each other and have the unit length) and one eigenvalue belongs to each eigenvector.

a) b)

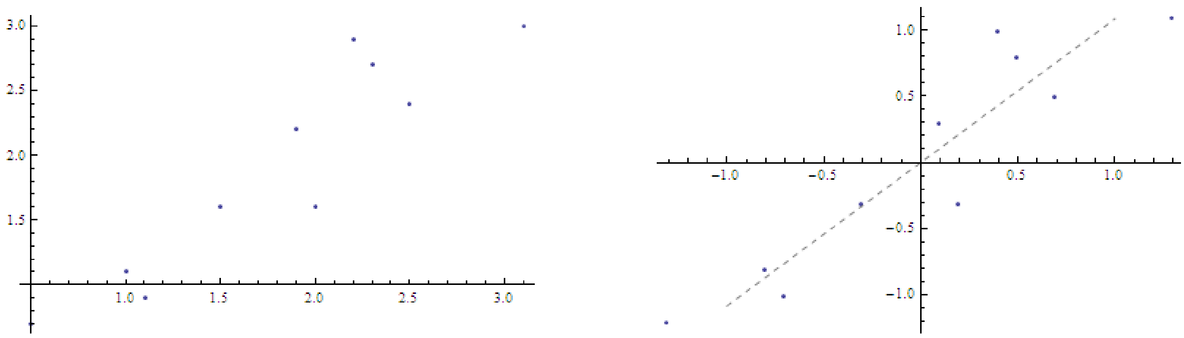

Fig. 100: Visualized data in various phases of the PCA method: a) the original data; b) data shifted into the position of zero mean.

The computed eigenvectors represent patterns in the data set. The eigenvector with the highest eigenvalue (called the principle component) determines the main direction in which the data is placed. If we sort all eigenvectors by their eigenvalues, we get the sequence where the vectors at the beginning have a significant influence on data distribution while the last eigenvectors affect the data distribution minimally.

The computed eigenvectors are orthonormal and so they can form a base of a new coordinate system. At this time we can transform data into the new coordinate system. We can use all dimensions or we can ignore several eigenvectors with the lowest eigevalues and so reduce the number of dimensions. The main reason is the elimination of tiny differences in dimensions with a low influence. The result of data from the example derived into the new coordinate system is shown in Fig. 101a. Before the transformation the minor eigenvector was ignored. It returns the original data just in the direction we have chosen. In fewer dimensions, it is easier to compare samples with each other.

Of course it is also possible to transform the data back into the original coordinate system. If we have ignored some eigenvectors, some information from the data is lost (as can be seen in Fig. 101b); otherwise we get the original data.

a) b)

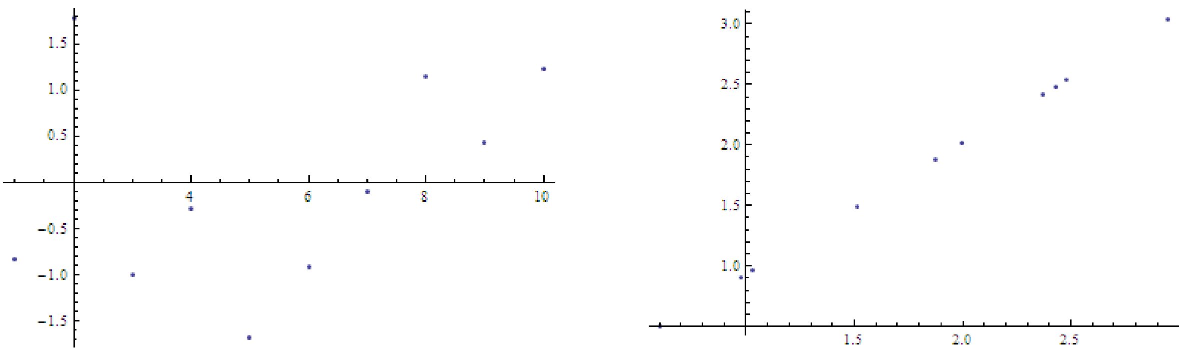

Fig. 101: Visualized data in various phases of the PCA method: a) data transformed into the new coordinate system after ignoring the minor eigenvector; b) data from Fig. 100a derived back into the original coordinate system.

For the representation of the height maps for the PCA processing each sample should be represented as one vector. It can be done by putting all sample rows after each another to create a vector of the length $M \times N$ (where M symbolizes the number of rows and N the number of columns of the sample). For all images that we want to compare, we have to create such a vector representation and from all these vectors, a matrix is composed – each image vector creates one matrix row. Then the covariance matrix has to be computed and for the covariance matrix the eigenvectors and the eigenvalues are determined. In the next step, the original images are recomputed into another coordinate system derived from the PCA. After the PCA analysis, the difference of images can be measured along the new axis.

The PCA method is successfully used for faces recognition [Zhang97], so maybe it could give results usable also for our problem. Proving it is the next task for the future research.

8.2 Samples Overlapping

To get the optimal result for simulation verification, it is necessary to overlay engraved pulses as exactly as possible. Otherwise, the error of comparison is growing in dependence on the relative shift of the engraved area in the samples. Manual overlapping is possible, but it can not be used for automatic verification and evaluation of results. That is why the system has to be able to find the best matching position independently.

One possible way how to match pulses automatically is to compute any parameter representing the difference of both samples (e.g. MSE) in a given position for all possible positions of both samples. It could be the optimal solution, if we were not concidering speed. That is why we have to reduce the number of repetitions as much as possible, but at the same time we have to preserve sufficient accuracy of the result.

First, we can eliminate all the positions in which only the borders are overlapped (as shown in Fig. 102). We can suppose that among these combinations, no optimum will be probably found.

We have to find the best starting position (a guess of optimal position of overlapped samples) and from this position, we have to start searching the real optimal position of the overlaid samples in its surrounding. We can use, for example, the centre of mass as the starting position (the method of centre of mass computation is described in Section 5.1.2). The centre of mass can be computed for both compared samples and samples can be shifted to overlay their centers of mass. Another approach offers the usage of the method of automatic pulse detection (possible approaches are outlined in Section 5.2) to detect pulses in both samples and to overlay the selected areas. In the second approach we can directly take the advantage of the pulse detection for the faster difference computation only in the selected area.

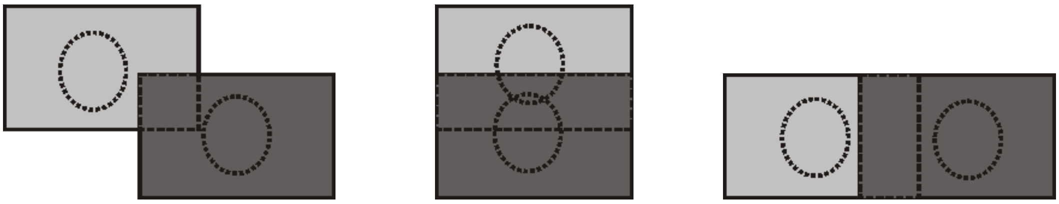

Fig. 102: Positions of the overlapped samples which can be most likely excluded from searching for optimum.

After finding the starting position, we just have to find the optimum by small shifting of samples over each other. In the further positions, the step for shifting is rougher, in the close surroundings the shift step is decreased. For each of these combinations the difference of the samples is computed and that is why the algorithm of difference parameter computation has to be quick enough to get some computation speed-up.

9 Data Exploration and Simulation Tool

In the research oriented to lasers and their usage, various sophisticated physical experiments have to be provided. Experiments are engraved, they can be measured and during the measurement, a detailed exploration of the results can be provided. Unfortunately, no appropriate tool for the subsequent visualization and comparison of measured samples data exists. That is why we were asked to prepare a data explorer and a system for the engraving process. The simulation should provide results as quick and cheap as possible. Moreover, it should enable optimization and elimination of unfeasible experiments. As a part of the simulation, an application for data visualization should also be implemented.

The first thing to be solved within the project was data preparation and processing. Because no tool for data exploration and its modification was available so far, we had to start development of a new software tool that would help us with data processing. Many functions for pulse detection, samples visualization, modification or comparison were required. Plenty of functions, which were grouped into several categories, were designed and implemented. The most often used functions were matched with key short cuts for easy usage. Thanks to internationalization, the tool can be translated into another language without any problem.

The tool works in two modes of data processing. The first one, which is described in Section 9.1, serves for sample viewing and exploration. In this mode, heat affected area of the sample can be detected, statistics over the sample are computed, samples can be measured or the cross-section curves can be explored. As a part of this way of research, the Laser Samples Explorer [LaSE_SW] was created. This tool is used also by our colleagues from the New Technologies Research Center for exploring the real measured samples. Besides the samples exploration, the pulse parameterization and artificial generation of new samples can also be provided in this mode.

The second mode serves for the samples comparison and result verification. It can be used for the comparison of real samples and the artificially generated samples. Details of this functionality are introduced in Section 9.2.

9.1 Sample Exploration

The sample exploration mode offers a broad range of functions for sample exploration and data preprocessing. For the sample preprocessing, a height map representation is loaded from a file and visualized. Format of files that can be processed is described in Section 3.2.

The sample can be explored in many ways. The main window offers a 2D visualization of the sample. The sample is shown in three views in the direction of three basic axes of the coordinate system. The part of the main window can be seen in Fig. 103. In the central part of the window, the explored sample is represented as a grayscale image. The intensity of the gray color reflects the height of the surface at the given position. The highest point of the sample is represented as a white color, the lowest point is black. To view the sample from the orthogonal directions, the cross-section curves of the surface in the vertical and horizontal direction are used. They are placed in the left and the bottom part of the window. In the left part of the window the cross-section in the vertical direction is projected, in the bottom part the horizontal cross-section curves can be seen. Both cross-sections are in the central window with the sample top view represented as two orthogonal (blue and red) lines. They show the column and row that are visualized in the form of cross-section curves.

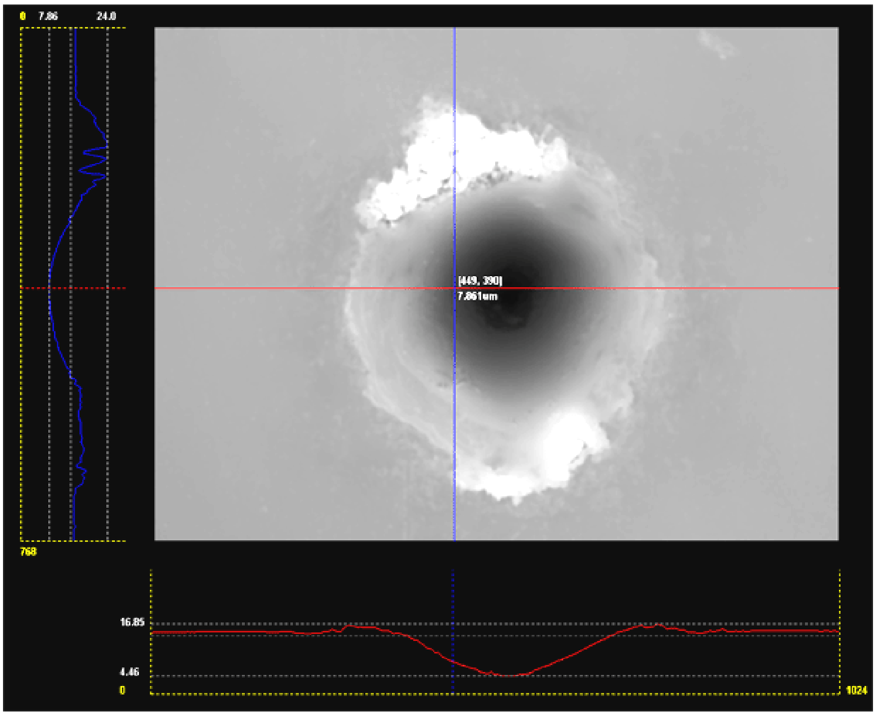

Fig. 103: 2D visualization of the explored sample – the top view represents the gray scaly image of the sample, in the left and bottom part, vertical and horizontal cross-section curves can be seen.

At the crossing of both lines, their image position and the real height of sample at the crossing point are given. The cross-section curve reflects the relief of the surface of one column or row of the sample. For both vertical and horizontal cross-sections, the maximal and minimal values are marked. The position of the cross-section lines can be changed by dragging the mouse or by using the user interface of the control panel in the right part of the main program window. In the control panel, both real and image units of placing the cross-section lines are indicated. The position of the cross-section lines is determined automatically after the automatic detection of the pulse into the position for sample parameterization (see Section 5.3).

Except the cross-section curves parallel with basic axes described above, the sample editor offers also the possibility of viewing the surface profile in any other direction. After setting end points of the line segment, the curve of surface cross-section along this line is visualized in a stand-alone window (see in Fig. 104a). The line segment between two defined points has to be computed and so we have to implement any algorithm for the line segment rasterization. For this case, DDA (digital differential analyzer) algorithm, described in [Žára05], was used.

For samples exploration, it is very useful to use any tool for lengths and depths measuring. That is why the tool of ruler is implemented into the system. It enables to measure distances in all views of the explored sample. The results of the measurements are given in real units. Using the ruler is simple and if the tool is activated, the user can measure distance by setting two points with the right mouse button clicks. The size of the pulse (width and length) can be measured in the central top view (see Fig. 104b). In the vertical and horizontal cross-sections, the ruler can be used for measuring the pulse depth. The result of cross-section depth measurement gives the difference between two points of the curve.

a) b)

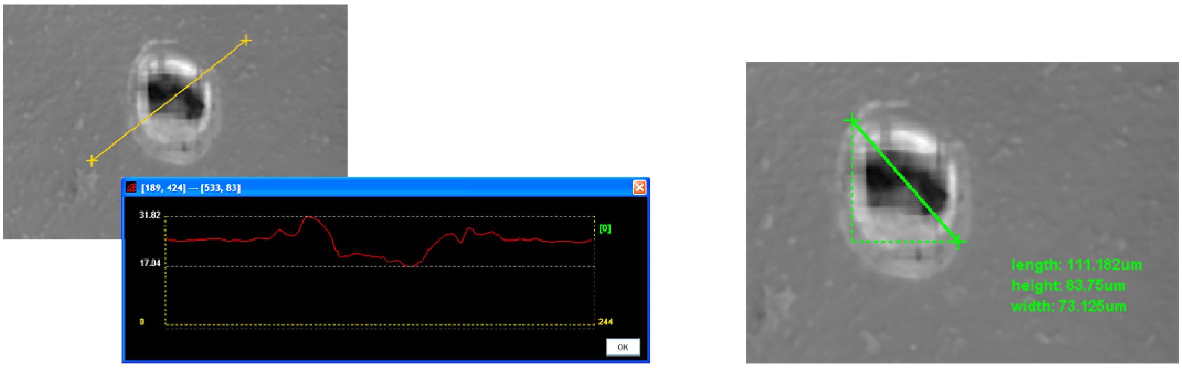

Fig. 104: a) Visualized curve of the sample surface cross-section along the line segment in a separate window. b) Size measurement of the pulse in the top view, distance of two points is measured in the real units.

For better knowledge of the sample surface height, the gray scale indicator can be activated. It shows the minimal and maximal height of the sample, which are represented black and white, and the gray scale between them (as shown in Fig. 105). The small horizontal line moves in the gray scale and it shows height of the point which is currently at the mouse cursor position. If the mouse cursor does not move over the sample top view, the actual height of the point on the cross-section lines intersection is represented by the movable horizontal line.

To have another view on the sample, it is possible to use a 3D visualization. Thanks to the mouse motion or using arrow keys, the viewing camera is rotated, moved or tilted to get the best position for exploring the sample. The spatial view on the sample surface offers a better imagination of the real sample surface shape. By rotating the camera and moving the sample, it can be explored perfectly from all sides. The 3D visualization is shown in Fig. 106. For the 3D visualization, we use OpenGL [Wrig04], [OGLOnl] and because the whole system is implemented in Java, for conecting OpenGL and Java, we use JOGL (Java for OpenGL) [JOGLOnl]. Its basics are described in [Tich07].

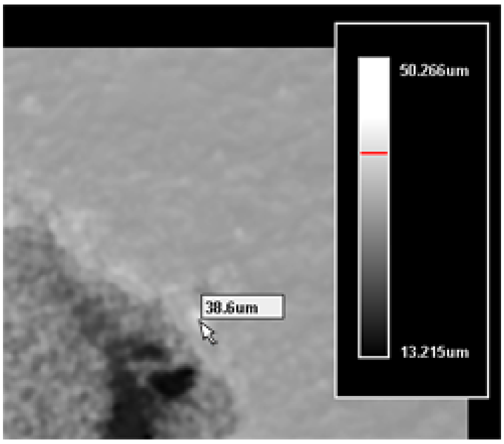

Fig. 105: Gray scale indicator shows actual height of the point at the cursor position as the red line in comparison with heights of the sample.

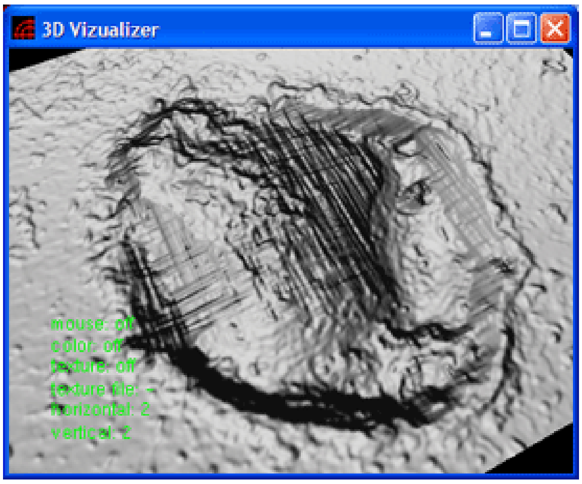

Fig. 106: 3D view on the sample.

Another very useful function for sample exploration is the statistics computation. Sample statistics information contains not only the basic values of sample dimension, minimal and maximal height of the surface, but also volumes of the pulse parts under and above the basic level of the material are computed. The results represent the amount of material which has vaporized (the volume of the pit measured under the basic material level) and the amount of material that creates the transition ring of the pulse. To get maximally exact result, two values are computed. The first one is computed for the whole sample and the second one only for the area of selection that borders the heat affected area of pulse. Volumes are computed by applying numeric integration.

Because in the sample viewing mode the heat affected area can be automatically detected, a function of sample part selection is needed. The selection function is used quite often and so it has to be manipulated in a direct and simple way. The borders of the selection can be changed manually by dragging the mouse in all 2D views. Another way how to set the border position exactly is to set selection border values in the right control panel of the window. Selection borders are changed automatically after the automatic pulse detection. The selection dimension is computed also in real units, the information about the selection dimension is written in the right control panel.

An example of the visualized sample with detected pulse (both the heat affected area and cross-section lines position) is shown in Fig. 107. All three views of the 2D visualization of the sample are shown; the pulse is bordered by the rectangle of the selection.

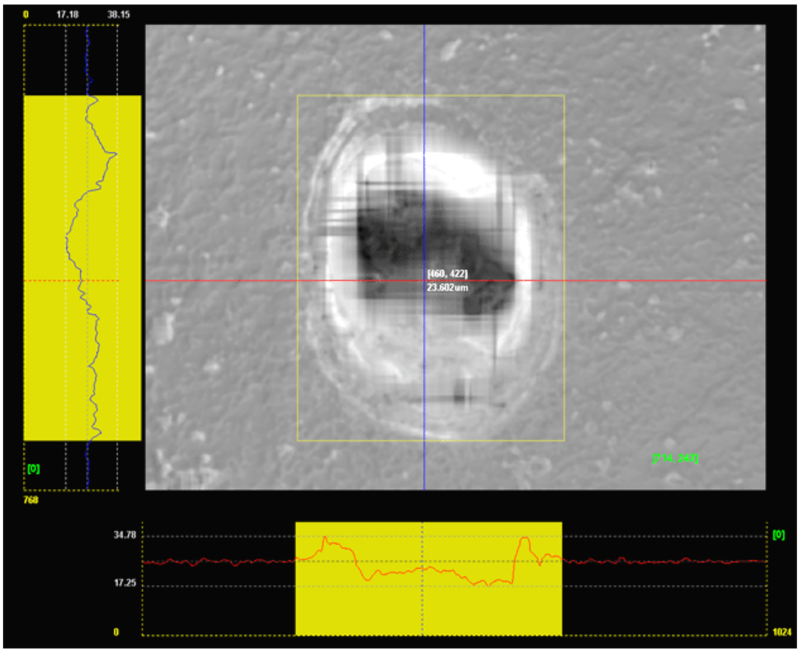

Fig. 107: The visualization part of the main window of the editor in the sample viewing mode; detected pulse is bounded by the selection rectangle.

Except exploring the real samples, also its parts can be saved as new samples, or the whole sample can be used as a gray scale image to be used for other purposes. It is also possible to export values of each visualized cross-section curve.

One of the most important functions of the simulation tool is the approximation of the loaded sample by the mathematically generated smooth surface, which is modified by methods described in Section 3.5. Before the sample simulation, the real sample is parameterized and according to these parameters a new sample is generated. The generated sample can be further explored, saved as a new sample or compared directly with the real sample.

9.2 Results Comparison

This mode is used for the results exploration and comparison and for the simulation verification. It enables to compare any two samples and to determine the size of their difference. Description of the simulation verification, its possibilities and problems are particularized in Chapter 8.

Before the comparison itself, we need to recompute the basic material levels of both samples to the same value. During the samples comparison the MSE (Mean Square Error) is computed to give information about similarity of both surfaces. The computed value is written in the right control panel. The MSE is computed for the whole sample and for the area bordered by the selection rectangle.

For the system verification both samples have to be compared in the position where engraved pulses overlap over each other in the most precise way. Reasons and methods of samples overlapping are outlined in Section 8.2. In the created system, both manual and automatic overlapping of samples is implemented. The manual sample shifting is provided simply by the mouse dragging.

Our tool enables to compare two samples and to visualize them in three possible ways. The user can choose during the results exploration from three ways of visualization: both compared samples shown together, the visualization of the standard difference image or the logarithm operator adaptation of the difference image.

The first visualization way shows both samples together in one window and enables to compare them directly. Each sample is highlighted by another color for better differentiation. The result of this visualization approach is shown in Fig. 108. The top view shows all parts of the sample which are higher then the surface of the second one; in the cross-section windows, both cross-section curves are shown. The blue pixels in the top view show points where the simulated sample is higher than the real one. The cross-section curves of the simulated sample are red and blue, for the real sample the yellow and green colors were chosen.

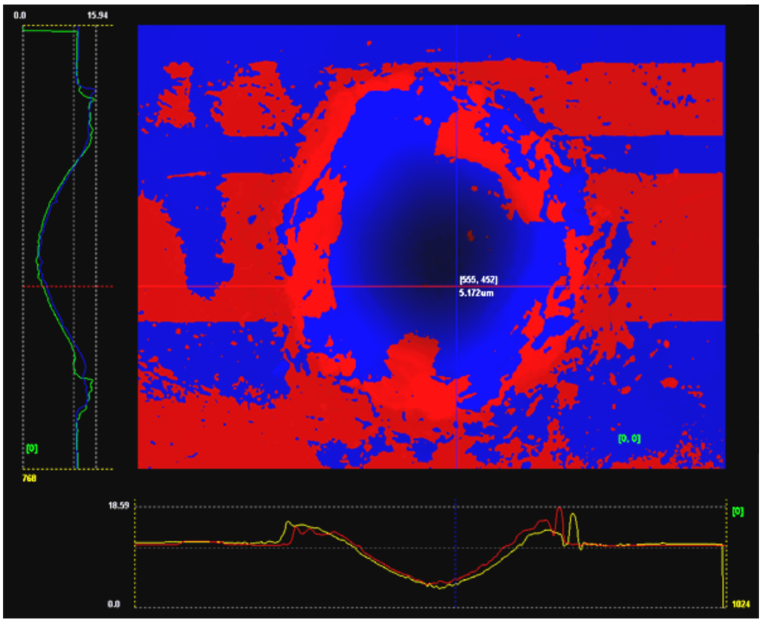

Fig. 108: Comparison of two samples visualized in the way of simultaneous visualization of both samples.

The second way of the comparison visualization is the standard difference image. The computation of the difference image is described in Section 8.1.2. Result of comparison of two similar samples can be seen in Fig. 109. From standard difference image, the distribution of height differences is visible well, but it is not easy to distinguish small changes, because they are displayed with the very similar or even the same color. These disadvantages are removed in the logarithm operator adaptation of the difference image. Its computation is outlined in Section 8.1.3. A result can be seen in Fig. 110. Because each way of comparison visualization brings several advantages and disadvantages, the implemented tool offers the possibility of choice.

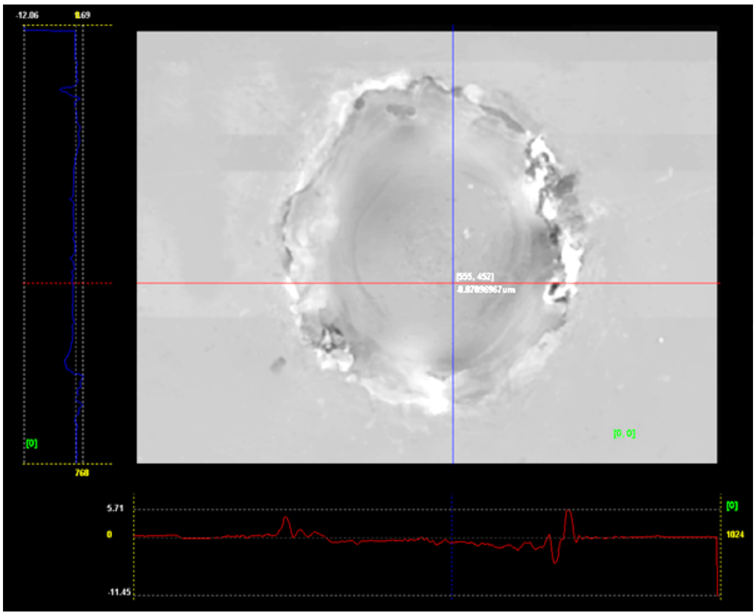

Fig. 109: Comparison of two samples visualized as a standard difference image.

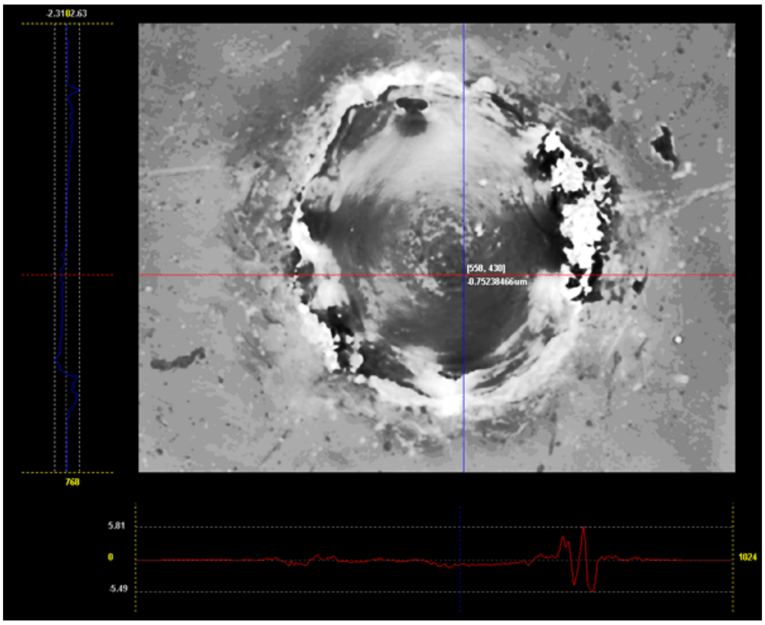

Fig. 110: Comparison of two samples visualized as the logarithm operator adaptation of the difference image.

10 Possible Ways of Future Research

As described in the previous text, the whole project includes many tasks to be done. We will not deal with all future plans of the project, but we will focus on plans from the data processing and simulation part. Some of them are solved in this thesis, but a lot of work should be done in the future research. The other (especially physical and hardware) parts of the project have of course their own individual plans for the future. Our future plans are divided into several groups in dependence on which activity they are related to.

10.1 Simulation

One of our most important aims for the project is to create a simulator of the laser engraving process. The main task is to get as realistic results as possible, and so we should create all important simulation components to make the whole system better and get a maximum accuracy of the simulation. Some of the tasks are connected with automation and program self-activity (they are described separately in Section 10.2), some of them depend on the ability of sample description (for more information see Section 10.3). Also steps related to including the material heating outlined in Section 2.1 into the simulation should be taken into account.

As written above, the data acquisition from the real experiments is time and money demanding, and so we want to minimize the amount of the real experiments required for a satisfactory system setting and verification. It is important to define the minimal required data set for the most often used materials and also to determine the requirements and parameters for experiment design that any new material should be used in the future.

Another challenge for the future research is the simulation of several pulses placed next to each other (creating the trajectory), which has a number of problems (e.g., starting and finishing laser motion inaccuracies) to be solved in the future. These problems are mostly related to the used mechanical parts of the laser, which are not currently specified and will be solved in the future.

Also the other simulation features and problems described in Section 2.2 have to be researched to finish the whole simulation, so that it could be used in the project.

10.2 Automation and Program Self-Activity

The whole system should work as automatically as possible. That is why all the subtasks of data processing should be self-acting in a maximum possible way. Of course, the reliability and speed of the system must be preserved across the automation.

At first, before the simulation itself is provided, we have to get input data. The basic level of the material has to be determined for each sample and then all pulses are automatically detected, samples are parameterized, and pulses can be extracted from the samples. All samples from the experiment should be processed automatically at once.

The first important aim of this thesis was to design methods for sample parameterization and further sample generation. Our development is described in Chapter 3. Till now, we still have not solved the automation of the whole pulse parameterization process, especially the determining of the sample roughness parameters optimally. Our future plans are described in Section 10.3.

Well working methods for the automatic pulse detection, which are reliable for the majority of processed samples, are described in Section 5.2 and their results are shown in Section 6.1. Regardless of them, we should keep working on the research in the field of automatic pulse detection in order to get method reliable for all samples.

Finally, to verify the system, the simulated samples must be compared with the real ones. Because pulses are not placed at the same position in the sample (as described in Chapter 8), it is necessary to overlay pulses over each other in the most accurate way. This operation is very time demanding and we have to find any suitable algorithm that quickly and exactly overlays both compared samples and determines the similarity of the real and the generated sample. In addition to searching for a new algorithm for samples overlapping, we can try to use a complete different approach of samples comparison that will be not based on comparison of raster images as the methods described in Section 8.1. One of the promising approaches seems to be the Principal component analysis described in Section 8.1.4.

10.3 Sample Parameterization

The way of real sample approximation and an artificial pulse generation process is described in the second part of Chapter 3. Some of the used parameters can be already detected automatically from the real samples. But the others, especially parameters for describing the sample roughness and pulse irregularity are so far set experimentally. In the future research, methods for the automatic pulse roughness parameterization should be designed, tested and implemented into the system.

If parameters can be detected for all the measured samples, we can try to find their dependence and to find a mathematical expression that will be able to describe also parameters for the other samples, which are not really engraved and measured. The dependence can be related to the number of laser pulses engraved into the material surface and also to the material itself which also affects the result of the engraving process. To do that, we will have to engrave various experiments, explore much more real samples and examine the trend of detected parameters values. For some parameters, it will be probably easier as shown in the plot in Fig. 54. For the others, it will be more complicated because of the high irregularity of the described pulse parts. An example was already described in Section 4.1 and the trend of some parameters was outlined in three plots. Then, we will be able to compute parameters for any describable experiment that we will need to.

To be able to create sufficiently general algorithms, all methods and procedures should be tested on a broad range of experiments engraved into several materials using various laser settings. According to the knowledge gained from the particularized experiments exploration, the techniques should be adjusted, so that we can get optimal results for parameterization of any sample.

11 Conclusion

After two and a half year of work, we have prepared a number of methods, which can be used especially for the real engraved and measured data processing and description. All these methods were tested, compared and the best of them are incorporated into a tool for data preprocessing and a groundwork for the simulation tool. For our tests, we can use data sets from experiments engraved and measured for two materials – cermet and steel.

At this state, we are able to explore samples in a very detailed way. The designed methods can be used for the automatic detection of the heat affected area. We are also able to describe the sample with a set of parameters and from their values, we can design a fully artificially generated new sample. In the second part of this thesis, two possible approaches for the simulation technique itself are suggested. Finally, to compare measured samples and our results, some methods for samples comparison were designed, implemented, tested and used for the results verification and real samples comparison.

As described in Chapter 10, we plan to work on the simulation process and improve it as much as we will be able. Moreover, we plan to maximize the self-activity of the system by finding suitable methods for the sample parameterization and other activities, which have to be done manually so far. Also methods for parametrizing unmeasured samples should be searched for and the trends of the measured parameters mathematically described.

To conclude the thesis, we should also summarize the fulfillment of our aims described in the introduction.

The first aim was to prepare a general methodology for the real input data sets processing that would result into the parametric description of a general sample engraved into any material. All these methods are described in Sections 3.4 and 3.5, where also the set of parameters is summarized.

Our second aim has depended on finishing the sample parameterization process that should be further used for the artificial sample surface generation. We have designed a number of methods which should be used for the basic sample surface generation and its modification so that the resulting surface corresponds to the real one as much as possible. The results of a practical usage of the surface generation from the set of parameters can be seen in Section 4.2. To fulfill this aim completely, only the exact computation of the parameters for non-measured samples should be finished.

The third important part of the data processing was the automatic detection of the pulse in any sample surface. Several algorithms were designed and they are explained in

Section 5.2. Their results can be found in Section 6.1, where their advantages and disadvantages are also discussed. The methods for automatic pulse detection can be further used for the automation of sample parameterization or for the validation and verification of the simulation model as outlined in Chapter 8.

For testing all the designed methods and evaluating the real measured and artificially generated samples, a data exploration and simulation tool was implemented. It is described in Chapter 9.

All completely or partly solved parts can be highlighted in the scheme of tasks shown in Fig. 111 with the gray rectangles. The other tasks remain white. The implemented sequences of tasks are symbolized as black arrows, gray arrows show connections, which are not used yet. In the figure, two new dotted arrows can also be found. They indicate the situation after the tasks relations simplification caused by the fact that the simulation model works in a limited mode yet. After finishing the simulation of the engraving process, all the tasks will work according to the original scheme shown in Fig. 1 (page 6).

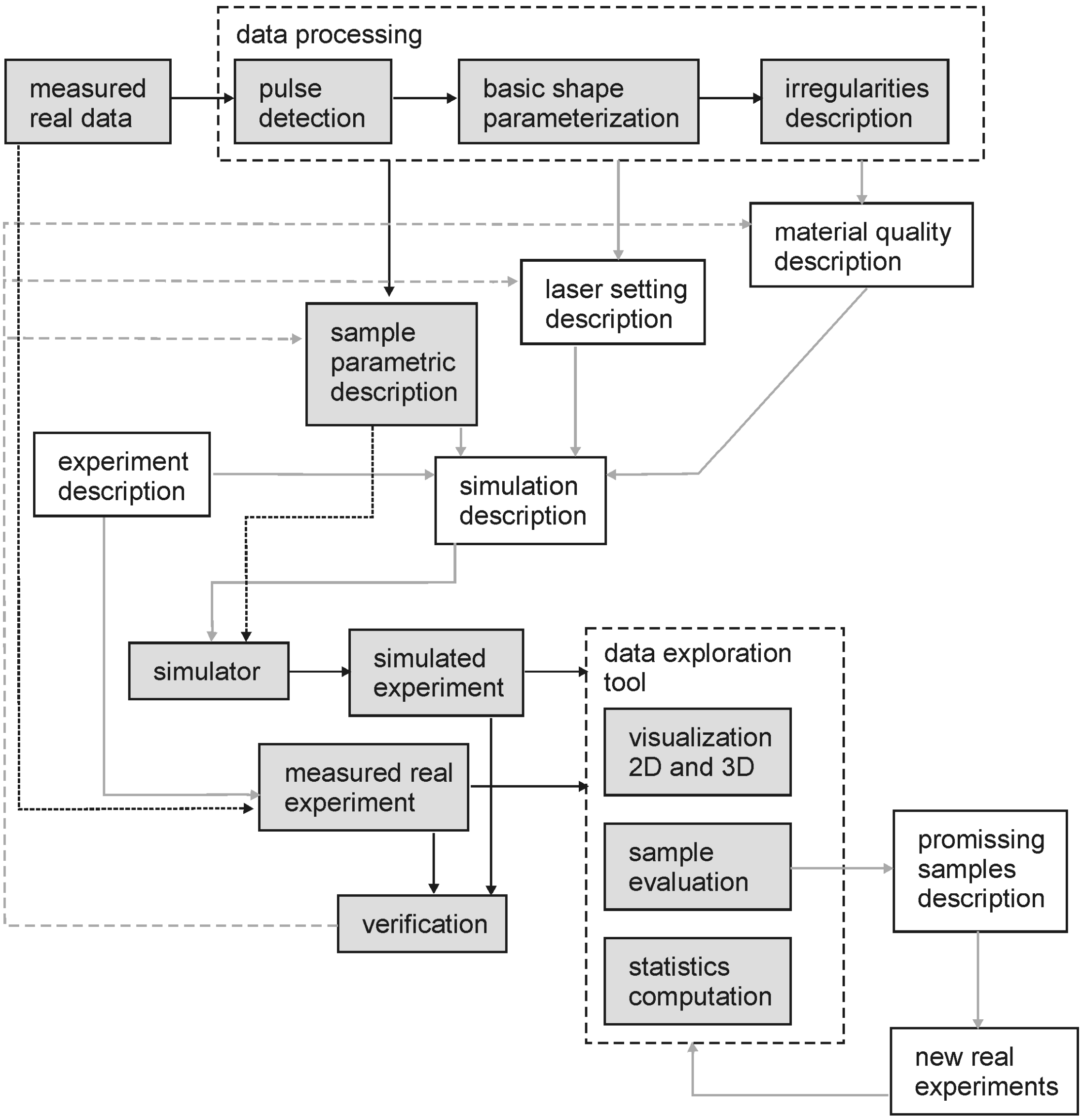

Fig. 111: Sequences of tasks with the solved parts highlighted.

The part of data processing has been solved and, as its result, we gain the parametric descriptions of samples which are used as inputs for the simplified simulation. The results of the sample surface generation are compared with the real measured data and all samples can be visualized and evaluated in the data exploration tool.

References

[Achry05] Acharya, T., Ray, A. K.: *Image Processing: Principles and Application*. Wiley-Interscience. 2005. ISBN: 978-0471719984

[Alex93] Alexiades, V., Solomon, A. D.: *Mathematical modelling of melting and freezing processes*. Taylor&Francis. 1993. ISBN: 1-56032-125-3

[Anis68] Anisimov, S. I.: *Vaporization of metal absorbing laser radiation*. Soviet Physics JETP, Vol. 27, pp. 182. 1968.

[Bäuer00] Bäuerle, D.: *Laser Processing and Chemistry*. Springer Verlag, Berlin. 2000. ISBN: 978-3540668916

[Blell01] Blelloch, E. G.: *Introduction to Data Compression*. [online], [cit. 2008-03-28]. http://www.cs.cmu.edu/afs/cs/project/pscico-guyb/realworld/www/compression.pdf

[Brigh88] Brigham, E. O.: The *fast Fourier transform and its applications*. Englewood Cliffs, N.J.: Prentice Hall, New Jersey, USA. 1988. ISBN: 0-13-307505-2

[Bulg07] Bulgakova, N. M., Stoian, R., Rosenfeld, A., Hertel, I. V., Campbell E. E. B.: Fast Electronic Transport and Coulomb Explosion in Materials Irradiated with Ultrashort Laser Pulses. *Laser Ablation and its Applications*, Springer Berlin/Heidelberg. 2007. ISBN: 978-0-387-30452-6

[Dah08] Dahotre, N. B., Harimkar, S. P.: *Laser Fabrication and Machining of Materials*, Springer, New York, USA. 2008. ISBN: 978-0-387-72343-3

[Dowd09] Dowden, J.: *The Theory of Laser Materials Processing: Heat and Mass Transfer in Modern Technology*. Canopus Academic Publishing Limited. 2009. ISBN: 978-1-4020-9339-5

[Ebert03] Ebert, S. E., Musgrave, F. K., Peachey, D., Perlin, K., Worley, S.: *Texturing & Modelling, A Procedural Approach*, Third edition. Elsevier Science. 2003. ISBN: 1-55760-848-6

[Grig07] Grigoropoulos, C. P., Chimmalgi, A., Hwang, D. J.: Nano-Structuring Using Pulsed Laser Radiation, *Laser Ablation and its Applications*, Springer Berlin / Heidelberg. 2007. ISBN: 978-0-387-30452-6

[Háj08a] Hájková, J., Herout, P.: Laser Simulation, *Proceedings of the 7th International Conference APLIMAT 2008*. STU Bratislava, Slovakia, pp. 823-828. 2008. ISBN: 978-80-89313-03-7

[Háj08b] Hájková, J.: *Pattern Recognition, Classification and Simulation of Laser Beam Impact*, The State of the Art and Concept of Doctoral Thesis, Technical Report No. DCSE/TR-2008-03, University of West Bohemia, Pilsen, Czech Republic. 2008.

[Háj08c] Hájková, J.: LASER SIMULATION - Methods of Pulse Detection in Laser Simulation, *Proceedings of the 3rd International Conference on Software and Data Technologies ICSOFT 2008*. INSTICC, Porto, Portugal, pp. 186-191. 2008. ISBN: 978-989-8111-57-9

[Háj08d] Hájková, J.: Approaches for Automatic Comparison of Laser Burned Samples, *Proceedings of the 9th International PhD Workshop on Systems and Control*. Izola, Slovenia. 2008. ISBN: 978-961-264-003-3

[Háj09a] Hájková, J.: Parameterization of Samples and Its Usage in Data Description and Simulation, *Proceedings of the 23rd European Conference on Modeling and Simulation ECMS2009*. Madrid, Spain. 2009. ISBN: 978-0-955301889

[Háj09b] Hájková, J., Herout, P.: Parameterization of Samples for Modeling of Laser Burning: Increasing the Lifelikeness of Synthetically Generated Samples, accepted to the *4th International Conference on Software and Data Technologies ICSOFT 2009*, Sofia, Bulgaria. 2009.

[Háj09c] Hájková, J.: Data Processing for Simulation of Laser Beam Impact – Statistical Method for the Heat-Affected Area Detection, accepted to *International Conference on Computer Modeling and Simulation*, Brno, Czech Republic. 2009

[Haral92] Haralick, R. M., Shapiro G. L.: *Computer and Robot Vision, Volume I*. Addison-Wesley, Longman Publishing Co., Inc. Boston, MA, USA. 1992. ISBN: 0-201-10877-1

[Hlav93] Hlaváč, V., Šonka, M., Boyle, R.: *Image Processing and Machine Vision*. Chapman & Hall Computing, London, UK. 1993. ISBN: 0412455706

[Hlav01] Hlaváč, V., Sedláček, M.: *Zpracování signálů a obrazů*. Vydavatelství ČVUT. Praha, Czech Republic. 2001. ISBN: 80-01-02114-9

[Hogg06] Hoggar, S. G.: *Mathematics of Digital Images: Creation, Compression, Restoration, Recognition*. Cambridge University Press. 2006. ISBN: 978-0-521-78029-2

[JOGLOnl] Java OpenGL [online], [cit. 2007-04-21]. https://jogl.dev.java.net/

[Klette04] Klette, R., Rosenfeld, A.: *Digital Geometry – Geometric Methods for Digital Picture Analysis*. Elsevier. 2004. ISBN: 1-55860-861-3

[LaSE_SW] *Laser Burned Samples Explorer* [online], [cit. 2009-02-26], authorized software. http://www.kiv.zcu.cz/en/research/software/detail.html?id=32

[Lintech] Lintech Homepage [online], [cit. 2008-02-21]. http://www.lintech.cz/en/

[LogOnl] Logarithm Operator [online], [cit. 2008-03-13]. http://homepages.inf.ed.ac.uk/rbf/HIPR2/pixlog.htm

[Lueb02] Luebke, D., Reddy, M., Cohen, J. D., Varshney, A., Watson, B., Huebner, R.: *Level of Detail for 3D Graphics*. The Morgan Kaufmann Series in Computer Graphic, Hardcover. 2002. ISBN: 1-55860-838-9

[Mitra01] Mitra, S. J., Sicuranza, G. L.: *Nonlinear Image Processing*. Academic Press. 2001. ISBN: 0-12-500451-6

[Nishi06] Nishiguchi, H., Imiya, A., Sakai, T.: Laplacian Based Non-Linear Diffusion Filtering. *Proceedings of 18th International Conference on Pattern Recognition ICPR 2006*, Hong Kong. IEEE Computer Society. 2006. ISBN: 0-7695-2521

[OGLOnl] OpenGL [online], [cit. 2007-09-01]. http://www.opengl.org/

[OlympOnl] Olympus LEXT OLS3100 [online], [cit. 2008-02-21]. http://www.olympusmicroimaging.com/index.cfm/page/products.index.cfm/cid/1085/navid/206/parentid/182

[Perlin85] Perlin, K.: An Image Synthetizer, *Proceedings of the 12th annual conference on Computer graphics and interactive techniques.* ACM New York, USA, pp. 287-296. 1985. ISBN: 0-89791-166-0

[Perlin02] Perlin, K.: Improving noise, In *Proceedings of the 29th annual conference on Computer graphics and interactive techniques*. ACM New York, USA, pp. 681-682. 2002. ISBN: 0730-0301

[PerlinOnl] Perlin Noise [online], [cit. 2008-10-22]. http://freespace.virgin.net/hugo.elias/models/m_perlin.htm

[Polack03] Polack, T.: *Focus on 3D Terrain Programming*. Premier Press, USA. 2003. ISBN: 1-59200-028-2

[Rami97] Ramirez, W. F.: *Computational Methods for Process Simulation*, Second edition. Butterworth Heinemann. 1997. ISBN: 0-7506-3541

[Rekt81] Rektorys, K:. *Přehled užité matematiky*. SNTL Praha, Czech Republic. 1981.

[Rich06] Richards, J. A., Xiuping, J.: *Remote Sensing Digital Inage Analysis*, 4th edition. Springer-Verlag Berlin Heidelberg New York. 2006. ISBN: 978-3-540-25128-6

[Robin04] Robinson S.: *Simulation: The Practice of Model Development and Use*. John Wiley & Sons, Ltd., England. 2004. ISBN: 0-470-84772-7

[Rosen66] Rosenfeld, A., Pfaltz, J. L.: *Sequential Operations in Digital Picture Processing*, Journal of the ACM (JACM), Volume 13. pp. 471 – 494. 1966. ISSN: 0004-5411

[Shap01] Shapiro, L., Stockman, G.: *Computer Vision*. Prentice Hall, New Jersey, USA. 2001. ISBN: 978-0130307965

[SHTOnl] Laser BLS-100 (Software – Hardware Technik) [online], [cit. 2008-02-21]. http://www.sht-mbh.de/webeng/530716975607ad305/5307169756083de22/5307169756084252b/index.html

[Silf04] Silfvast, W. T.: *Laser Fundamentals*, Second edition, Cambridge University Press, United Kingdom. 2004. ISBN: 0-512-83345-0

[Smith02] Smith, I. L.: *A Tutorial on Prinicpal Component Analysis*. [online], [2008-03-20]. http://www.cs.otago.ac.nz/cosc453/student_tutorials/principal_components.pdf

[Sonka07] Sonka, M., Hlavac, V., Boyle, R.: *Image Processing, Analysis, and Mahine Vision*, International Student Edition Nelson Engineering; Student Ed edition. 2007. ISBN: 978-0495244387

[Steen91] Steen, W. M.: *Laser Material Processing*. Springer-Verlag, New York Berlin Heidelberg. 1991. ISBN: 0-387-19670-6

[Tich07] Tichava, J.: *OpenGL v Javě*. Bachelor Thesis. University of West Bohemia, Pilsen, Czech Republic. 2007.

[Weiss99] Weisstein, E. W:. *The CRC Concise Encyclopedia of Mathematics*. CRC Press LLC, USA. 1999. ISBN: 0-8493-9640-9

[Wrig04] Wright, R.S., Lipchak, B.: *OpenGL SuperBible (3rd Edition)*. Sams. 2004. ISBN: 0672326019

[WolfOnl] Wolfram Mathematica® [online], [cit. 2008-03-20]. http://www.wolfram.com/

[Wool99] Woolfson, M. M., Pert, G. J.: *An Introduction to Computer Simulation*. Oxford University Press, New York. 1999. ISBN: 0-19-850423-3

[Zapl07] Zapletal, J.: *Application of radial Basic Functions*. Diploma Thesis, University of West Bohemia, Pilsen, Czech Republic. 2007.

[Zhang97] Zhang, J., Yan, Y., Lades, M.: *Face Recognition: Eigenfaces, Elastic Matching, and Neural Nets*. Proceedings of the IEEE, Vol. 85, Issue 9. 1997. ISSN: 0018-9219

[Žára05] Žára, J., Beneš, B., Felkl P.: *Moderní počítačová grafika*. Computer Press, Brno, Czech Republic. 2005. ISBN: 80-251-0454-0

Basic Expressions Explanation

Ablation
The process of material melting and vaporizing that starts after the laser beam strikes the material surface *(pp. 9).*

Cross-section curve
A curve created as the visualization of the sample surface along any cross-section line *(pp. 21).*

Cross-section line
A line segment along which the cross-section curve is generated – most often a row or a column of the sample *(pp. 49).*

Difference image
A method of samples comparison; in fact MSE visualization *(pp. 79).*

Experiment
The described pattern burned into the material; it can be further measured and processed *(pp. 4).*

Heat-affected area
The part of the material surface modified during the burning process by the thermal action of the laser beam *(pp. 9).*

Local defect
The roughness on the material surface caused, for example, by a damage on the original material surface *(pp. 19).*

Material roughness
The irregularities on the material caused by a very detailed measuring of the sample and its structure *(pp. 19).*

MSE (Mean Square Error)
A computation of heights differences of two compared samples *(pp. 78).*

PCA (Principal Component Analysis)

A method usable for data analysis that is based on computing eigenvalues and eigenvectors *(pp. 82).*

Pulse

An analogous expression for the heat affected area *(pp. 9).*

Pulse pit

The shape of the pulse area that is created in the heat-affected area as the result of material ablation during the laser burning process *(pp. 9).*

Pulse transition ring

The shape of the pulse area created around the irradiated area during the laser burning process especially as the result of the melt expulsion process *(pp. 9).*

Sample

A part of the measured experiment represented as the height map of its surface *(pp. 4).*

Appendix: Activities

Publication Related to the Doctoral Thesis

Hájková, J.: Data Processing for Simulation of Laser Beam Impact – Statistical Method for the Heat-Affected Area Detection, accepted to *International Conference on Computer Modeling and Simulation*, Brno, Czech Republic. 2009.

Hájková, J., Herout, P.: Parameterization of Samples for Modeling of Laser Burning: Increasing the Lifelikeness of Synthetically Generated Samples, accepted to *4th International Conference on Software and Data Technologies ICSOFT 2009*, Sofia, Bulgaria. 2009.

Hájková, J.: Parameterization of Samples and Its Usage in Data Description and Simulation, *Proceedings of the 23rd European Conference on Modelling and Simulation ECMS2009*. Madrid, Spain. 2009. ISBN: 978-0-9553018-8-9

Hájková, J.: Approaches for Automatic Comparison of Laser Burned Samples, *Proceedings of the 9th International PhD Workshop on Systems and Control*, Izola, Slovenia. 2008. ISBN: 978-961-264-003-3

Hájková, J.: LASER SIMULATION – Methods of Pulse Detection in Laser Simulation, *Proceedings of the 3rd International Conference on Software and Data Technologies ICSOFT 2008*, INSTICC, Porto, Portugal, pp. 186-191. 2008. ISBN: 978-989-8111-57-9

Hájková, J.: *Pattern Recognition, Classification and Simulation of Laser Beam Impact*, The State of the Art and Concept of Doctoral Thesis, Technical Report No. DCSE/TR-2008-03, University of West Bohemia, Pilsen, Czech Republic. 2008.

Hájková, J., Herout, P.: Laser Simulation, *Proceedings of the 7th International Conference APLIMAT 2008*, STU Bratislava, Slovakia, pp. 823-828. 2008. ISBN: 978-80-89313-03-7

Other Publications

Zelenka, P., Hájková J.: Structural Components in Multiadjustable Road Traffic Models: Their Role and the Means of Generating Their Topology, *Proceedings of the 23rd European Conference on Modelling and Simulation ECMS2009*. Madrid, Spain. 2009. ISBN: 978-0-9553018-8-9

Hájková, J., Šašek, M., Herout, P.: Simulation of Human Body Thermoregulation, *Proceedings of MOSIS 2006*. Přerov, MARQ, Ostrava, Czech Republic, pp. 123-128. 2006. ISBN: 80-86840-21-2

Hájková, J.: *Graphical Editor of Street Graphs*, final contribution in ACM Student Research Competition 2005.

Hájková, J.: Graphical Support of the Traffic Simulation System, *Proceedings of the 9th Central European Seminar on Computer Graphics*, Budmerice, Slovakia, pp. 51-57. 2005.

Hájková, J.: *Grafický editor schémat dopravních systémů*, Diploma Thesis, University of West Bohemia, Pilsen, Czech Republic. 2005.

Authorized Software

Laser Burned Samples Explorer [online], [cit. 2009-02-26], http://www.kiv.zcu.cz/en/research/software/detail.html?id=32

Related Talks

Hájková, J.: *Laser Simulation*. DSS Working Group Seminar, University of West Bohemia, Pilsen, Czech Republic, 17. 12. 2007.

Hájková, J.: *Methods for Laser Burning Data Preprocessing – Parameterization of Pulses*. DSS Working Group Seminar, University of West Bohemia, Pilsen, Czech Republic, 8. 4. 2009.

Teaching Activities

2005 – 2009: PPA1 – Computers and Programming 1 (Java basics)

2005 – 2009: PPA2 – Computers and Programming 2 (Data structures)

2006 – 2009: PRJ5 – Semester Project

2006 – 2009: BPINI – Bachelor Thesis Tutorial